UPMC HILLMAN CANCER CENTER ACADEMY

FRIDAY, AUGUST 1, 2025

ABSTRACT BOOK

UPMC | HILLMAN CANCER CENTER

University of Pittsburgh

Welcome

Thank you for joining us today to honor our hard-working scholars and laboratories from the Hillman Academy! We strive to provide cutting-edge research and career preparatory experiences to a diverse group of highly motivated high school students who are interested in pursuing higher education and careers in STEM fields. In this hands-on summer program, scholars are placed in laboratories directed by dedicated faculty and trainee mentors across the University of Pittsburgh Campus.

Over the course of its history, the Hillman Academy has become an award-winning science, technology, engineering, and mathematics (STEM) program that prepares students for successful college careers and beyond. The Academy was initiated in 2009 under the directorship of Michael Lotze, MD, and has grown to the program it is today with generous support from the NIH, Doris Duke Charitable Foundation, Jack Kent Cooke Foundation, UPMC, Hillman Foundation, Ear and Eye Foundation, Beckwith Funds, Stan Marks Foundation, Shadyside Hospital Foundation, University of Pittsburgh, grateful parents and patients, and the many University faculty, trainees, and staff who give selflessly of their time.

Please join us in honoring these students and mentors, as well as the hard work they did this summer to complete an authentic research project. We are so glad that you chose to join us today and are pleased that you have given your scholar a chance to work with our talented faculty, students, and fellows!

Hillman Academy Staff

Program Director: David Boone

Associate Director: Joseph Ayoob

Project Manager: Steven Jones

Hillman Academy Site Directors

Cancer Biology (CB): Dr. Deborah Galson and Dr. Ines Lohse

Computer Science, Biology and Biomedical Informatics (CoSBBI): Dr. David Boone

Computational Biology (CompBio): Dr. Joseph C. Ayoob and Dr. Keisuke Ishihara

Immunology and Cancer Immunotherapy (ICI): Dr. Tullia Bruno and Dr. Greg Delgoffe

Ophthalmology (VISION): Dr. Yuanyuan Chen

Pathobiology: Dr. Andrew Duncan and Dr. David Gau

Surgery: Dr. Emilia Diego

Tech Drive X (TDX): Dr. Justin Weinbaum and Serafina Lanna

Women's Cancer Research Center (WCRC): Dr. Partha Roy and Dr. Michelle M. Williams

Thank You

This program was made possible with the help of the following people and organizations.

Funding

National Institutes of Health (NIH)

National Cancer Institute (NCI) Youth Enjoy Science (YES) R25

Doris Duke Charitable Foundation (DDCF)

Hillman Foundation

Ear and Eye Foundation

Dr. Edwina C. Kinchington

Magee Womens Research Institute

Jack Kent Cooke Foundation - past

Stan Marks Foundation

University of Pittsburgh

Pittsburgh Cure Sarcoma

Shadyside Hospital Foundation - past

NIH CURE – past

Jack Kent Cooke Foundation - past

The Beckwith Institute – past

UPMC Center for Engagement and Inclusion – past

UPMC Parking and Security – past

Grateful parents and patients

Partners

Fund for the Advancement of Minority Education (FAME)

Homeless Children's Education Fund (HCEF)

Pittsburgh Public Schools (PPS)

Remake Learning

YWCA

MPowerhouse

Investing Now

Propel Schools

STEM PUSH Network

Precollege STEM Programs at Pitt

The Citizen Science Lab

Gene Team

BioZone

Community Engagement Centers

Pittsburgh Promise

Neighborhood Learning Alliance

Hillman Academy Leadership Team

Dr. Kathryn Schmitz
Dr. Devin Dressman
Dr. Joe Ayoob
Dr. Christopher Bakkenist
Dr. David Boone
Steven Jones

Administration

Beth Baic
Barbara Karnbauer
Samantha Reagan
Genine Bartolotta
Karla Kichi
Chanel Reid
Michael Becich
Jon Klosinski
Rayleigh Richards
Amanda Bytzura
Vladislav Leskovtec
Fritz Roth
Rob Ceccehetti
Alison Lithgow
Jose-Alain Sahel
Greg Cooper
Renee Mandell
Genaida Salgado
Eli Coutch
Michael Mazarei
Amanda Shaheen
Dawn Cziczin
Christy McCrory
Alejandro Soto-Gutierrez
Dianna Fennell
Kelsey Meyer
Lawton Syner
Carrie Fogel
George Michalopoulos
Lola Thompson
Harry Hochheiser
John Moretti
Gina Toy-Cutler
Emma Hudson
Carolyn Nolte
Justin Wideman
Rozlynn James
Liron Pantanowitz
Emily Woodard
Steven Jones
Toni Porterfield

Technology

Keith Durst
Ethan Hay
Peter Lennon
Roland Frasher
Bryan Krinberg

UPMC Hillman Cancer Center Communications Team

Gera Jochum
Anna Daniels

The Warhol Creative

Mason Williams

HDS and Interpreters

Josh Stresing

Doris Duke Scholars

Marcus Jones
August Kollar
Trinidy Manison

Pittsburgh Cure Sarcoma Undergraduates

Caelan McCormack
Norah Niesz

Pittsburgh Cure Sarcoma High School Intern

Zacharias Barron

SciTech and Dr. Edwina Kinchington Scholar

Kai Lewis

TECBio REU @ Pitt Mentoring Committee

Eliza Callahan
Tehreem Fatima
Zach LaFrankie
Kelvin Lartey
Karla Martinez
Ksenia Mats
Messiah Ridgley
Jeremiah Satcho
Samuel Wales-McGrath

Instructors, TAs, and Education Team

Alyssa Arminan
John Ash
Sarah Bradley
Hannah Bumgarner
Kun-Che Chang
Yuanyuan Chen
Kelsey Ertwine
Kevin Fuller
Deborah Galson
Jess Jana
Hye Mi Kim
Ines Lohse
Patrick Mayo
Lauren McCue
Kaylee Montanari
Angelica Phan
Rufiaat Rashid

Speakers, Lecturers, and Guests

Alyssa Arminan
Shoumei Bai
Michael Becich
David Boone
Allyn Bove
Ron Buckanovich
Casey Cargill
Yuanyuan Chen
Katherine Davoli
Wei Du
Ian Eder
Luisa Escobar-Robledo
Julia Foldi
Jon Fura
Lawrence Garvin, II
Dave Gau
Dave Gau
Yi-Nan Gong
Ritwik Gupta
Lexi Hill
Tom Hintelmann
Huda Issa Atiya
Steven Jones
Daiki Kitano
Yekaterina (Katya) Krutsenko
Stella Lee
John Maier
Kacey Marra
Steph Masotti
Curtis McCloskey
Noelle Michel
Ava Miller
Kaylee Montanari
Christopher Morii-Sciolla
Jessie Nedrow
Angie Odeniyi
Charles Patterson
Eddie Perez
Billy Reynolds
Alexa Rivera del Rio Hernandez
Brent Schlegel

Speakers, Lecturers, and Guests (cont.)

Hannah Schriever

Jane Siwek

Eric Strobl

Erin Wheeler

Sara Beth Winikoff

Professional Development Seminar Series Speakers

Joe Ayoob, PhD

Tullia Bruno, PhD

Carolyn De La Cruz, MD

Kai Ding, PhD

Fen Guo, PhD

Emma Hudson

Michael Mazarei

Nolan Priedigkeit, MD/PhD

Chanel Reid, MD, MS

Offices and Departments

University of Pittsburgh

UPMC Hospital System

UPMC Hillman Cancer Center

UPMC Children's Hospital of Pittsburgh

Pitt School of Medicine

Eye & Ear Foundation of Pittsburgh

UPMC Security Office

UPMC Volunteer office

Disability Resources and Services

Pitt IT/ Technology Help Desk

Pitt Health Sciences IT

Panther Central

Department of Biomedical Informatics

Department of Ophthalmology

Computational and Systems Biology

Department of Immunology

Department of Pathology

Department of Cell Biology

Department of Surgery

Center for Transcriptional Medicine

Pittsburgh Liver Research Center

Cellular & Molecular Pathology Graduate Training Program

Department of Bioengineering

Magee-Womens Research Institute

McGowan Institute of Regenerative Medicine

Office for Equity, Diversity, & Inclusion

University Counsel

And the many other departments that support this program

Mentors

Thanks to the hundreds of mentors across campus each of which is recognized on the individual student abstracts and site schedule

UPMC HCC Summer Academy
Cancer Biology Site 2025 Research Symposium

August 1, 2025, 8:20 am-12:45 pm

Auditorium in Assembly Building on 5051 Center Ave

Join Zoom Meeting: https://pitt.zoom.us/j/98430307436 Passcode: 711916

8:20 AM **Welcoming Remarks -** CB Site Education Team:
Deborah L. Galson, PhD (Site Director) & Ines Lohse, PhD (Site Co-Director)

8:30 AM **#1** **Norah Niesz (Undergrad @ St. Lawrence University)**
PI: Jessie Nedrow, PhD; Lab Mentor: Abhinav Bhise, PhD

8:45 PM **#2** **Summer Ji**
PI: Tatiana Moiseeva, PhD; Lab Mentor: Rohan Harolikar, BS

9:00 AM **#3** **Andrea Halun Ramirez**
PI: Kathryn Demanelis, PhD

9:15 AM **#4** **Mylo Carter**
PI: Dennis Hsu, MD; Lab Mentor:Marwa Ibrahim, PhD & David Man, PhD

9:30 AM **#5** **Andy Weng**
PI: Dennis Hsu, MD; Lab Mentor: David Man, PhD

9:45-10:00 AM ---------- **BREAK** ----------

10:00 AM **#6** **Zacharias Barron (2nd yr YES student)**
PI: Ines Lohse, PhD, Kurt R. Weiss, MD; Lab Mentor: Tanya Heim, MS

10:15 AM **#7** **Caelan McCormack (Undergrad @ St. Lawrence University)**
PI: Ines Lohse, PhD, Kurt R. Weiss, MD; Lab Mentor: Tanya Heim, MS

10:30 AM **#8** **Matthew Chu**
PI: Ines Lohse, PhD, Kurt R. Weiss, MD; Lab Mentor: Tanya Heim, MS

10:45 AM **#9** **Christian Tabler**
PI: Ines Lohse, PhD, Kurt R. Weiss, MD; Mentor: Karen Schoedel, MD

11:00 AM **#10** **Comfort Fayomi**
PI: Diwaker Davar, MD, MSc; Lab Mentor: Drew Hurd, BS

11:15-11:30 AM ---------- **BREAK** ----------

11:30 AM **#11** **Hussain Raza (2nd yr YES student)**
PI: Wei Du, MD, PhD; Lab Mentor: Jian Xu, PhD & Logan Sund, BS

11:45 AM **#12** **Joanna Li**
PI: Wei Du, MD, PhD; Lab Mentor: Jiayang Bao, PhD & Logan Sund, BS

12:00 AM **#13** **Alayna Button**
PI: Xiaosong Wang. MD, PhD; Lab Mentor: Bashir Lawal, PhD

12:15 AM **#14** **Alastair Watt (2nd yr YES student)**
PI: Patricia Opresko, PhD; Lab Mentor: Samantha Sanford, PhD

12:45 PM **#15** **Marann Buchanovich**
PI: Kathy Shair, PhD; Lab Mentor: Benjamin Warner, PhD

12:45 PM ------ **LUNCHEON (Atrium, Crane Shed)** ------

2:00 PM **ACADEMY-WIDE CLOSING CEREMONY (Assembly Auditorium)**

Computational Biology Site Agenda

2025 Research Symposium • Hillman Academy

August 1, 2025
Murdoch Building (3420 Forbes Ave, Pittsburgh, PA 15213) Floor 8, Room 814
Virtual link: https://pitt.zoom.us/j/92098276298

9:00 – 9:30 AM	**Students check their slides on shared computer**
9:30 – 9:35 AM	**Dr. Keisuke Ishihara, CompBio Site Head**
9:35 – 9:50 AM	**Zenon Cieslak** Mentor: Dr. Jim Faeder, Alex Di Basi
9:50 – 10:05 AM	**Jocelyn DeVito** Mentors: Dr. David Koes, Fareeda Abu-Juam
10:05 – 10:20 AM	**Mia Eldaher** Mentors: Dr. Dennis Kostka, Elizabeth Gilfeather
10:20 – 10:35 AM	**Allison Shi** Mentors: Dr. Jianhua Xing, Dr. Yong Lu
10:35 – 10:45 AM	**Break**
10:45 – 11:00 AM	**Avery Mills** Mentors: Dr. Fritz Roth, Dr. Warren van Loggerenberg
11:00 – 11:15 AM	**Matayo Wankiiri-Hale** Mentor: Dr. Nate Lord, Alison Guyer
11:15 – 11:30 AM	**James Hsieh** Mentor: Dr. Keisuke Ishihara
11:30 – 12:00 AM	**Rachel Kim** Mentors: Dr. Maria Chikina, Dr. Tina Subic
12:00 – 12:30 PM	**Group Photo** **Lunch for Students, Mentors, Family, and Friends** **Murdoch Classroom 814**

Hillman Academy - CoSBBI

August 1, 2025, 8:00 AM
The Offices at Baum, Room 407 A/B
https://us02web.zoom.us/j/85754282549?pwd=elordlNjOE43cFNXOEM4M3RhNGRjZz09

8:00 AM **Welcoming Remarks**

David Boone, PhD

8:05 AM **CoSBBI Scholars Research Presentations – Session 1**

Ruth Joel
Mentors: Dr. Olga Kravchenko, K. Kindler, S. Visweswaran and M. Samayamuthu
Matei Zivanov
Mentors: Dr. Harry Hochheiser and Eddie Perez
Oscar Martinez
Mentors: Dr. Liang Zhan, Kun Zhao, and Siyuan Dai
Bolutito Ojo
Mentors: Dr. Lujia Chen and Aodong Qiu
Lucia Nanda
Mentor: Dr. Inhee Lee

9:20 AM **BREAK**

9:30 AM **CoSBBI Scholars Research Presentations – Session 2**

Trinidy Manison* Doris Duke Undergraduate
Mentors: Dr. Ana Radovic and Dashawna Fussel-Ware
Nana Kwame Dwomoh
Mentors: Dr. Natasa Miskov-Zivanov and Haomiao Luo
Kenneth Ding
Mentors: Dr. Natasa Miskov-Zivanov and Haomiao Luo
Yuriy Bidochko
Mentors: Dr. Jacob Biehl, Griffin Hurt, and Brock Gjesdal
Ethan Small
Mentors: Dr. Murat Akcakaya, Yifan Zuo, and Richard Gall

10:45 AM **BREAK**

11:00 AM **CoSBBI Scholars Research Presentations – Session 3**

Husniya Nurmuhammad
Mentors: Drs. Margaret Rosenzweig and Ruth Modzelewski
Asher Peng
Mentor: Dr. Madhavi Ganapathiraju
Kylie King
Mentors: Drs. Erik Wright and Shu-Ting Cho
Einstein Lee
Mentors: Dr. Matt Wohlever and Brian Acquaviva
Hannah Luo
Mentor: Dr. Eric Strobl

12:30 PM **Lunch – Baum 4th floor foyer and 407A/B RSVP REQUIRED**

2:00 PM **Hillman Academy Closing Ceremony**

Assembly Building – First Floor Auditorium
5051 Centre Ave or **Zoom for students**:
https://us02web.zoom.us/j/86021100717?pwd=dmVQQ0NvYzFnMUVIOUxKWFdwd2U5UT09

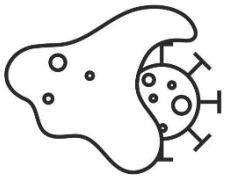

Immunology and Cancer Immunotherapy

Hillman Summer Academy Final Day

Friday, August 1, 2025

9 AM-2 PM EST (West Wing Auditorium)

Time	Presenter and Mentor
9:15-9:45 AM	Breakfast (optional)
9:45-10:00 AM	**Opening remarks**
10:00-10:15 AM	**Laila Golla** *Mentor: Dr. Adam Soloff*
10:15-10:30 AM	**Ivan Chen** *Mentor: Dr. Greg Delgoffe*
10:30-10:45 AM	**Anabella Phelps** *Mentors: Dr. Tullia Bruno and Caroline Sweeney*
10:45-11:00 AM	**Rayan Majumdar** *Mentors: Drs. Tullia Bruno and Medard Kaiza*
11:00-11:15 AM	*Short networking break*
11:15-11:30 AM	**Luke Morcos** *Mentor: Dr. Ali Kohan*
11:30-11:45 AM	**Christie Koyo** *Mentor: Dr. Ali Kohan*
11:45-12:00 PM	**Reina Majumdar** *Mentor: Dr. Jishnu Das*
12:00-12:15 PM	**Amelia Balet** *Mentors: Drs. Youjin Lee and Ziran Zhu*
12:15-12:30 PM	*Short networking break*
12:30-12:45 PM	**Rhea Arya** *Mentor: Dr. Daniella Schwartz*
12:45-1:00 PM	**Catherine Yang** *Mentor: Dr. Amanda Poholek*
1:00-1:15 PM	**David Boehm** *Mentors: Drs. Dario Vignali, Erica Braverman, Andrew Baessler*
1:15 PM	**Final remarks, group picture, and grab and go lunch**
2:00 PM	**Start of final ceremony in Assembly Auditorium**

All presentations will be <u>in person only</u>. If able, we will record student presentations for distribution!

Pathobiology

2025 Research Symposium • Hillman Academy

August 1, 2025

S120 BST, 200 Lothrop St., Pittsburgh, PA 15261
Virtual: https://pitt.zoom.us/j/94861128729

9:00 AM **Morning Mixer**
Join us for coffee, juice, and pastries.

9:30 AM **Welcome**
Drs. Dave Gau & Andrew Duncan, Pathobiology Site Heads

9:45 AM **Oral Presentations** (10 min. presentations + 5 min. questions); introductions by lab mentors

9:45 AM **Brandon Williams**
Lab & Mentor, Dr. Rodrigo Florentino

10:00 AM **Elise Dressman**
Lab, Dr. Christi Kolarcik; *Mentor,* Breanna Sullivan

10:15 AM **Najih Haider**
Lab, Dr. Bharat Bhushan; *Mentor,* Dr. Siddhi Jain

10:30 AM **BREAK**

10:45 AM **Ezra Hardy**
Lab & Mentor, Dr. Tim Perkins

11:00 AM **Alberto Gildengers**
Lab, Dr. Wendy Mars; *Mentor,* John Stoops & Ann Orre

11:15 AM **Kai Lewis**
Lab, Dr. Karina Vargas; *Mentors,* Ian Mooney & Dr. Grant Daskivich

11:30 AM **Eric Chen**
Lab, Dr. Evan Delgado; *Mentor,* Daniel Green

12:00 PM **Lunch – S120 BST**

2:00 PM **Closing Ceremony**
Assembly Building, First Floor Auditorium
5051 Centre Ave, Pittsburgh, PA 15213

Surgery Site

2025 Research Symposium • Hillman Academy

August 1, 2025
Herberman Conference Center Room 202 A
5230 Centre Ave
Join the meeting now
Meeting ID: 280 070 898 101 2
Passcode: Vb6CX2G6

10:30 **Opening Remarks**
Dr. Emilia Diego

Time **Research Presentations**

10:45 **Brooklyn Brewington**
Mentor, Dr. Carolyn De La Cruz

11:00 **Blake Whiteman**
Mentor, Dr. Joshua Brown and Dr. Christine Leeper

11:15 **Charles Bottoms**
Mentor, Dr. Genia Dubrovsky

11:30 **Rose-Carlie Pierrre**
Mentor, Dr. Melanie Scott

11:45 **Mia Fritz**
Mentor, Dr. Farzad Esni

12:00 **Lunch - Herberman Conference Center Room 202 A**

2025 Research Symposium • Hillman Academy

August 1, 2025

5th Floor Conference Room, Bridgeside Point 1, 100 Technology Drive, Pittsburgh, PA 15219
Virtual: https://pitt.zoom.us/j/92872002471

9:00 AM **Breakfast and Socializing!**

9:15 AM **Welcome**
Dr. Justin Weinbaum, Serafina Lanna, TDX Site Heads

9:30 AM **Oral Presentations** (10 min. presentations + 5 min. questions); introductions by lab mentors

9:30 AM **August Kollar**
Lab, Dr. TK Kozai; *Mentor,* Vanshika Singh

9:45 AM **Sophia Mazer**
Lab, Dr. Vaughn Cooper; *Mentos,* Dr. Abigail Matela

10:00 AM **Angie Odeniyi**
Lab, Dr. Justin Weinbaum; *Mentor,* Amanda Pellegrino

10:15 AM **Nithila Vijayan**
Lab, Dr. Amrita Sahu; *Mentor,* Jagruti Kosaraju

10:30 AM **Casey Yang**
Lab, Dr. Yuan Liu; *Mentor,* Dr. Bill Chen

11:00 PM **Lunch – Conference room and porch, weather permitting**

2:00 PM **Closing Ceremony**
Assembly Building, First Floor Auditorium
5051 Centre Ave, Pittsburgh, PA 15213

VISION

2025 Research Symposium • Hillman Academy

August 1st, 2025, 9:30 to 1:00 pm EST

IN-PERSON meeting at MHP-PAV 4.402A

Zoom link: https://pitt.zoom.us/j/92632365992

Each session will be started by a brief intro of each student by his/her mentor followed by a 10 min presentation leaving 2-3 min Q&A and picture time.

9:30 am Welcome

Presentations

9:40 am	**Sofia De La Cruz** Mentors: Dr. Silmara de Lima
9:55 am	**Sara Beth Winikoff** Mentors: Drs. Constanza Potilinski and John Ash
10:10 am	**Alexander Small** Mentors: Dr. Ethan Rossi
10:25 am	**Elif Rana Buyukkaya** Mentors: Dr. Kevin Fuller
10:40 am	**Break and Awards Announcement**
10:55 am	**Aubrey Sudor** Mentors: Dr. Patrick Mayo
11:10 am	**William Zhang** Mentors: Dr. Issam Al Diri
11:25 am	**Marcus Jones** Mentors: Dr. Kip Kinchington
11:40 am	**Jacquelyn Tang** Mentors: Kun-Che Chang

11:55 am Pictures, Award announcement and Lunch

2:00 pm Closing Ceremony – Assembly Building, Richards Auditorium

Women's Cancer Research Center Site Agenda

2025 Research Symposium • Hillman Academy

August 1, 2025
Assembly Building, Room 2001
5051 Centre Ave
https://pitt.zoom.us/j/95593704035

10:00 am **Welcome**
Michelle Williams & Partha Roy, WCRC Site Heads

10:05 am **Research Presentations** (10-12 min. presentations + 3-5 min. questions); introductions by lab mentors

10:05 am **Sunny Pham**
Mentors: Dr. Michelle Williams & Angelica Phan

10:20 am **Ava Miller**
Mentors: Dr. Katherine Aird & Dr. Naveen Kumar Tangudu

10:35 am **Roshini Umesh**
Mentors: Dr. Adrian Lee &Dr. Steffi Oesterreich & Dr. Rahul Kumar

10:50 am **Sai Saharsh Gumudavelly**
Mentors: Dr. Ron Buckanovich & Dr. Shoumei Bai

11:05 am **Shamael Rahamani**
Mentors: Dr. Steffi Oesterreich & Dr. Adrian Lee & Chris Merkel

11:20 am **---Break----**

11:30 am **Siddh Kapil**
Mentors: Dr. Kathryn Schmitz & Michele Sobolewski

11:45 am **Ruth Ayers**
Mentors: Dr. Ioannis Zervantonakis & Matt Laird

12:00 pm **Elijah Bullock**
Mentors: Dr. Partha Roy & Ishani Sharma

12:15 pm **Angelina Li**
Mentors: Dr. Lan Coffman & Dr. Huda Issa Atiya

12:30 pm **Lunch – Assembly Building, Room 2001**
2:00 pm **Closing Ceremony – Assembly Building, Richards Auditorium**

Creating Plasmids of Epitope Tagged ORF62 Genes of wild type (pOka) and the Vaccine (vOka) strains of Varicella Zoster Virus

Scholar: Marcus Jones
College: Allegheny College
Lab: Paul Kinchington, PhD
Mentor: Paul Kinchington, PhD
Site: Vision

The live attenuated virus of Varicella Zoster Virus, also known as Chickenpox, has nucleotide changes that have been shown to mostly affect a gene called ORF62. This gene encodes for a protein called IE62, which has unknown proteins associated with it that we want to uncover. To uncover those proteins, an epitope-tagged version of IE62 needs to be produced. The purpose of this project is to produce plasmids that contain an HA-tagged ORF62 gene from wild-type and vaccine strains so that they can be used as a template for insertion into the VZV virus to make the tagged IE62 protein in the future. This would be achieved through the insertion of the epitope called HA through PCR, plasmid DNA preparation, cutting DNA plasmids, ligation, and transformation. Imaging of stained gels and grown bacteria colonies pointed toward unsuccessful production of all but one sample. One sample displayed DNA fragments pointing toward successful cuts of both enzymes used, and sequencing confirmed successful production of plasmids containing the HA-tagged ORF62 gene. This sample was confirmed to be a tagged vaccine strain. Although only one sample was successful, the purified DNA made during this experiment will be used to produce the remaining samples that did not work for this project later on. Having these plasmids with epitope tagged ORF62 gene in them will allow for Immunopercipation of IE62 protein of both wild type and vaccine strains in the future. This will allow for identification of the unknown proteins associated with the IE62 protein.

Developing Methods to Decode Microglia Calcium Activity in Response to Intracortical Microstimulation

Scholar: August Kollar

High School/College/City/State: Rochester Institute of Technology, Rochester, NY

PI: TK Kozai, PhD.

Mentor: Vanshika Singh

Site: TDX

Background: Implanting electrodes into the brain allows for both stimulating and recording the brain's activity. These implants can be used for both studying the electrical signals from the brain as well as administering stimulation to treat specific conditions such as Parkinson's Disease, epilepsy, and depression. This interfacing, called intracortical microstimulation (ICMS), excites the activity of neurons near the probe. Microglia, the immune cells of the brain, naturally respond to neuron activity, observable via changes in their calcium activity. Studying calcium events in microglia enriches our understanding of their intracellular changes in response to electrical stimulation induced neural activity.

Methods: For this project, we implanted single-shank Michigan style electrodes into transgenic mice expressing red fluorophore and green fluorescent calcium indicator in microglia. These mice were imaged for 20 minutes before, 60 minutes during, and 20 minutes after a 10 Hz stimulation interval under a 2-photon microscope. Using this imaging data and images from previous experiments, a MATLAB script was designed with the goal of algorithmically detecting microglial calcium events based on the signals of each individual pixel of imaging data.

Results: Although the script worked on images from past experiments, it struggled to process the data for this experiment. This failure to successfully process data is likely a result of fluorescence intensity decay as a result of longer imaging intervals, as well as noisy data as a result of issues with equipment. It is also possible that events in the collected images were too small to be detected, or the stimulation paradigm was not strong enough to elicit observable events.

Conclusion: Past algorithms that were designed to detect microglial calcium events worked better on datasets representing shorter timeframes—when imaging is performed for longer periods of time, the effects of fluorescence decay become non-negligible.

Title: Train the Trainer: A Youth-Led Approach to Mental Health Education

Scholar: Trinidy Manison

High School/College/City/State: Pennsylvania State University

PI of group/lab: Dr. Ana Radovic

Mentor(s): Ana Radovic, Dashawna Fussell-Ware, Sierra Geisler

Site: CoSBBI

Black youth continue to experience rising rates of depression, anxiety, and suicide, especially within communities facing economic disadvantage. This project aimed to address these challenges by developing a peer-led “Train the Trainer” mental health education model using the Supporting Our Valued Adolescents (SOVA) platform. The resulting E-HEAL curriculum showed feasibility, engagement, and potential for broader implementation based on feedback from youth and adult facilitators during its pilot phase at the Boys and Girls Club McKeesport site.

Supporting Our Valued Adolescents (SOVA) is an initiative by the University of Pittsburgh focused on youth mental health, especially among underserved and marginalized communities such as BIPOC (Black, Indigenous, and People of Color) and LGBTQ+ youth. Originally developed for use in primary care, SOVA provides online tools, youth-created content, and moderated support to promote mental health awareness and help-seeking behaviors.

This project aimed to expand SOVA’s reach by developing and testing a youth-led “Train the Trainer” curriculum. The goal was to prepare young people to deliver peer-led presentations that promote mental health literacy and self-advocacy within job readiness and community programs.

In 2024, youth-led presentations were delivered at a Boys and Girls Club (BGC) site. Three focus groups used the “Rose, Bud, Thorn” method to gather feedback and explore barriers to peer-led education. These insights informed the creation of the SOVA E-HEAL curriculum.

In 2025, the curriculum was piloted at BGC McKeesport. Three youth and one adult facilitator completed all modules, created presentations on panic attacks and depression, and presented to peers. Youth found learning from peers more engaging, and staff emphasized the need for facilitator guides and expert support. This study shows that youth-led mental health education is possible and well-received. Next steps include academic publication and expanding the model’s reach and evaluation.

Title: Metastatic Patient Plasma Increases Migration of Primary Osteosarcoma Cells

Scholar: Caelan McCormack

High School/College/City/State: St. Lawrence University, Canton, NY

PI of lab: Dr. Ines Lohse

Mentors: Tanya Heim and Dr. Ines Lohse

Site: Cancer Biology

Osteosarcoma (OS), although a rare cancer, is the most common primary bone cancer in children and adolescents, occurring most frequently during periods of rapid bone growth. Osteosarcoma has a tendency to metastasize to the lungs, significantly decreasing patient survival. However, the mechanisms underlying metastasis remain poorly understood. Small signaling vesicles called exosomes have been implicated in regulating cancer cell migration in various malignancies including osteosarcoma. While the importance of exosomes for cancer progression and metastasis is clear, the specific underlying mechanisms remain elusive. We have examined changes in migration potential of primary osteosarcoma cells in response to treatment with patient-derived plasma from patients with only primary osteosarcoma and patients with metastases using scratch assays. To perform the scratch assay, SaOS-2 cells were cultured to 100% confluency in a six well plate. Once fully confluent, three scratches were introduced per well using 200ul pipette tip. Cells were then treated with either patient-derived plasma, PBS, or OS media. Scratches were photographed every 12 hours for 72 hours and ImageJ was used to measure the width of each scratch to quantify migration rates. We found that primary osteosarcoma cells treated with primary and metastatic patient plasma migrated at a faster rate than controls. Additionally, we observed that after 36 hours, primary osteosarcoma cells treated with metastatic patient plasma showed increased migration rates compared to primary osteosarcoma cells treated with primary patient plasma. As next steps, we will perform Boyden Chamber migration assays to validate whether the migration phenotype is observed across different assays. Finally, we will isolate exosomes and perform proteomic analysis to identify the underlying molecular pathways driving metastatic behavior.

Title: Evaluation of VH-Fc Fusion Proteins for Mesothelin-Targeted PET Imaging in Triple-Negative Breast Cancer Models

Scholar: Norah Niesz

High School/College/City/State: St. Lawrence University, Canton, New York

PI of group/lab: Dr. Jessie Nedrow

Mentor(s): Dr. Abhinav Bhise

Site: Cancer Biology

Mesothelin (MSLN) is a membrane protein expressed in a variety of cancers but shows limited expression in normal tissue making it an ideal target for cancer therapies. Conventional IgG antibodies (~150 kDa) targeting MSLN often exhibit prolonged circulation, high background noise and limited tumor cell penetration due to their large size. VH-Fc fusion proteins (~80 kDa), consisting of the variable heavy (VH) domain linked to an Fc fragment, offer a smaller alternative with improved pharmacokinetics and tumor penetration. In this study, anti-MSLN VH-Fc fusion proteins using the 2A10 VH domain and mutant Fcs were evaluated in a model of triple negative breast cancer (HCC1806 tumor-bearing mice). PET imaging was performed at 1.5-, 24-, 48-, and 120-hours post-injection to assess the pharmacokinetic profiles. Quantitative image analysis using VivoQuant determined the mean standard uptake value (SUV) in tumor and major organs. Comparative analysis of the SUV identified [^{89}Zr]Zr-DFO-2A10-VH-Fc$_{LALAPG}$ as showing the most favorable tumor targeting and pharmacokinetic profile. Additionally, PEGylation of the 2A10-VH-Fc$_{LALAPG}$ and an alternative Fc mutation, 2A10-VH-Fc$_{FEA,}$ effectively reduced renal retention due to improved *in vivo* stability, but reduced tumor accumulation. These findings support the utilization of PET imaging to optimize anti-MSLN VH-Fc fusion proteins for improved pharmacokinetic profiles, minimizing renal uptake without compromising tumor targeting. Additionally, this study has identified the 2A10-VH-Fc$_{LALAPG}$ as the lead agent for advancing preliminary studies to investigate the potential of radiopharmaceutical therapy.

Th9-arterial endothelial cell crosstalk promotes autoimmunity-associated cardiovascular disease

Scholar: Rhea Arya

College: University of South Alabama, Mobile, AL

PI of group/lab: Dr. Daniella Schwarts

Mentor: Dr. Ishita Baral

Site: Immunology and Cancer Immunotherapy

Psoriasis and atherosclerosis are chronic inflammatory diseases linked by a distinct “Th9-high” immune endotype, marked by expansion of IL-9–producing Th9 cells and increased cardiovascular risk. Recent evidence suggests that inflammatory mediators within atherosclerotic plaques—such as nitric oxide (NO) and key cytokines—can modulate Th9 differentiation, potentially amplifying vascular inflammation and endothelial dysfunction in autoimmunity. Splenocytes were isolated from C57BL/6 mice and cultured under Th9-polarizing conditions (IL-4 and TGF-β). Experimental groups were treated with 200 μM NOC-18 (a nitric oxide donor), anti–IL-2 blocking antibodies, recombinant IL-1β, or a combination of anti–IL-2 and IL-1β. After three days, intracellular flow cytometry quantified the percentage of IL-9–producing CD4+ T cells. Isotype antibody and solvent controls were included. Experiments were optimized in a single mouse, then performed using splenocytes from two additional mice to provide three biological replicates. Treatment with 200 μM NOC-18 increased the frequency of IL-9–producing Th9 cells compared to controls. Blockade of IL-2 reduced Th9 polarization and IL-9 production, while IL-1β produced a variable effect. Co-treatment with anti–IL-2 and IL-1β further modulated Th9 differentiation, highlighting a complex interplay between nitric oxide and cytokine signaling pathways in regulating Th9 responses relevant to inflammatory cardiovascular disease.

Comparative Analysis of Presumptive Mesothelial Cell Marker Expression in Ovarian Cancer and Endometriosis

Scholar: Ruth Ayers
School: Pittsburgh Science and Technology Academy, Pittsburgh, PA; Carnegie Mellon University, Pittsburgh, PA
PI of Lab: Ioannis Zervantonakis
Mentors: Ioannis Zervantonakis, Matthew Laird
Site: Women's Cancer Research Center

Rationale:
Ovarian cancer frequently metastasizes to the omentum, where tumor cells disrupt the mesothelial lining. This disruption may drive mesothelial-to-mesenchymal transition (MMT), a process thought to facilitate tumor invasion and stromal remodeling. However, the molecular features of mesothelial activation in this context are poorly understood. This study aimed to characterize how ovarian cancer metastases alter expression of mesothelial and stromal markers across tissue types and spatial regions.

We analyzed mesothelial changes in:
(a) tumor-infiltrated vs. adjacent normal (NAT) tissue within patients,
(b) NAT tissues across patients,
(c) tumor-adjacent vs. endometriosis tissues (a benign inflammatory control), and
(d) different regions within a tumor-infiltrated sample.

Methods:
We used multi-round immunofluorescence on fixed omental tissue (tumor-infiltrated, NAT, and endometriosis) to detect mesothelial (calretinin) and mesenchymal (αSMA) markers. WT1, SNAIL, and HIF1α were excluded due to low specificity.

Results:
In tumor-infiltrated regions, calretinin expression was significantly reduced, while αSMA was consistently elevated compared to paired NAT, though this trend did not consistently reach statistical significance across all patients. Notably, calretinin levels were higher in regions farther from tumors, while αSMA expression increased closer to tumors, suggesting spatially localized effects of tumor presence. Expression of both markers varied between patients, indicating inter-individual heterogeneity. Endometriosis samples showed higher αSMA than tumor-adjacent NAT, but similar calretinin levels, suggesting that stromal remodeling in cancer is distinct from benign inflammation.

Conclusion:
Ovarian cancer metastases induce spatial and patient-specific alterations in mesothelial and stromal marker expression. Tumor proximity correlates with decreased calretinin and increased αSMA expression, indicating localized microenvironmental remodeling. The differential marker profile in endometriosis versus tumor-adjacent tissues suggests that cancer-associated stromal activation involves tumor-specific mechanisms beyond inflammation. These findings may inform therapeutic strategies targeting the tumor–stroma relationship to limit metastatic progression.

Effects of CCR3 In Treg Cells On the Central Nervous System

Scholar: Amelia Balet
Education: The Ellis School, Pittsburgh, PA
Mentors: Ziran Zhu and Youjin Lee
Site: Immunology and Tumour Immunotherapy (ICI)

Abstract:

Introduction: Regulatory T-cells play an important role in mediating immune responses within the Central Nervous System. These pro-tumour cells can mitigate neuroinflammation, promote neuronal survival, and assist in viral resistance. Their infiltration of the brain is CCR3 dependent, a type 3 C-C chemokine receptor that aids in immune responses and inflammation. When CCR3 is expressed in Treg cells, its specific effects on the cell and interactions with the CNS is unknown; however, this receptor has been linked to many neurological diseases.

Procedure: To identify CCR3's effects on Treg cells and the CNS, we decided to overexpress the receptor in a mouse model. I created a vector with CCR3 and thy1.1, a cell membrane protein that is used as a marker for mouse T cells. My mentor, Ziran Zhu, used pCL-Eco and my vector to produce a retrovirus which she infected Treg cells with. I then performed qPCR to check the cells' mRNA levels and flow cytometry to check the cells' CCR3 protein levels.

Results: Our experiment was successful, with the qPCR showing that cells with an overexpression of CCR3 had higher relative mRNA levels. The flow cytometry revealed that 98% of Treg cells with CCR3 expressed thy1.1, the marker that indicates that our vector successfully infected the Treg cells and was replicated.

Discussion: To fully understand the effects of overexpressed CCR3, these modified Treg cells must be injected into a mouse model, something that we were unfortunately unable to do this summer. By observing these mice, we could have come to conclusions about the role of CCR3 in regulatory T cells and the CNS. Our findings could impact the way researchers approach treatments for neurodegenerative diseases and disorders, such as Multiple Sclerosis. Hopefully, we can help scientists better understand the immune system's role in these issues.

Investigating the Effect of Panobinostat on Osteosarcoma Cells

Scholar: Zacharias Barron

Education: Woodland Hills High School (‘25); Johns Hopkins University (‘29)

Lab: Kurt Weiss, MD; Ines Lohse, PhD

Mentors: Ines Lohse, PhD; Tanya Heim, MS

Site: Cancer Biology

Osteosarcoma (OS) is a primary malignant bone tumor affecting children, adolescents, and young adults[1]. Before 1970, surgical resection was the standard treatment, with long term survival rates under 20 percent[1]. The introduction of multiagent chemotherapy improved outcomes, raising survival to 65 to 70 percent[1]. However, in patients with lung metastases, seen in 90 percent of metastatic cases, there is no standard treatment, and five-year survival remains below 30 percent[2]. Panobinostat, a histone deacetylase (HDAC) inhibitor, has been shown to reduce OS growth and lung metastases in preclinical models[3]. SaOS-2 cells were cultured in OS media (DMEM plus 10 percent FBS, 1 percent Pen Strep, 1 percent NEAA, 1 percent vitamins) at 37 °C with 5 percent CO_2. Cells (2×10^4 per well) were seeded in 96 well plates. After 24 hours, cells were treated with an 8-point dilution of panobinostat starting at 10 μM. DMSO (0.1 percent) was used as control. After 48 hours, 100 μL of WST 1 reagent was added and incubated for 30 minutes. Absorbance was measured at 420 nm. SaOS-2 and LM2 were successfully plated and treated with the specified concentrations of panobinostat. Early results indicate that lower concentrations led to greater reductions in SaOS-2 cell viability. In contrast, LM2 cells, which exhibit higher migratory and proliferative behavior, did not show significant viability reduction at lower concentrations. Higher concentrations of panobinostat may be required in LM2 cells to observe accurate effects on cell viability, and future trials will further investigate this dose-dependent response. Lower concentrations of panobinostat show promise in reducing SaOS-2 viability and may be tested with disulfiram. Further testing will clarify cell line-specific responses.

References:

1. Isakoff SM et al. *Osteosarcoma: Current treatment and a collaborative pathway to success.* J Clin Oncol. 2015;33(27):3029–35.
2. Heim ET et al. *RNA-sequencing predicts the role of AR and ALDH1A1 in OS lung metastases.* Oncogene. 2024; 43:1007–18.
3. McGuire JJ et al. *HDAC inhibition prevents growth of primary and metastatic OS.* Int J Cancer. 2020;147(10):2811–23.

Realtime Seizure Prediction: A Personalized Approach

Yuriy Bidochko, Dr. Jacob Biehl, Griffin Hurt, Brock Gjesdal
Penn-Trafford High School, Harrison City, PA; University of Pittsburgh, Pittsburgh, PA

Abstract

This projects investigates a personalized approach to seizure prediction with real-time use in mind. I aimed to build a patient-specific seizure prediction system that uses a patient's ongoing EEG to predict what that patient's EEG would look like prior to a seizure, continuously updates the predicted pre-seizure EEG to make it more fit to patient EEG data, and constantly validates ongoing EEG with the predicted pre-seizure EEG to output a warning once the two resemble each other.

Introduction

Seizures often occur during Neurosurgery. Procedures like an electroencephalogram (EEG) measure electrical activity in the brain using probes placed on the scalp to send electrical impulses to be graphed as data. EEG increases the chance one undergoes a seizure due to the nature of sending electricity into the brain. Many have attempted to use machine learning to predict seizures before they occur, but there has been limited success incorporating seizure prediction into the operating room due to limited real-time prediction accuracy. Many past approaches were made with the assumption that EEG data is generalizable across patients, but this might not be the best approach. My novel approach aims to predict seizure onset using a personalized approach because EEG data may not generalizable across patients.

Methods

I utilized the CHBMIT dataset which uses EEG data from 22 subjects to obtain 664 total files with 198 seizures. I first created a global pre-seizure class by extracting 10 minute windows prior to every seizure in the dataset. Those pre-seizure windows were then transformed with a variational autoencoder (VAE) and then combined via mean to create one universal window of what the average pre-seizure looks like. For every patient, I process 10s of EEG data at a time (simulating real time) to predict what a pre-seizure window would actually look like and comparing that predicted pre-seizure window to the current EEG reading. This is done by continuously updating the predicted pre-seizure window using VAE to adapt it to the patient's EEG. This results in a more accurate prediction of what the pre-seizure window would look like as more data is fed in for a patient. The current EEG is continuously compared to the predicted pre-seizure using cosine similarity, and once the similarity reaches a set threshold, the current window is flagged as pre-seizure, signaling a seizure to come in the future.

Results

Across all 23 patients validated on from the CHBMIT dataset, I have been able to predict every single seizure present in their total EEG timeline within 10 minutes prior of the seizure, but my model has predicted false positives in the process, and thus invalidated the model's usefulness.

Discussion

My model is still in the early stages and thus has not produced satisfactory results. I aim for my approach to overall be built open in the future as personalized approaches in seizure prediction are not mainstream yet. The assumption of the past has been that EEG data is generalizable across patients, but this steers seizure prediction in the wrong direction. The future of seizure prediction is personalized approach because every seizure is different. Every person is different.

LAG3 limits CD8 T-cell Migration

Scholar: David Boehm Jr.

High School/College/City/State: Pittsburgh Science and Technology Academy, Pittsburgh, PA

PI: Dario Vignali, PhD

Mentors: Andrew Baessler, PhD, Erica Braverman, PhD

Site: ICI

A CD8 T cell is a type of white blood cell that plays a crucial role in the immune system's defense against infections and cancer. LAG3 is an inhibitory receptor that helps to regulate their activity. However, it is unknown if LAG3 impacts chemokine receptor expression and influences migration toward a chemokine gradient. For this project, we utilized flow cytometry and transwell migration assays to test whether LAG3 impacts chemokine receptor expression and to test whether or not LAG3 influences migration towards a chemokine gradient. We found that whilst chemokine receptor expression was not different, LAG3 deficient cells migrate more efficiently in the transwell assay. These data suggest that LAG3 may act to restrict T cell movement. Ongoing studies will examine whether LAG3 also impacts the ability of T cells to infiltrate into tumors.

In another set of experiments, we wanted to examine how therapies targeting inhibitory receptors impact the composition of the tumor microenvironment using a mouse melanoma model. We found that there was greater amount of CD8 and CD4 T cells in mice treated with antiPD1 and antiLAG3 immunotherapy. We also saw that the ratio of CD8 T cells to Tregs was greater in the treated mice. Ongoing work will examine how treatment impacts the spatial relationships of these cells in the tumor microenvironment.

Mitigating CR-POPF After DP: Pancreatic Stenting

Scholar: Charles Botoms

High Schol: Obama Academy 6-12, Pittsburgh Pennsylvania

Lab: Emilia Diego

Mentor: Genia Dubrovsky, MD

Site: Surgery

Background: This study explores the use of pancreatic stents as a method to prevent clinically relevant postoperative pancreatic fistula (CR-POPF) after distal pancreatectomy. A mold for stent manufacturing was developed using a 3D designing tool that is ready to be 3D-printed. Although the stent was not manufactured due to the lack of access, the project highlights the potential utilization of stent-based prevention. Clinically relevant post-operative pancreatic fistula (CR-POPF) is a frequent complication occurring in 20-30% of cases after distal pancreatectomy (DP). It is caused by the leakage of pancreatic enzymes.

Methods: To simulate the design of a suitable pancreatic stent, a 3D modeling tool was used to create prototypes for stent molds. These molds would be used for stent manufacturing via heated extrusion. Designs were based on average duct sizes and aimed to produce stents 1-5 mm in diameter and 5-10 mm in length. The 3D software allowed for adjustments and flexibility, providing a framework for how the stent would adapt to the pancreatic duct.

Results: Autodesk Fusion was used to generate prototypes for manufacturing pancreatic duct stents. The molds had different diameters, lengths, and shapes, so that multiple different stents could be easily manufactured with reproducibility. Figure 1 shows an example of one stent mold. Features include stent dimensions, and ease of stent retrieval after hardening within the mold. These mold prototypes were created in a CAD file, so they can be easily 3D printed and ready to be used.

Conclusion: The use of 3D design tools provided insight into the function of a pancreatic stent and customization to match anatomy-based requirements. The project highlights the potential of prototyping for surgical innovation, and the models created here will be used to manufacture stents for testing and optimization. Partnerships with engineers and manufacturers should be prioritized for future clinical testing.

Title: Developing a serologic assay to type EBNA-1 variants in Epstein-Barr virus-associated cancers for cancer risk prediction

Scholar: Marann Buckanovich

Highschool: Winchester Thurston, Pittsburgh PA

PI: Dr. Kathy Shair, PhD

Mentors: Dr. Benjamin Warner, PhD, Dr. Joshua Walton, PhD

Site: Cancer Biology

Abstract: Epstein-Barr Virus (EBV) is a herpesvirus associated with cancers including nasopharyngeal carcinoma (NPC) and gastric carcinoma (GC). Over 90% of the global population is chronically infected with EBV. However, NPC is endemic to certain geographic regions, such as Southeast Asia, and specific ethnic populations. This suggests the possibility of EBV variants that may increase NPC risk. Epstein-Barr Virus Nuclear Antigen 1 (EBNA1) is a multi-functional protein that is essential for viral replication and persistence. It is expressed in all EBV-associated cancers, and NPC tumors almost exclusively harbor one variant. Two EBNA1 variants (B95-8 and Akata) have been characterized, but how variation contributes to risk remains inconclusive. Previous studies have shown that, compared to B95-8, human antibodies against Akata more accurately predict NPC risk. Viral sequences from “dbEBV” were analyzed to identify EBNA1 variants and prevalence in tumor samples (NPC and GC) and saliva, across different geographies. In parallel, a panel of rabbit polyclonal antibodies spanning conserved and variant epitopes were tested against B95-8 or Akata by immunofluorescent staining to identify an antibody specific to B95-8. Histology sections and western blotting of HEK293 cell lines transfected with FLAG-tagged EBNA1 variants were used to define antibody reactivity and specificity. Histograms were used to rank order antibodies by signal-to-noise. Antibodies that scored highest were further validated in EBV-infected cell lines. Antibody (K67-3) spanning both conserved and variant residues detected both EBNA1 variants comparably. In contrast, antibodies (K96/5, K96/16, K96/9, K96/11-v) showed specificity for B95-8. A hypervariable amino acid (a.a. 487) found in EBNA1 hybrids would require additional antibodies to distinguish subtypes. This data demonstrates the feasibility of a custom antibody panel to type EBNA1 B95-8, which may also be developed for EBNA1 Akata and other subtypes. This could aid the development of an antibody-based assay to survey the EBNA1 variants in EBV-associated tumors.

Investigating the Role of MRTF in Endocrine Resistance of ER+ Breast Cancer

Scholar: Elijah Bullock

High School/College/City/State: Winchester Thurston School, Pittsburgh, PA

PI of group/lab: Dr. Partha Roy

Mentor(s): Ishani Sharma

Site: Woman's Cancer Research Center

Background: Luminal breast cancers (BC) account for 70% of BC cases. A hallmark of luminal BCs is overexpression of estrogen receptor-alpha (ERα), which initially renders these cancers responsive to endocrine therapies that block estrogen signaling. However, prolonged treatment often leads to therapy resistance, resulting in therapeutic failure and disease progression. Myocardin-related transcription factors (MRTFs) belong to a family of transcriptional co-activators that play a key role in the activation of transcription factor (TF) serum-response factor (SRF). Increased activity of the MRTF with its binding partner SRF drives transcriptional programs that are linked to enhanced tumor aggressiveness, metastasis, and, interestingly, a few studies have linked MRTF-A activity in promoting endocrine resistance in ER+ BC cells. The resistance is through downregulating the expression of hormone receptors and massive reorganization of ERα. The study is guided by the hypothesis that if MRTF overexpression contributes to the loss of ER expression in BC cells and endocrine resistance, then silencing MRTF or its cofactor SRF can restore ER expression and resensitize BC cells to treatment. The overarching goal of this study is to determine whether suppressing MRTF/SRF signaling can reverse acquired endocrine resistance in ER^+ breast cancer cells. Toward this goal, my project specifically investigates the impact of suppressing the expression of either MRTF isoforms or SRF on ERα expression in breast cancer cells.

Methods: The project will utilize the MCF-7 cell line, a well-established model of ER+ breast cancer. The experimental approaches were as follows: MCF7 cell cultures were transfected with either MRTF-A/B-targeting siRNA or SRF-targeting siRNA (control siRNA transfection served as a control), and cell lysates were probed for ERα expression with Western Blotting.

Results: The results supported the central hypothesis. Silencing MRTFA, MRTFB, and SRF led to an increase in ERα expression, as demonstrated by the Western blot analysis. These findings confirm the effectiveness of the transfection and gene knockdown procedures. Compared to the control, ERα expression was elevated following MRTFAB and SRF silencing. This suggests a negative regulatory relationship, whereby MRTFA, MRTFB, and SRF act to suppress ERα expression under normal conditions.

Conclusion: By reducing MRTF and SRF expression in ER+ breast cancer cells, this study highlights that targeting the MRTF-SRF can restore ERα expression. These findings provide a conceptual foundation for the potential utility of targeting MRTF/SRF signaling to overcome endocrine resistance in ER+ breast cancer.

The Discovery of KIR-reg, a Transcriptional Factor-Based Program For Predicting Immunotherapy Outcome in Kidney Cancer

Scholar: Alayna Button

High School/City/State: Thomas Jefferson High School, Jefferson Hills, Pennsylvania

PI: Xiaosong Wang, M.D., Ph.D.

Mentor: Bashir Lawal, Ph.D.

Site: Cancer Biology

Backgrounds: Immunotherapy holds promise as an effective cancer treatment by targeting the immune system, but predicting patient response remains a clinical challenge, particularly in renal cell carcinoma (RCC), where treatment resistance can lead to adverse effects and wasted resources. To address this, a transcription factor–based signature predictive of immunotherapy resistance, termed KIR-reg (Kidney cancer Immunotherapy Resistance Regulon), was developed.
Methods: Using four RCC clinical trial datasets, transcription factor (TF) activity scores were computed for each patient by ranking the expression of TF target genes. AUROC values were calculated to assess each TF's ability to discriminate responders (1) from non-responders (0), with lower AUROC indicating stronger association with resistance. The top resistance-predictive TFs across datasets were integrated to form the KIR-reg score.
Results: The predictive activities of the KIR-reg were tested on the 4-datasets, yielding 0.71, 0.59, 0.88, and 0.56, with average AUROC scores of 0.69. Mechanistically, cybersort immune cell deconvolution revealed that the KIR-reg demonstrated a significant negative association with key anti-tumor immune cells including the M1 macrophage and cluster of differentiation 8 (CD8). In addition, physiological analysis of KIR-reg enrichment using bulk-RNA and single cell transcriptomic data of healthy tissue revealed that KIR-reg was highly expressed in immune-privileged body including the brain, testis, and eyes.
Conclusion: In conclusion, KIR-reg is a robust transcriptional signature capable of predicting immunotherapy resistance in RCC. RNA sequencing of tumor biopsies can be used to measure KIR-reg expression, aiding clinicians in identifying patients unlikely to benefit from immunotherapy and avoiding unnecessary treatment-related risks and costs.

Keywords: KIR-reg (Kidney cancer Immunotherapy Resistance Regulon); Immunotherapy; transcriptional factors; Renal cell carcinoma

Repurposing mammalian protein kinase A inhibitors as novel antifungals to treat fungal keratitis

Scholar: Elif Rana Buyukkaya
High School: North Allegheny Senior High, Hillvue Lane Pennsylvania
Lab: Kevin Fuller, PhD
Mentor: Manali Kamath, Kevin Fuller
Site: VISION

Background: Fungal keratitis (FK) is a potentially blinding infection of the cornea that affects 1-2 million people annually and is most prevalent among agricultural workers in tropical climates. Current antifungals, including natamycin and voriconazole, fail to save the cornea in up to 40% of cases, thus underscoring the need to develop better treatment modalities. The protein kinase A (PKA) pathway is a conserved eukaryotic signaling cascade that regulates the virulence of several fungal pathogens, including the common FK agent, *Aspergillus fumigatus*. In this study, we seek to test the antifungal activity of commercially available mammalian PKA inhibitors *in vitro*, with long-term aim of developing such drugs as novel therapeutics for FK.

Methods: The minimum inhibitory concentration (MIC) of H89 against *A. fumigatus* was determined in a broth microdilution assay. After 24 and 48 h incubation at 37 °C, optical density (OD) at 530 nm was measured to assess fungal biomass. The assay was similarly conducted against voriconazole, with or without the presence of 125µg/mL H89. In a separate assay, *A. fumigatus* conidia were spot-inoculated on nutrient agar containing 60µg/mL H89 or vehicle (DMSO). Colony diameters were marked daily and plates were photographed at end point (72h).

Results: In the microdilution assay, H89 completely inhibited *A. fumigatus* spore germination at 125µg/mL, where presence of 60µg/mL in solid media significantly reduced the hyphal growth rate. Moreover, the presence of 60µg/mL H89 shifted the MIC of voriconazole from 1 µg/mL to 0.5-0.25µg/mL.

Conclusion: These data demonstrate that H89 harbors direct antifungal activity against *A. fumigatus* that is additive when combined with voriconazole. Future studies will evaluate the impact of H89 on *A. fumigatus* PKA activity, its activity against other FK relevant fungi, and its toxicity against corneal cells before moving to treatment studies in a mouse model of FK.

The role of THUMPD3 in arginine translation during arginine limitation in colorectal cancer

Scholar: Mylo Carter

High School/College/City/State: Taylor Allderdice, Pittsburgh, PA

PI of group/lab: Dr. Dennis Hsu, MD

Mentor(s): Marwa Ibrahim, PhD

Site: Cancer Biology

Arginine limitation has been found in many cancer microenvironments, including colorectal cancer. When there is not enough arginine in the surrounding area, tRNA molecules are unable to properly load the arginine onto the RNA to translate into a protein. Based on the results of a focused siRNA screen, we hypothesize that the tRNA modifying enzyme THUMPD3 is linked to ribosome stalling under arginine starvation conditions. To test this, we designed a luciferase reporter system in which Renilla luciferase was modified to be "stalling prone" via the addition of additional arginine codons. Decreased arginine availability results in less Renilla luciferase translation which in turns diminishes bioluminescence. Additionally, we modified Renilla luciferase with two glycine codons as an external control. In order to test THUMPD3's hypothesized connection to ribosome stalling under arginine starvation conditions, we silenced it in the colorectal cancer cell line RKO, which stably expressed the luciferase reporter and measured luciferase activity at different levels of arginine limitation. Each condition was tested with THUMPD3 either expressed or silenced using two independent siRNAs. After normalizing for cell viability in each well, we found that in cells with THUMPD3 silenced, luciferase activity dropped by an average of 20% under starvation compared to the fully-fed condition. In contrast, cells expressing THUMPD3 showed an average 50% decrease in bioluminescence under the same conditions. We also performed a Western Blot assay to determine the amount of the enzyme. This assay confirmed our findings from the luciferase assay, showing that the percent expression when THUMPD3 was expressed was 40%, as compared to when it was silenced, where it was 70%. These findings support the hypothesis that THUMPD3 contributes to ribosome stalling during arginine limitation, and that silencing THUMPD3 potentially lessens the effects of arginine limitation on protein translation.

Title: Identifying whether epigenetic inhibitors can promote gene expression in HCC cells

Scholar: Eric Chen

High School/College/City/State: Seneca Valley High School, Harmany, PA

PI of group/lab: Evan Delgado, Ph.D.

Mentor(s): Evan Delgado, Ph.D.

Site: Pathobiology

Background: Hepatocellular carcinoma (HCC) is the most common type of primary liver cancer. Currently, liver transplantation is the most effective treatment, but a lack of healthy donor livers impacts the use of this method. New approaches to treating HCC are crucial because HCC is a heterogeneous disease, causing the efficacy of immunotherapy to only demonstrate a response in approximately 30% of patients. Some groups have turned to utilizing a combination of histone deacetylase inhibition (HDACi) and DNA methyltransferase inhibition (DNMTi) to promote the expression of genes that assist immune cell recruitment and function. Prior investigation suggests high levels of HDACi are detrimental to the expression of immune-related genes in HCC cell lines, while low levels are beneficial. This study aimed to investigate the effects of HDACi on gene expression in normal and cancerous human hepatocytes.

Methods: The murine cell line AML12, primary human hepatocytes, and primary mouse hepatocytes were treated with varying doses of Belinostat while 5-aza concentrations remained constant. Quantitative PCR was used to assess gene expression of chemokines (CCL5, CXCL1, CXCL2, IFN-γ, IFN-γ receptor 1/2), and luminescence-based assays were used to measure changes in cell viability.

Results: Expression of pro-inflammatory genes in AML12 cells, primary human hepatocytes, and primary mouse hepatocytes is suppressed after twenty-four hours of treatment with Belinostat and 5-aza. Expression of pro-inflammatory genes in these cells is increased in comparison to the control. Cell viability was also impacted in a dose-dependent and time-dependent manner with respect to altering Belinostat.

Conclusion: Our study determined that doses of Belinostat may impact the expression of immune-related genes to a higher degree in HCC cell lines than in normal hepatocytes. Further studies will be conducted to determine whether Belinostat significantly alters the expression of genes in cancerous human hepatocytes and in animal models.

Exploring the NK-like receptor CD161 as a potential immunotherapeutic target

Scholar: Ivan Chen

High School/College/City/State: Seneca Valley, Zelienople, PA

PI of group/lab: Greg Delgoffe

Mentor(s): Supriya Joshi

Site: ICI

Background: Immunotherapy has changed the landscape of cancer therapy. However, checkpoint blockade fails when a sufficient initial tumor response isn't carried out. Thus, alternate immunotherapies, such as chimeric antigen receptor T (CAR T) cell therapy, that works through specific targeting of tumor antigens through genetic modification, have been developed. However, both forms of immunotherapy often fail due to barriers like poor infiltration and exhaustion due to constant antigen exposure. Exhausted T cells express inhibitory molecules such as PD1, Tim3 and LAG3 that can be targeted through checkpoint blockade therapy e.g. PD1 therapy. Checkpoint blockade therapy has shown remarkable success in patients but is not perfect. There is thus always a search for more therapeutic targets such as PD1. One such target that has been of interest is the NK-like receptor CD161. Recent studies have shown that exhausted T cells may show an NK-like phenotype like the expression of CD161 alongside PD1. This project will focus on confirming whether CD161 is another viable target for immune checkpoint blockade by analyzing its effects on T-cells once blocked during exhaustion.

Methods: Human anti CD19-CAR T cells were generated using a standard retroviral transduction protocols. Expression of CD161 was observed throughout expansion on Day 0,2,6 and 12. Expanded CD19 CAR T cells were subjected to continuous antigen exposure through a Nalm6 leukemia serial killing assay and both CD161 expression and killing efficacy were tracked using flow cytometry staining and bioluminescence respectively.

Results: We confirmed CD19 CAR T cell generation through flow cytometry. We observed that a small population of naive CD4/CD8 T cells express CD161. This expression gradually goes down post activation and expansion and goes back up as the cells get exhausted.

Conclusion: CD161 could be a potential immunotherapy target; but this needs to be confirmed through CD161 blocking studies to observe improvements in T cell function.

Investigating Exosomes in Sarcoma Patients

Scholar: Matthew Chu

Education: Chantilly High School, Fairfax, Virginia

Lab: Ines Lohse, PhD; Kurt Weiss, MD

Mentors: Tanya Heim, MS; Ines Lohse, PhD

Site: Cancer Biology

Background: Osteosarcoma (OS) is a primary malignant bone tumor with bimodal age distribution, primarily affecting individuals aged 10–14 and over 65.[1,2] Standard treatments include surgery and chemotherapy, achieving about 60% long-term survival for localized cases.[3] However, OS frequently metastasizes to the lungs, a complication with limited understanding of its metabolic profile.[4] This leads to clinical uncertainty—patients are overtreated for indolent tumors or receive insufficient intervention. Exosomes, which carry DNA, RNA, and proteins, are promising biomarkers for metastasis prediction.

Methods: Two OS cell lines were used: LM2 (lung metastasis) and SaOS-2 (primary tumor). Cells were cultured in supplemented OS Media (DMEM, +10% FBS, +1% Vitamins, +1% Pen/Strep, +1% Non-essential amino acids) until 60–80% confluency. We evaluated 9 patient plasma samples and 2 conditioned media samples. A 6-well growth assay was initially conducted with 1.0×10^5 cells to optimize dilution groups. A cytotoxicity assay followed, with 1.0×10^4 cells per well in 96-well plates. Cell viability was quantified using a standard curve and analyzed via a Tecan microplate reader.

Results: We hypothesized that exosomes from metastatic plasma promote cell migration, while those from localized plasma enhance proliferation. Early results indicate distinct group responses, supporting our hypothesis that exosomal cargo influences metastatic behavior.

Discussion: Our study aims to determine whether exosomal factors from OS patients can stimulate sarcoma cell proliferation and migration. These findings may offer insight into the metastatic potential of OS tumors, supporting the development of risk-adapted therapies, and future grant proposals.

Works Cited:

1.Misaghi et al. 018;4:12. doi:10.1051/sicotj/2017028
2.Kim et al. 2023;15(20):5044. doi:10.3390/cancers15205044
3. Hu et al. 2022;11(21):3507. doi:10.3390/cells11213507
4. Rathore et al. 2021;10(6):1182. doi:10.3390/jcm10061182

Modeling Density-Dependent Trivalent LAT Aggregation Using BioNetGen

Zenon Cieslak, James R. Faeder, PhD, Alex A. DiBiasi, Student: CPCB

[1]Shaler Area, Pittsburgh, PA
[2]University of Pittsburgh Hillman Cancer Center Academy, Pittsburgh, PA

Abstract

T cells and T cell receptor (TCR) signaling defend the body against infections and cancer; however, the specific biochemical mechanisms remain unresolved. To investigate this mechanism, White et al.[1] proposed that aggregation of the Linker for Activation of T Cells (LAT) is the rate-determining step in T cell activation, using a spatial, probabilistic model. We test whether rule-based modeling in BioNetGen within a well-mixed, non-spatial system can replicate their conclusions.

Introduction T cells initiate immune responses through the T cell receptor signaling pathway, which begins when the TCR binds to peptide-MHC complexes on antigen-presenting cells. Upon recognition of a threat, the TCR signaling pathway activates and eventually results in the formation of LAT aggregates on the T cell plasma membrane. LAT can form aggregates because it has four binding motifs–or in other words, tetravalent. These aggregates promote essential phenomena such as acute antigen sensitivity, selectivity, and the ability to provide a dynamic response. These abilities lie within the mechanisms of the Y132 site on LAT, which produces stronger bonds as compared to the other GRB2-SOS-mediated bonds of the other three LAT binding sites. The speed at which the Y132 site is phosphorylated determines the speed at which LAT condensates or clusters form, which then continues the TCR pathway.

Methods We constructed a simplified BioNetGen model simulating trivalent LAT molecules, excluding the Y132 phosphorylation site. This simplified model can still be used to prove the validity of modeling spatial processes through BioNetGen, despite a parametrized effect of density. Parameters presented in White et al.[1] were used as a foundation for the model. Several simple rules were then written to allow the LAT molecules to form aggregates. This style of aggregate modeling is not standard to BioNetGen; without the use of the package NFsim, which is a tool that allows the use of local functions. We used local functions to query, or ask, the LAT clusters for the total number of LATs in each cluster. This allows us to model the forward rate of cluster growth as exponentially decaying with every LAT added. As LAT clusters have a physiological limit to their size, this style of modeling coincides with reality. Parameter "a" was fit to align with findings from White et al.[1]

$$k_f' = k_{f0} \exp\left(- a \left(\mathrm{LAT}_{\mathrm{clust}} \right) \right)$$

Results The model succeeds in replicating the density-dependent trivalent LAT graphs C and D located on page 12 of the supplement for White et al.[1] Our replicated graphs are below in Figure A. This proves the efficacy of spatial modeling in BioNetGen, but also has implications for expanding the model further. With the simplest aspects of LAT aggregation modeled, further changes to the model can be made to implement the phosphorylation of the Y132 to allow stronger bonds to form. Additionally, TCR signaling can be modeled, and the system will not initially contain a finite number of phosphorylated LAT molecules, yet it will instead begin as an inactive T cell.

Discussion Our work is proof that BioNetGen, combined with the use of NFsim, can be used to simplify spatial biological models into zero dimensions; however, this does have a limit due to the complexity of functions that NFsim offers. Specifically, when we attempted to model the coagulation of two independent LAT aggregates, we were unable to query the size of each aggregate and use them in a singular local function, as both cluster sizes should be used to model the forward rate constant. As a workaround, we decided only to query the size of the smaller cluster during cluster aggregation. While we ultimately did produce viable results, our inability to model per our desires represents a great pitfall in both BioNetGen and NFsim; however, there is a straightforward solution–add more features to NFsim. More features would allow for more complex modeling, but this solution is a double-edged sword because, without the specific challenge of modeling LAT aggregates, we would not know what features to add.

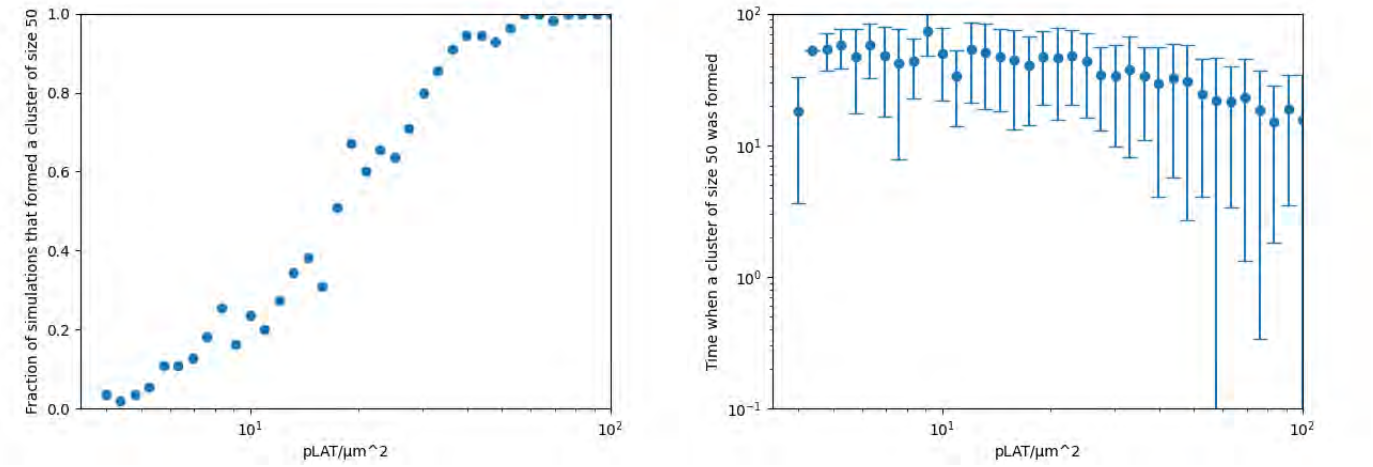

Figure A: BioNetGen simulations in accordance with supplemental figures C and D in White et al.[1].

References

[1] White, W. L., Yirdaw, H. K., Ben-Sasson, A. J., Groves, J. T., Baker, D., and Kueh, H. Y. (2025). *Proofreading and single-molecule sensitivity in T cell receptor signaling by condensate nucleation.* Proceedings of the National Academy of Sciences, 122(22). https://doi.org/10.1073/pnas.2422787122

Optimization of immunostaining protocol for visualization of whole optic nerve tissue with clearing method

Scholar: Sofia De la Cruz

High School/College/City/State: Hawken School, Gates Mills, OH

PI of group/lab: Silmara de Lima, PhD

Mentor(s): Silmara de Lima, PhD and Rusy Lee, M.Sc.

Site: Vision

Optic pathway gliomas (OPGs) are the most common type of tumor in patients with neurofibromatosis 1 (NF1), a genetically inherited disease that predisposes patients to tumor formation in the central and peripheral nervous system. Understanding the microenvironment around the tumor and the interaction between tumor cells and the axons in the optic nerve is crucial for studying NF1-OPGs. Existing protocols to visualize these interactions are extremely laborious as they require imaging of serial sections using regular microscopy, or using electron microscopy, the latter being costly. The aim of this project was to overcome these limitations by optimizing a clearing protocol to be able to visualize the cellular and axonal organization at the glioma area. In our first trial using optic nerves from a control NF1-OPG mouse line, tissues were subjected to a delipidation reagent (CUBIC-R1), to successfully clear the tissue and attain optical transparency, followed by standard immunofluorescence protocol using the oligodendrocyte specific markers CC1 and Olig2 (a cell body and nuclear marker for the oligodendrocyte lineage, respectively), together with the nuclear marker TO-PRO. Although CC1 was successfully detected in the optic nerve tissue, the nuclear markers Olig 2 and TO-PRO were not detected in the tissues. In a second trial, aiming at improving permeabilization of the optic nerve tissue to be able to detect the signal from nuclear markers, we used the SWITCH buffer system which has sodium dodecyl sulfate (SDS), an anionic detergent that can improve permeabilization of antibodies. The CUBIC-SWITCH protocol is expected to provide an adequate visualization of the cellular and nuclear markers and fully permeate optic nerve tissue for proper imaging and analysis. At the completion of this training we had not yet received imaging of our second trial though we expect to see fully penetrated antibodies due to the SDS system.

Analysis of the E954K Mutation's Effect on the Nav1.1 Protein

Jocelyn C. DeVito[1], Fareeda E. Abu-Juam, BA[2], David R. Koes, Ph.D[2]

[1]Pine-Richland High School, Gibsonia, PA; [2]University of Pittsburgh, Pittsburgh, PA, Country

Abstract

More than 400 mutations of the Nav1.1 ion channel protein are associated with epileptic disorders. An understanding of each mutant would aid the development of molecular therapies. We performed molecular dynamics simulations to simulate the E954K mutation inside of the cell membrane and used MDAnalysis to evaluate its effects on the channel's behavior to help inform the development of treatments. In later work, we plan to analyze the channel across multiple activation states by simulating it longer and analyze wild-type simulations to further evaluate the effects of the E954K mutation on the channel.

Introduction

Dravet syndrome, a severe form of epilepsy characterized by cognitive impairments, affects as much as 1 in 20,000 people globally. (Epilepsy Foundation) Mutations in the human voltage gated sodium channel (NaV1.1), crucial for regulating the nerves' ability to respond to signals, leads to Dravet. Encoded by the gene SCN1A, which has up to 900 epilepsy-associated mutations, the NaV1.1 channel is the most frequent target of epileptic mutations out of the 9 sodium channel subtypes (Pan et al. 2021). Mutations in SCN1A either lead to truncated forms of NaV1.1 protein or loss of protein function. For example, replacement of negatively-charged Glu954 on the P2II helix of the selectivity filter by positively-charged lysine disturbs cation (Na+) attraction because NaV1.1 selectively filters ions based on changes in electric potential in the cell membrane (Pan et al. 2021). Here, we used an AlphaFold3 predicted structure of NaV1.1structure to simulate the E954K mutation in the cell membrane. Using molecular dynamics analysis on these simulations, we will compare differences in interactions with ions to evaluate the E954K mutation's effect on the Nav1.1 protein. In this work, the E954K mutation did not show drastic changes in selectivity. In future work, we plan to run the simulation for longer to potentially see a transition in activation states and also analyze wild-type simulations to analyze whether there are changes in comparison to that such as less ion flow.

Methods

We predicted the mutated structures of Nav1.1 with AlphaFold3 using an edited version of the protein sequence from UniProt. The system was set up by using Charm-GUI and PPM2.0 to orient and place the protein in a cell membrane, add ions, and insert water molecules resulting in 600,000 atoms in the system. We ran an MD simulation using amber with the charmm36 forcefield for a 50 ns equilibration and ~200 ns production. We applied an electric field along the z-axis and employed a 2fs timestep. Results were analyzed using the MDAnalysis package to obtain a comparison of both channels' rates of ion flow through the membrane and activation states of the membrane based on pore size.

Results

Pore allows sodium ions to pass through, but blocks the flow of chloride ions (Figure 2).Ion gap between top and bottom residues (black lines) shows pore opening and few chloride ions within chosen pore. The ion gap between top and bottom residues shows flow of sodium ions through pore.

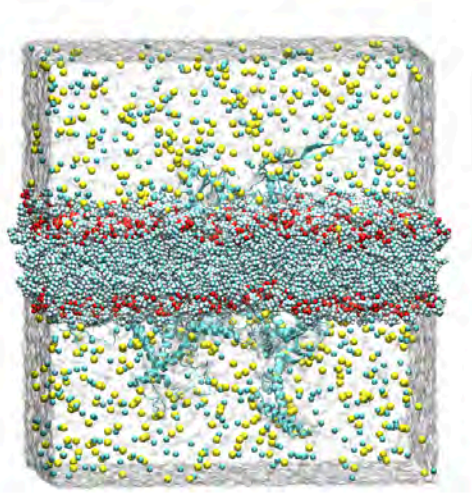

Figure 1- **Fully Solvated Nav1.1 System**. Nav1.1 system shown carrying the E954K mutation embedded in the cell membrane, sodium ions (yellow), chloride ions (cyan), membrane (red), water (transparent surface).

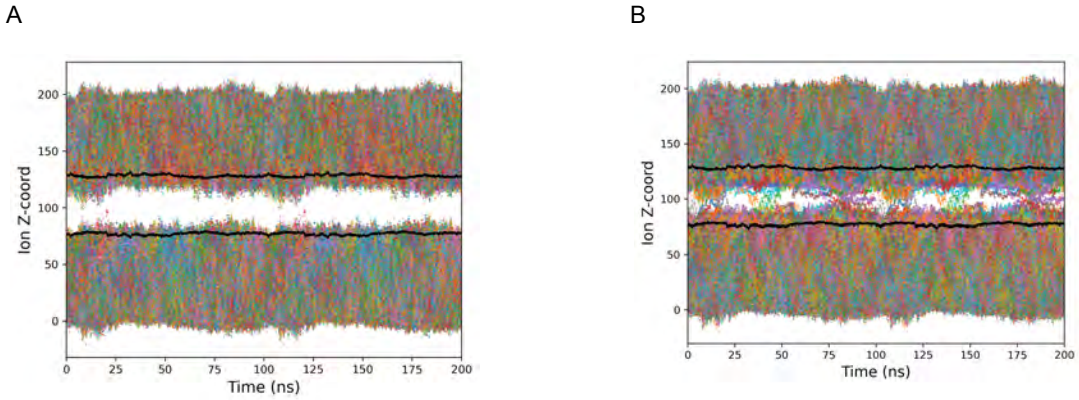

Figure 2- **E954K mutation doesn't significantly impact cation attraction.** (A) Chloride Density graph shows little passing of chloride ions through the Nav1.1 channel. (B) Sodium density graph shows ions passing continuously through the channel.

Discussion

The E954K mutation does not appear to have a significant effect on cation attraction. Despite changing negatively charged lysine to a positively charged Glutamate amino acid, sodium ions still flow through the channel and chloride ions rarely pass through the channel. This suggests that ion selectively is not being drastically affected. However, with a comparison to the wild-type simulation we may see changes (in the shown simulation, in comparison to wild-type) such as less ion flow which explain the malignant effects of the E954K mutation. In further work, we plan to run a longer simulation, and perform extended ion pass rate analysis to further quantify the mutation's effect. Additionally, we plan to include the wild-type simulation in order to understand how these results compare to the wild-type system.

References

1. Pan, Xiaojing et al. "Comparative structural analysis of human $Na_v1.1$ and $Na_v1.5$ reveals mutational hotspots for sodium channelopathies." *Proceedings* of the National Academy of Sciences of the United States of America vol. 118,11 (2021): e2100066118. doi:10.1073/pnas.2100066118
2. Joshi, Charuta, and Elaine Wirrell. "Dravet Syndrome." Epilepsy Foundation, 24 Aug. 2020, www.epilepsy.com/what-is-epilepsy/syndromes/dravet-syndrome.

Curation of a Gold-Stand Corpus of Intracellular Interactions to use in Benchmarking Different Algorithmic Readers

Kenneth Ding[1], Haomiao Luo[2], Miskov-Zivanov[2]
[1]Newton South High School, Newton, MA, [2]University of Pittsburgh Hillman Cancer Center Academy, Pittsburgh, PA

Abstract In this project, a manually curated corpus of protein-to-protein interactions was compiled with the goal of comparing the manually made dataset against machine made datasets. The two are compared by the number of matches and non-matches to evaluate the accuracy of the machine made datasets.

Introduction Large sets of intracellular interactions are essential to train accurate computer models of cells and their functions, particularly in fields like cancer research. While human curations from primary literature exist, the amount of information is always growing, and these databases will always be incomplete. To remedy this, machine reading algorithms like INDRA were developed to extract these data at large scales. To benchmark these algorithms, a high-quality, human-curated "gold-standard" corpus is needed. This project describes the curation of such a corpus to evaluate the machine reading systems REACH and INDRA.

Methods The broad methodology was based on an evaluation of 56 sentences related to CAR-T cell interactions, a key area in cancer immunotherapy. A gold-standard corpus was made through manual curation and compared to machine curators. For manual, human curation of the dataset, two annotation tools were used: Doccano and INCEpTION. Doccano provided a user-friendly interface and fast performance, but did not have advanced capabilities like protein ID matching. INCEpTION; however, had more advanced capabilities, notably auto-suggestions for annotations and ID matching, and was used for the majority of annotations. For automatic curation, the sentences were fed through INDRA and REACH, both algorithmic reading programs. Both of these extractions were then converted to BioRECIPE, a format that allows for both human and machine accessibility. An attempt to use a Python script to compare the outputs was attempted, but it was unreliable; thus, human analysis was performed to analyze and assess the accuracy of each machine-generated interaction prediction.

Results Manual comparison revealed that machines had correct predictions (i.e. true positives) approximately 1/3 of the time (Fig. 1A, Fig. 1B). Annotation methodology was a key feature of the errors; especially in terms of entity length. INDRA commonly annotated too much redundant or unnecessary information in one entity, leading to multiple entities being annotated as one. In REACH outputs, it would often take a name like PD-1/CD28 CAR-T and only output CAR-T or PD-1 as an entity, and not the full name. Furthermore, both programs, REACH and INDRA, suffered from the same issue regarding classifying entities. Both very often could not match a database ID or type to an element, leading to large numbers of "other" or "TEXT_NORM" classifications, hence why a Python script could not be used, as there would be difficulty matching IDs (Fig. 2A, Fig. 2B). Furthermore, machines also commonly misunderstood text, or did not grasp the full context. When tackling longer sentences, INDRA, and especially REACH, both often missed a second or third regulated entity. This was also a common error for nested relations, or chains of results, in which the automatic readers may not pick up on every interaction in a sentence. Crucially, both readers suffered from misunderstanding of important context. For example, sentences that indicated a hypothesis, or an interaction that was proven to be false, would be annotated as true interactions.

Discussion Large, accurate databases of intracellular interactions are necessary to efficiently advance research related to the many different molecular and genetic processes within the body. However, these findings indicate that machine reading models, which can help gather these large databases, come with a high risk of error and should be used cautiously. In order to help aid research in immunology and oncology especially, further development of algorithmic reading models is necessary in order to ensure a higher accuracy rate, lessen the need for human curators, and help establish accurate datasets of molecular interactions for hypothesis generation and testing.

Figure 1A. REACH Accuracy

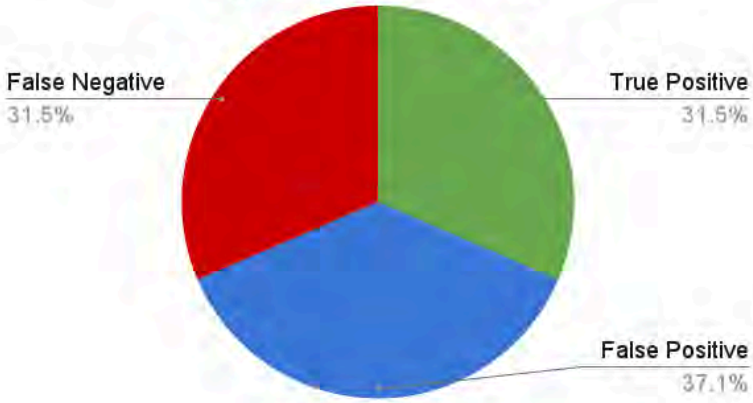

Figure 1B. INDRA Accuracy

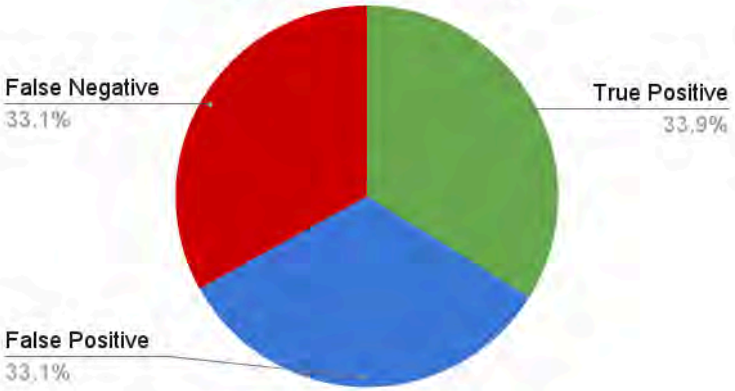

Figure 2A. Entity Types (Regulator)

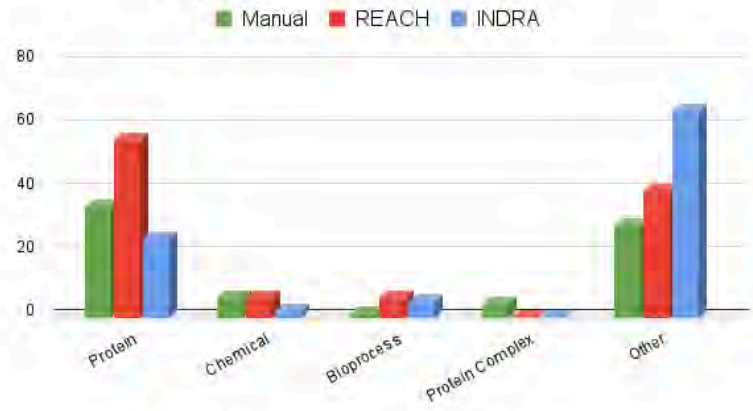

Figure 2B. Entity Types (Regulated)

Title: Structural changes in the neurocircuitry of a Profilin1-linked mouse model of amyotrophic lateral sclerosis

Scholar: Elise Dressman

High School/College/City/State: Fox Chapel Area Highschool, Pittsburgh, PA

PI of group/lab: Dr. Christi Kolarcik

Mentor(s): Breanna Sullivan

Site: PathoBiology

Introduction: Amyotrophic lateral sclerosis (ALS) is a progressive and fatal disease characterized by motor unit degeneration and network-level dysfunction. Although sporadic and inherited forms of ALS share common pathological features, no definitive cause and effect relationship has been determined. A better understanding of timing and changes to the neural network connectivity could provide insight into underlying disease mechanisms. Further, the characterization of ALS mouse models is critical for evaluating future drug therapies. We hypothesize that compared to healthy controls, ALS mouse models will have significant differences in network-level measures prior to the onset of clinical symptoms.

Methods: In this study we characterize neural network structural changes over the disease course in Profilin1 (PFN1)-linked mouse model, which express key clinical and pathological features of human ALS. PFN1 mice and age-and sex-matched healthy control mice were injected in the hindlimb with rabies virus, which is a tracer for ALS, and is retrogradely and trans-synaptically transported. Mice were studied at various stages corresponding to pre-symptomatic, symptomatic, and end-stage disease states to study structural changes over the disease course. Mouse brains were paraffin fixed and embedded, and subsequently sectioned on a microtome for ongoing immunohistochemistry and immunofluorescence experiments to label various cell subtypes and rabies-positive cells. Serial brain tissue sections will be imaged using a confocal microscope and analysed using the software package, NeuroInfo.

Results: Ongoing histology experiments will allow us to calculate and compare the percentage of rabies-positive neurons in the motor cortex of PFN1 mice versus healthy controls, representing the number of cortical motor neurons connected to the injected hindlimb muscles. Co-staining with various antibodies (e.g., somatostatin for GABAergic interneurons) will allow us to study selective neuronal vulnerability or resilience in PFN1 mice. Further, we can make longitudinal comparisons of structural changes in the neurocircuitry at symptom onset versus end-stage disease. We will also consider sex differences in our analysis.

Conclusions: While histology experiments are ongoing, we expect to find structural changes in the neurocircuitry even prior to overt clinical symptoms in PFN1 mice. These results will provide a foundation for ongoing work aimed at better understanding connectivity resilience of cortical neural circuits in ALS. Further, investigating the PFN1-linked mouse model of ALS may offer insight into human ALS, with implications for evaluating future therapies.

Enhanced INDRA-to-BioRECIPE Translation and Comparative Analysis of Biological Text Mining Systems

Nana Kwame Dwomoh[1], Dr. Natasa Miskov-Zivanov[2], Haomiao Luo[2] [1]Brookings High School, Brookings, SD; [2]University of Pittsburgh Hillman Cancer Center Academy, Pittsburgh, PA

Abstract

My mentors, Dr. Natasa Miskov-Zivanov and Haomiao Luo developed BioRECIPE[1], a human-readable format for modeling biological networks. They built a Python translator for converting INDRA[2] statements to BioRECIPE[1] tables. I enhanced it by adding entity type mapping, translocation support, and bug fixes. Context parsing yielded limited results due to format incompatibility. I also used Claude AI to compare INDRA[2] and REACH[3] outputs, showing INDRA extracted 34% more interactions and doubled gene resolution.

Introduction

Biological research creates vast amounts of knowledge from papers and databases. However, lack of standardized formats creates barriers to analysis. INDRA (Integrated Network and Dynamical Reasoning Assembler)[2] extracts mechanistic statements using natural language processing, while BioRECIPE (Biological system representation for Evaluation, Curation, Interoperability, Preserving, and Execution)[1] provides a human-readable tabular format for biological networks. The INDRA-to-BioRECIPE translator had four key issues: regulated type parsing errors, incomplete entity mapping, missing translocation support, and missing context parsing.

Methods

I enhanced the Python translator by fixing four key issues. Entity type mapping was implemented for Gene (HGNC), Protein (UniProt, EGID), Protein Family (FamPlex, InterPro, Pfam), Simple-chemical (ChEBI, PubChem, HMDB), and Bioprocess (GO, MeSH) categories. A bug incorrectly assigning entities to 'text' type was fixed. Context parsing was attempted but yielded limited results as complex interactions containing context aren't included in the BioRECIPE format[1]. Regulated type parsing errors were fixed, and translocation interaction support was implemented. A comparative analysis was performed using Claude AI to evaluate Excel datasets comparing INDRA[2] and REACH[3] (Reading and Assembling Contextual and Holistic Mechanisms from Text) performance across interaction counts, entity resolution, and mechanism classification.

Results

The enhanced translator successfully fixed three of the four issues. Context attribute parsing remained limited due to BioRECIPE format[1] constraints, as complex interactions containing context are not included in the current specification. INDRA[2] extracted 11,058 total interactions compared to REACH's[3] 8,249 interactions (34% increase) and demonstrated superior entity resolution (Figures 1-2). Entity resolution quality demonstrated marked differences, with INDRA[2] achieving 35% HGNC symbol coverage compared to REACH's[3] 16.4% coverage. INDRA[2] achieved 100% mechanism classification versus REACH's[3] 67% unspecified, with distinct database grounding strategies.

Discussion

The translator improvements enable better biological data standardization. INDRA's[2] superior performance provides clear guidance for text mining platform selection. The 34% increase in extraction and better gene resolution demonstrate significant advantages for automated knowledge systems. Future work will expand comparisons to additional systems and improve context parsing as format specifications evolve.

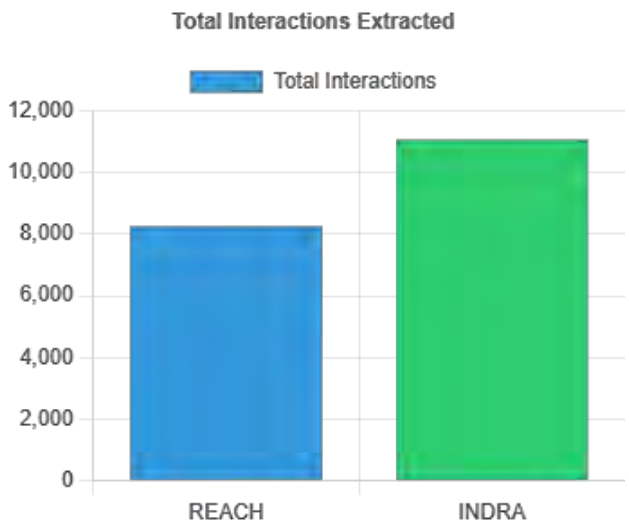

Figure 1. Total interactions extracted by INDRA[2] versus REACH[3] from comparable paper datasets.

INDRA[2] demonstrated superior extraction efficiency, processing 11,058 interactions compared to REACH's[3] 8,249 interactions, representing a 34% improvement in automated paper mining performance.

Figure 2. HGNC symbol coverage comparison showing entity resolution quality across regulator and regulated entities.

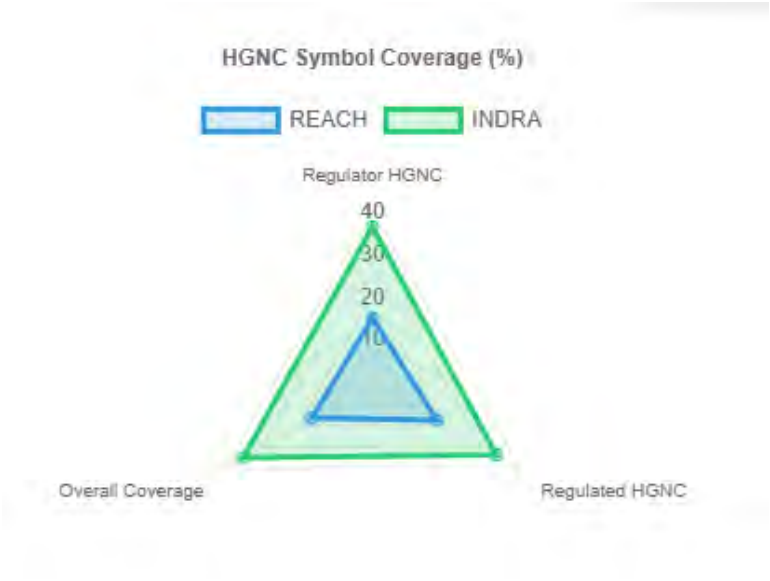

References

1. Holtzapple E, Zhou G, Luo H, Tang D, Arazkhani N, Hansen C, Telmer CA, Miskov-Zivanov N. The BioRECIPE Knowledge Representation Format. ACS Synth Biol. 2024;13(8):2621-2624.
2. Gyori BM, Bachman JA, Subramanian K, Muhlich JL, Galescu L, Sorger PK. From word models to executable models of signaling networks using automated assembly. Mol Syst Biol. 2017;13(11):954
3. Valenzuela-Escárcega MA, Babur Ö, Hahn-Powell G, Bell D, Hicks T, Noriega-Atala E, Wang X, Surdeanu M, Demir E, Morrison CT. Large-scale automated machine reading discovers new cancer-driving mechanisms. Database (Oxford). 2018;2018:bay098.

Title: Predicting functional mechanisms behind fine-mapped GWAS variants related to coronary artery disease
Scholar: Mia Eldaher
High School/College/City/State: Shady Side Academy, Pittsburgh, PA
PI of group/lab: Dennis Kostka, PhD
Mentor(s): Dennis Kostka, PhD, Elizabeth Jane Gilfeather
Site: Computational Biology

The genomes of the population vary greatly, and variants in DNA sequences can cause differences in phenotype and disease. By identifying the causal variants for a specific phenotype, we can create treatments for the disease. Genome wide association studies (GWAS) statistically measure the correlation between variants in a population and disease prevalence. Variants are often found together within populations, making it harder to find the causal variant for a trait. Fine mapping is a statistical method to identify which closely linked variant is causal. When causal sequence variants are in regions of the genome that are not genes (regulatory, or non-coding regions), it is harder to determine the functional cause of a variant's effect. Many deep learning models, including sSei, have been developed to resolve this issue. The project's aim is to analyze variants in the UK BioBank dataset pertaining to coronary artery disease (CAD), by predicting functional scores for variants using a machine learning model. We used sSei, a model that calculates a functional score for a variant based on 40 sequence classes, then analyzed the correlation between the functional scores and GWAS effect sizes. We isolated variants with an association to CAD and analyzed variants of interest based on the functional score and effect size, then looked at the relationship between variants and genes associated with CAD. We identified variants with a significant effect size, but no functional score, suggesting that although this was called a causal variant by finemapping, there is no functional change in mechanism for the variant, as indicated by sSei In the future we will investigate variants like these further and identify true causal variants.

Processed Food Intake as a factor of Socioeconomic Status affected Response to Immune Checkpoint Inhibitor therapy in Advanced Melanoma

Comfort Fayomi[1], Dr. Diwakar Davar[2], Drew Hurd[2].

[1]Plum Senior High School, Pittsburgh, PA; [2]University of Pittsburgh Hillman Cancer Center, Pittsburgh, PA

Introduction

Immune checkpoint inhibitor (ICI) therapy has been a major treatment driving oncology research in the past decade, with much research revealing the role of the gut microbiome in ICI response.[1,4] While much is known about the relationship between diet and gut microbiome, the relationship of this system to ICI response has not yet been researched. We know that many public health factors such as insurance status, level of education, and income can affect the diversity found in the gut microbiome.[5] Our research seeks to link the connection between public health factors, the gut microbiome, and response to ICI therapy in patients with advanced melanoma.

Methods

Patient data was collected under an IRB approved bio-banking protocol at the UPMC Hillman Cancer Center for patients receiving Immune Checkpoint Inhibitor therapy as part of their cancer treatment. Enrolled patients (n=114) were administered the DHQIII recall questionnaire to collect patterns of dietary data. Using the NOVA classification system, all food types were categorized in terms of processing, and the percentage of gram intake was used to determine each patient's level of Ultra-processed food (UPF) intake.[2,3] Patients were classified using cutpointr to determine the most significant cutoff for UPF intake as a percentage of diet (threshold = 20.079).[6] Patients were classified as above or below the threshold, and used in combination with progression statistics, were run through a Kaplan-Meier Survival Analysis.

Results and Discussion

Kaplan-Meier Survival Analysis shows a significant correlation (p=0.0022) between Ultra-processed food intake and diminished progression-free survival in ICI-treated advanced melanoma patients. This supports our hypothesis that a diet high in UPF will lead to poorer outcomes to immune therapy. Inflammation, a known driver of response to ICI therapy is well documented to be increased in diets containing large amounts of highly processed foods.[7] Further exploration of this topic will include metagenomic analysis of the gut microbiome and proteomic analysis of patients classified by ultra processed food intake. This will allow us to define the biological differences in patients that are driving the differences in response.

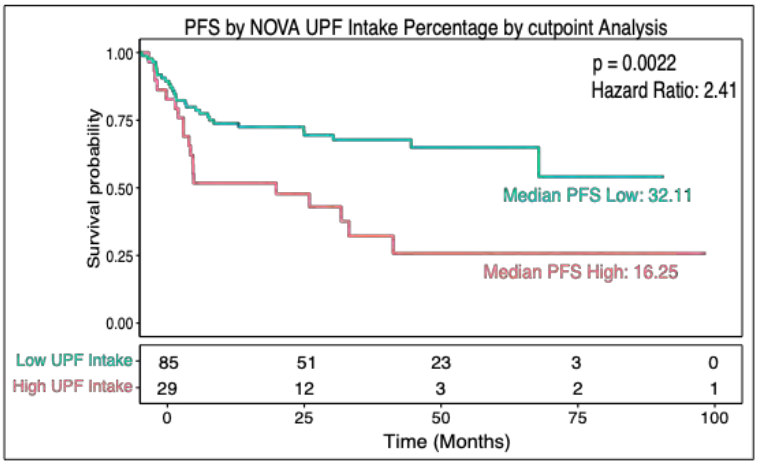

References

1. Zhao J, Graetz I, Howard D, Yabroff KR, Lipscomb J. Immune Checkpoint Inhibitors and Survival Disparities by Health Insurance Coverage Among Patients With Metastatic Cancer. JAMA Netw Open. 2025;8(7):e2519274. doi:10.1001/jamanetworkopen.2025.19274
2. Subar AF, Midthune D, Kulldorff M, Brown CC, Thompson FE, Kipnis V, Schatzkin A. Evaluation of alternative approaches to assign nutrient values to food groups in food frequency questionnaires. Am J Epidemiol. 2000 Aug 1;152(3):279-86. doi: 10.1093/aje/152.3.279. PMID: 10933275.
3. Frade EODS, Gabe KT, Costa CDS, Neri D, Martínez-Steele E, Rauber F, Steluti J, Levy RB, Louzada MLDC. A novel FFQ for Brazilian adults based on the Nova classification system: development, reproducibility and validation. Public Health Nutr. 2025 Mar 27;28(1):e83. doi: 10.1017/S1368980025000412. PMID: 40143737; PMCID: PMC12100568.
4. Fortman DD, Hurd D, Davar D. The Microbiome in Advanced Melanoma: Where Are We Now? Curr Oncol Rep. 2023 Sep;25(9):997-1016. doi: 10.1007/s11912-023-01431-3. Epub 2023 Jun 3. PMID: 37269504; PMCID: PMC11090495.
5. Kwak S, Usyk M, Beggs D, Choi H, Ahdoot D, Wu F, Maceda L, Li H, Im EO, Han HR, Lee E, Wu AH, Hayes RB, Ahn J. Sociobiome - Individual and neighborhood socioeconomic status influence the gut microbiome in a multi-ethnic population in the US. NPJ Biofilms Microbiomes. 2024 Mar 11;10(1):19. doi: 10.1038/s41522-024-00491-y. PMID: 38467678; PMCID: PMC10928180.
6. Thiele, C., & Hirschfeld, G. (2021). cutpointr: Improved estimation and validation of optimal cutpoints in R. Journal of Statistical Software, 98(11), 1–27. https://doi.org/10.18637/jss.v098.i11
7. Tristan Asensi M, Napoletano A, Sofi F, Dinu M. Low-Grade Inflammation and Ultra-Processed Foods Consumption: A Review. Nutrients. 2023 Mar 22;15(6):1546. doi: 10.3390/nu15061546. PMID: 36986276; PMCID: PMC10058108.

Dynamic Expression of Stathmin-1 during pancreatic cancer progression

Mia Fritz

High School: Pine-Richland High School, Pittsburgh, Pa

Lab: Dr. Farzad Esni, PhD

Mentor: Dr. Farzad Esni, PhD

Site: Surgery

Background: Acinar-to-ductal metaplasia (ADM) is a reversible process during inflammation or injury, which has been generally considered to play an active role in acinar regeneration. However, upon oncogenic *Kras* expression these metaplastic events become irreversible and may act as precursors to neoplastic lesions (PanINs). Due to the inherent heterogeneity among acinar cells, those displaying higher plasticity may play a more significant role during pancreatic regeneration and tumorigenesis. Stathmin-1 (STMN1) is a cytoplasmic protein involved in regulating microtubule polymerization and facilitating mitotic spindle formation during cell division, which has been associated with the control of cell proliferation by inducing various cell cycle regulators. A subset of acinar cells expressing STMN1 has been identified as a potential population of facultative progenitor-like cells in the adult pancreas. Given that chronic pancreatitis (CP) is considered a risk factor for pancreatic cancer, here we studied the expression of Stmn1 in mouse models for chronic pancreatitis and cancer.

Methods: Pancreatic tissues from wild type mice treated with caerulein for 8 weeks (CP model) or Ptf1aCre;$Kras^{G12D}$ (PK) mice harvested at 3-, 5-, or 12-months were immunostained for expression of Stmn1 in conjunction with E-cadherin.

Results: ADMs in CP and PK mice at 3 months of age, exhibited high Stmn1 expression, whereas early PanIN lesions demonstrated reduced levels. Interestingly, more advanced PanINs as well as tumor cells expressed high level of Stmn1.

Conclusion: STMN1 appears to play a role in early metaplastic transformation and tumor proliferation. ADMs and tumors show increased STMN1 consistent with active proliferation, while PanINs demonstrate reduced expression, suggesting a non-proliferative state. These findings implicate STMN1 in both early transformation and late-stage proliferation.

Future Direction: Future studies will explore the role of STMN1 in chronic pancreatitis, and pancreatic cancer.

Human neutrophil alpha-defensins and an aberrant role in liver disease: A preliminary study

Scholar: Alberto Gildengers

High School: Taylor Allderdice High School, Pittsburgh, Pennsylvania

Lab: Wendy Mars, PhD

Mentors: John Stoops, Anne Orr, and Rodrigo Florentino, PhD

Site: Pathobiology

Background: Alpha-defensins are antimicrobial peptides with multifaceted immune functions that enable the regulation of pathogens via membrane disruption—a role crucial to the maintenance of liver health. Preliminary findings via immunostaining showed an unexpected presence of the leukocyte-specific alpha-defensins (DEFA1-3) in the bile duct epithelia (BDE) of patients exhibiting significant liver disease. To determine if a relationship between disease status and the expression of DEFA1-3 in BDE exists, we expanded upon these preliminary data regarding DEFA1-3 expression in diseased livers.

Methods: Formalin-fixed human liver tissue samples were obtained from 42 patients (23 male, 19 female) with varying disease prognoses, and immunohistochemistry staining was performed to analyze staining for DEFA1-3 in BDE. A blinded analysis was conducted and subsequently correlated with sex and disease status. For *in vitro* studies, an immortalized human BDE cell line was plated into two twelve-well plates and treated with either 20 μM sorafenib or a DMSO control for 24 or 48 hours. Wells were fixed with formalin and then stained for DEFA1-3.

Results: Data analyses indicated a statistical difference in BDE staining levels between patients diagnosed with alcoholic liver disease (ALD) and metabolic dysfunction-associated steatohepatitis (MASH). Furthermore, a positive correlation between BDE staining and a history of chemotherapy was observed in resected “normal” tissue from patients with liver cancer. To test if staining indicated induction by chemotherapy, an *in vitro* experiment with a BDE cell line was conducted. Immunohistochemistry indicated DEFA1-3 was only present in the chemotherapy-treated (sorafenib) samples, with staining prominence decreasing from 24 to 48 hours.

Discussion: The relevance of DEFA1-3 staining in BDE remains unclear. However, enhanced expression of alpha-defensins in the BDEs of chemotherapy versus non-chemotherapy treated samples suggests expression in BDEs is inducible. Furthermore, the *in vitro* experiment suggests this induction is transient as no staining was observed after 48 hours and the sorafenib half-life in culture is reportedly 9–13 hours. As such, these findings warrant further research on the relationship between alpha-defensin expression in BDEs and liver disease.

The impact of microplastics on macrophage phagocytosis of tumor cells

Scholar: Laila A. Golla
School: Fox Chapel Area High School, Pittsburgh, PA
Lab: Adam Soloff, PhD
Mentors: Adam Soloff, PhD; Hannah Udoh, MS; Naila Noureen, PhD
Site: ICI

Background: The leading cause of cancer death in the United States is lung cancer, and it has disproportionately occurred in females in recent years. Air pollutants have been proven to correlate to lung disease, but the role of increasing microplastics concentrations in these phenomena remains unknown. Since the immune system is prevalent in the body's defense against cancer and the most prevalent immune cell in the lung is the macrophage, we wanted to examine how microplastics may impact the macrophage's ability to carry out its function of phagocytizing tumors. Additionally, macrophages are responsible for tissue development and remodeling and have varying reproductive demands between the sexes, which may help to explain the differences in male-female ratios of lung cancer incidence.

Methods: 250,000 Orange RAW 264.7 macrophage cells were treated with varying concentrations of microplastics for 1 hour and co-cultured with 500,000 CFSE-labeled 4T1 tumor cells for an additional 3 hours in FACS tubes. The experiment was then run using flow cytometry and analyzed for relative concentrations of macrophages with tumor uptake. Additionally, primary macrophage cells from mouse bone marrow were treated with microplastics and cocultured with the 4T1 cells to examine differences in the effects between sexes. Controls used include macrophages with heat-killed 4T1 cells, macrophages with 4T1 cells incubated at 4 degrees Celsius, and macrophages with 4T1 cells suspended in media that were treated with no microplastics

Results & Conclusion: As the microplastic exposure to the macrophages increased in concentration and size, less phagocytosis was observed on the flow cytometer. Differences between sexes are still being analyzed and tested. Next steps include analyzing digestion of the tumor cells by microplastic-treated macrophages, as microplastics can induce frustrated-phagocytosis in macrophages and likely have an impact to their overall function.

EGFL6 as a Driver of Obesity-Driven Endometrial Cancer Through Stem Cell Marker Upregulation

Scholar: Sai Saharsh Gumudavelly
High School: North Allegheny Senior High School, Pittsburgh, PA
Lab: Ronald Buckanovich, MD+PhD
Mentor: Dr. Shoumei Bai
Site: WCRC

Introduction: The rate of endometrial cancer (EC) growth in incidence and mortality is increasing and directly correlates with increasing obesity rates, marking it an obesity-related cancer. EGFL6 is a growth factor that is known to be expressed in fat, regulate stem cells in development, and increase cancer cell growth. We found that induced expression of EGFL6 in all mouse tissue (iEGFL6) and in adipose-only tissue (FQE) resulted in obesity development and high-grade uterine cancers. Through RNA sequencing, in EGFL6 exposed uteri, compared to control uterine tissue, markers of uterine stem/progenitor cells were increased. We hypothesized EGFL6 overexpression induces cancer by increasing the expression of these markers, thereby increasing proliferation of the endometrial stem cells.

Methods: We performed immunofluorescence for BCAM and SOX9, and immunohistochemistry for LGR5 on uteri of control, iEGFL6, and FQE tissue. We analyzed 30-40 high-powered microscopy images from 3 uteri from each gene and used image analysis to quantify how many cells show expression. Results were compared using t-tests and visual analysis.

Results: Compared to control tissue, iEGFL6 uteri demonstrated an average 2.5-fold increase in expression of SOX9 ($p<.05$), but showed no significant difference compared to FQE ($p\sim.73$). For BCAM, both iEGFL6 and FQE tissue both showed a significant increase ($p<.05$ for both tissues), demonstrating a 2.1-fold increase in expression. LGR5 also showed a significant increase in expression and change in color for FQE and iEGFL6 tissue compared to the control samples.

Conclusion: The findings show that tissue with induced expression of EGFL6 expressed more progenitor markers than control tissue, the difference being greater in iEGFL6 than FQE tissue, showing that induced expression of EGFL6 can be associated with an increase in uterine stem and progenitor cells, suggesting EGFL6 may be an important driver of obesity-associated cancer.

EGFR Inhibition Reduces Liver Injury Following Acetaminophen Overdose in a Mouse Model

Najih Haider[1, 2], Siddhi Jain[2], Gillian Williams[2], Bharat Bhushan[2]

1. Winchester Thurston School, Pittsburgh, PA, USA; 2. Department of Pathology School of Medicine, University of Pittsburgh, Pittsburgh, PA, USA

Abstract

Acetaminophen (APAP) is a pain reliever, but overdose can lead to acute liver failure, treatable only with N-acetylcysteine (NAC) if given early. This emphasizes the need for new therapies targeting later liver injury phases. Studies show that the EGFR worsens damage during APAP overdose, despite promoting regeneration in partial hepatectomy (PHx). Investigating its role in AILI using EGFR inhibitors like Afatinib and Osimertinib revealed that these inhibitors resulted in lower ALT levels, reduced necrosis, and less DNA damage, suggesting potential protection against liver injury.

Introduction

Acetaminophen (APAP) is a widely used pain reliever, but its overdose is the leading cause of acute liver failure (ALF) in the U.S. Unfortunately, the only treatment available, N-acetylcysteine (NAC), must be given within 8 hours of overdose, but many patients seek care too late. This underscores the pressing need for novel interventions that extend therapeutic viability beyond the early phase of APAP-induced liver injury (AILI). Previous studies have explored the role of the epidermal growth factor receptor (EGFR), a key regulator of liver regeneration following PHx (1). However, our group has previously demonstrated that EGFR activation worsens AILI and inhibition of EGFR using Canertinib, a non-clinically available EGFR inhibitor (2), or hepatocyte-specific deletion of EGFR significantly reduced liver injury. Despite these promising findings, the therapeutic potential of clinically approved EGFR inhibitors in AILI remains unexplored. Therefore, the objective of the present study is to evaluate the efficacy of two FDA-approved EGFR inhibitors, Afatinib and Osimertinib, in attenuating liver damage.

Methods

Male C57BL/6 mice (~8 weeks old) were administered APAP (500 mg/kg) followed by treatment with either Afatinib or Osimertinib (20 mg/kg). Liver damage was assessed through serum ALT levels, H&E staining, and TUNEL staining of liver sections.

Results

6 hours post-APAP overdose, serum ALT levels were elevated in the vehicle-treated group, while Afatinib-treated mice showed slightly reduced ALT, and Osimertinib-treated mice exhibited a significant decrease, indicating reduced hepatocellular injury (Fig. 1A). Histopathological analysis supported these findings, with widespread centrilobular necrosis observed in the vehicle group. Afatinib-treated mice showed comparable necrosis, whereas Osimertinib-treated mice had notably less (Fig. 1B). To further validate these results, TUNEL staining revealed markedly reduced DNA fragmentation and hepatic injury in the Osimertinib group (Fig. 1C).

Discussion

These findings align with previous studies that indicate the role of EGFR in liver damage following acetaminophen (APAP) overdose (2). Deleting EGFR from hepatocytes has been associated with decreased JNK activation and mitochondrial damage, which limits the release of AIF and subsequent DNA damage (unpublished data). Our data suggest that clinically approved EGFR inhibitors may yield similar protective effects. Treatment with Osimertinib resulted in lower initial liver injury, as indicated by ALT levels, and a reduction in necrotic areas and DNA damage. By expanding on these findings with FDA-approved medications, our research underscores EGFR as a potential therapeutic target in cases of APAP overdose.

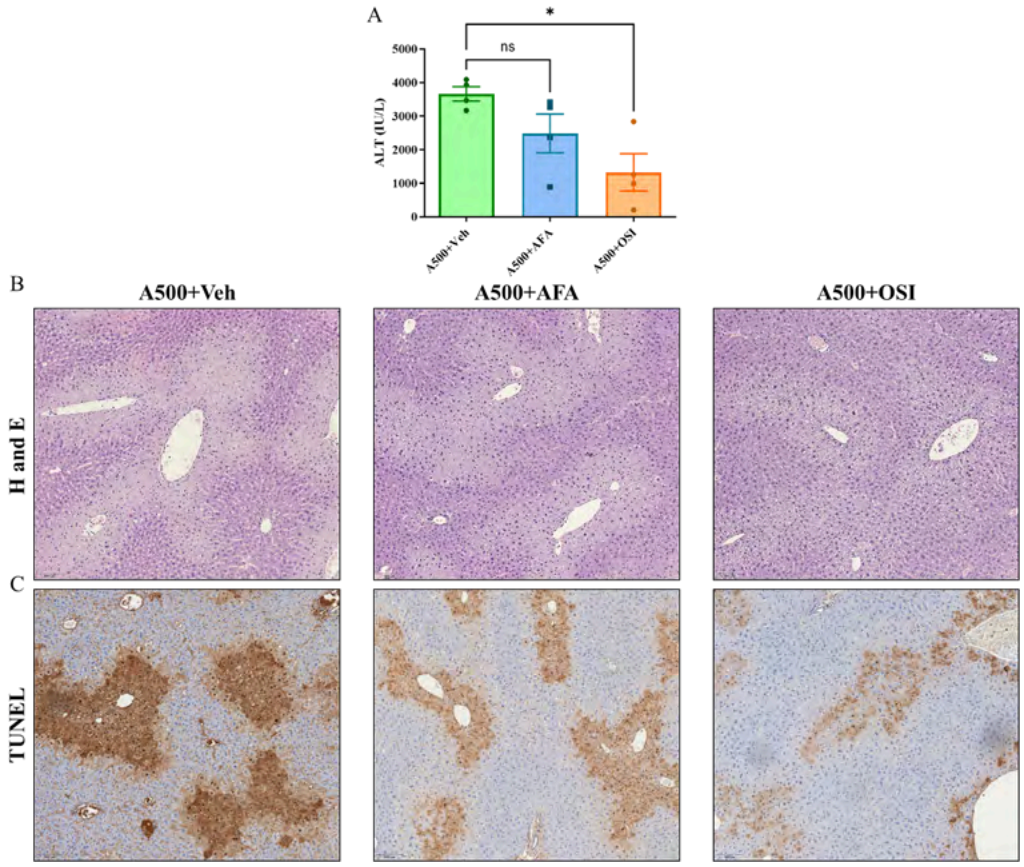

Figure 1: EGFR Inhibition Reduces Liver Injury Following Acetaminophen Overdose in a Mouse Model. (A) Bar graph representing serum ALT levels after 6hr post APAP overdose. Representative photomicrographs of (B) H&E stained liver sections showing necrotic areas (scale bar 100 µm) and (C) TUNEL-stained liver sections showing DNA fragmentation (scale 100 µm) after 6hr post APAP overdose. A500: APAP 500 mg/kg, Veh: Vehicle control, AFA: Afatinib 20 mg/kg, and OSI: Osimertinib 20 mg/kg.

Reference

1. Paranjpe S, Bowen WC, Mars WM, Orr A, Haynes MM, DeFrances MC, et al. Combined systemic elimination of MET and EGFR signaling completely abolishes liver regeneration and leads to liver decompensation. Hepatology (Baltimore, Md). 2016;64(5):1711.

2. Bhushan B, Chavan H, Borude P, Xie Y, Du K, McGill MR, et al. Dual role of epidermal growth factor receptor in liver injury and regeneration after acetaminophen overdose in mice. Toxicological Sciences. 2017;155(2):363-78.

Acknowledgments

I, Najih Haider, would like to express my sincere gratitude to Dr. Bharat Bhushan, Dr. Siddhi Jain, Gillian Williams, Saidikrom Mardiev, and all members of the Department of Pathology at the University of Pittsburgh School of Medicine for their time, guidance, and support throughout this research. It was a privilege to work with such a knowledgeable and dedicated team. I am deeply thankful for the opportunity to be part of this study and for all the mentorship I received along the way.

Neighborhood-level factors and their interaction with race/ethnicity on adenocarcinoma, squamous cell carcinoma, and small cell lung cancer incidence and survival in the United States

Andrea Halun Ramirez[1], Kathryn Demanelis, PhD[2]
[1]West Allegheny High School, Imperial, PA, Country; [2]University of Pittsburgh Hillman Cancer Center Academy, Pittsburgh, PA

Abstract. Lung cancer accounts for the most cancer deaths both in the US and worldwide. Among the three main subtypes of LC, incidence and mortality differ significantly. Our study sought to determine how specific neighborhood level factors influence the incidence and survival rates of the subtypes of LC and by race/ethnicity.

Introduction. Disparities related to race/ethnicity, urban-rural residence, and neighborhood level (NL) socioeconomic status (SES) are known to impact lung cancer (LC) diagnosis, treatment, and survival. Studies have attributed this to varying smoking patterns and differences in healthcare access among these groups. However, the influence of these factors on specific subtypes of LC has not been extensively explored. Our study sought to determine the impact of neighborhood level SES and rurality and their interaction with race/ethnicity, on the incidence and survival of three subtypes of LC in the US: adenocarcinoma, squamous cell carcinoma (SCC), and small cell.

Methods. We used data from the Surveillance, Epidemiology, and End Results (SEER) Program, maintained by the National Cancer Institute, to gain access to a specialized dataset (SEER-17) that included census tract attributes for all cancers diagnosed from 2006-2020. We included all malignant lung and bronchus cancer cases diagnosed from 2006-2019. Cases were specified as adenocarcinoma, squamous, and small cell, by their ICD-O-3 histologic codes. We examined the following variables and disparity factors: NL SES (Yost US-Based Quintiles, where Quintile 1 corresponds to the lowest NL SES), race/ethnicity, urban-rural residence (USDA Rural-Urban Commuting Area codes), and sex. Age-adjusted incidence rates were calculated through the SEER*Stat program, and Joinpoint regression analyses determined the annual percent change of incidence by subtype from 2006-2019. We extracted the mean (and standard deviation) age at diagnosis for each NL factor and race/ethnicity within each subtype, and linear regression models evaluated disparities in age of diagnosis based on NL factors. The five-year relative survival for each histology was computed using SEER*Stat and by race/ethnicity, NL SES, and NL rurality.

Results. From 2006-2019, 682,672 lung and bronchus cancer cases were included in our analysis, with 40.3% (age-adjusted incidence = 22.0 [95% CI: 21.9, 22.1] per 100,000) were adenocarcinoma, 19.9% (age-adjusted incidence = 11.0 [95% CI: 10.9, 11.1] per 100,000) were SCC, and 11.5% (age-adjusted incidence = 6.2 [95% CI: 6.2, 6.3] per 100,000) were small cell cases. Incidence substantially differed by NL SES for SCC (16.5 per 100,000 in Quintile 1 [lowest NL SES] and 7.1 per 100,000 in Quintile 5 [highest NL SES], $p < 0.001$) and small cell (9.2 per 100,000 in Quintile 1 and 4.0 per 100,000 in Quintile 5, $p < 0.001$). However, differences in incidence of adenocarcinoma were smaller across NL SES (23.6 per 100,000 in Quintile 1 and 20.9 per 100,000 in Quintile 5, $p <0.001$). Incidence in rural areas was higher across all subtypes when compared to urban areas. Across all subtypes, the mean age of diagnosis was ~3.5 years younger for cases in Quintile 1 compared to Quintile 5, and ~1 year younger for cases residing in rural areas than urban areas. The 5-year survival rate substantially differed by NL SES for adenocarcinoma with ~ 10% difference between Quintile 5 and Quintile 1 across all races/ethnicities. A much smaller difference was observed in SCC, and no strong difference in small cell LC.

Discussion. NL SES and rurality contributed to more noticeable disparities in SCC and small cell LC incidence and survival, compared to adenocarcinoma. Given that smoking rates are higher in rural areas and areas with lower SES, our results provide support for the hypothesis that adenocarcinoma has a more multifactorial etiology compared to SCC and small cell, where smoking is the predominant risk factor. Further research is warranted to improve our understanding of how NL factors contribute to the etiology and disparities among LC subtypes.

Understanding the role RAGE plays in type 2 low and type 2 high obstructive lung disease

Scholar: Ezra Hardy

High School/College/City/State: Pittsburgh Science and Technology Academy, Pittsburgh, PA

PI of group/lab: Dr. Tim Perkins

Mentor(s): Dr. Tim Perkins

Site: Pathobiology

Background: Obstructive lung disease is a group of disorders that affects the upper airways that can lead to complications such as inflammation and mucus hypersecretion impeding the patient's ability to breathe. Some examples of obstructive lung disease are: type 1 and type 2 Asthma, Cystic Fibrosis, and Chronic obstructive Pulmonary Disease. The Receptor for Advanced Glycation Endproducts (RAGE) is a cell surface receptor primarily expressed in the lungs that promotes inflammation. Previous experiments performed by my mentor demonstrated that RAGE contributed to the symptom of type 2 low and type 2 high obstructive lung disease. The purpose of these experiments is to better understand the role RAGE plays in different types of obstructive lung disease.

Methods: We used a mouse model to determine the role of RAGE in neutrophilic airway inflammation. We also used the in-vitro models of primary human bronchial epithelial cells to evaluate the effects of type-2 cytokines on epithelial function.

Results: Using a mouse model of severe neutrophilic airway disease we found that mice that did not express RAGE showed less type 1 neutrophilic inflammation while mice that did express RAGE did have type 1 inflammation.

Conclusions: These results suggest that RAGE not only contributes to but is required for symptoms of all obstructive lung diseases.

Future Directions: The mechanisms through which RAGE mediates these effects is not currently well understood so by using future studies to understand this process we can get a better idea of how to treat the symptom of obstructive lung disease.

Physical Modeling of Cell Mechanical Interactions

Scholar: James Hsieh

High School: Taylor Allderdice High School, Pittsburgh, Pennsylvania

Lab: Keisuke Ishihara, PhD

Mentor: Keisuke Ishihara

Site: Computational Biology

Intro & Background: Mechanical interactions among cells is important for organ development and disease. Mechanical forces can affect the proliferation and migration of cancer cells in tumors. Previous experiments in the Ishihara lab showed that externally applied osmotic pressure prevents cancer cells from clumping. However, it is unknown how mechanics affect cell-cell interactions.

Methods: To explore mechanical interactions at different length scales, I used a particle simulation framework called HOOMD to model cell movement over time, following the implementation of Dunjova et al. 2025. Here cell interactions are defined by the potential energy as a function based on their distance and Brownian dynamics. I varied motility functions and force parameters to more realistically capture cell behaviour, using custom force terms to test the effects of both random and directed cell actions. Simulation results were compared to microscopy movies of cancer cells under osmotic pressure.

Results: First, I found that while changes to the cell cutoff distance had a noticeable effect on clumping, changes to the cell radius resulted in little change. Second, I found that when cells didn't clump as much, they gradually spread to a more uniform distribution across the entire confine. Third, I added a density-based stopping condition to mimic the shift in cell behaviour when they became separated from other cells. Now, I observed cell interactions that qualitatively matched the experiments in vitro.

Discussion: In this study, I modeled cell-cell interactions with simulations. By modifying forces, I found conditions that resemble cancer cell interactions under osmotic pressure. However, I have yet to find the precise scaling for the conditions that mimics the behaviour of cancer cells. Understanding different mechanical conditions may lead to new therapeutic strategies to inhibit malignant tumor growth.

Exploring the role of the interaction between MCM and TIMELESS in DNA replication in human cells

Scholar: Summer Ji

High School: North Allegheny Senior High School, Wexford, Pennsylvania

Lab: Tatiana Moiseeva, Ph.D.

Mentor: Rohan Harolikar

Site: Cancer Biology

Background: Cancer cells divide faster and are prone to replication stress, so it is important to understand the processes of DNA replication and cell proliferation for developing treatment strategies. MCM is a helicase that promotes the unwinding of DNA strands during DNA replication. Additionally, MCM interacts with TIMELESS (TIM) – a part of the fork protection complex. TIM maintains genome stability and helps replication of difficult-to-replicate regions. TIM is often overexpressed in cancers. In this project, we studied the effect of disrupting the interaction between TIM and MCM on cell proliferation. We hypothesized that without TIMELESS-MCM interaction, DNA replication and cell proliferation are slower.

Methods: A human osteosarcoma cell line (U2OS) was modified so that, upon treatment with doxycycline and 5Ph-IAA (auxin) (dox/aux), TIM is replaced by a mutated version TIM*, unable to interact with MCM. Four cell lines, which deplete endogenous TIM upon auxin treatment, were used. Upon doxycycline treatment, cell lines 3W2 and 3W4 express wild-type TIM, while cell lines 3M1 and 3M4 express TIM*. 3×10^5 cells of each line were seeded to 6 cm dishes and treated with DMSO or dox/aux. Cells were counted at 24, 48, and 72 hours. Data was analyzed on Prism.

Results: Significantly slower proliferation was observed for 3M1 and 3M4 treated with dox/aux, compared to those treated with DMSO. 3W2 and 3W4 showed no significance of dox/aux treatment on cancer cell proliferation.

Conclusion: We showed that disrupting the interaction between TIM and MCM results in slower cell proliferation. This supports the hypothesis that this interaction is important for DNA replication and cell proliferation. Cancer is a disease of proliferation; thus, by better understanding DNA replication, researching methods to control these processes can pave the way for new, innovative therapeutics.

Effect of Early Pharmacological Intervention on 5-Year Cardiovascular Outcomes in Early-Onset Hypertension

Ruth Joel[1], Kevin Kindler, MD[2], Olga Kravchenko, PhD[2]

[1]Providence Day School, Charlotte, NC; [2]University of Pittsburgh, Pittsburgh, PA

Abstract

We compared 5-year incidence of major adverse cardiovascular events (MACE) between hypertensive patients initiating antihypertensive therapy early (≤ 1 year) versus late (> 1 year) post-diagnosis using UPMC aggregate data extracted via the i2b2 tool. Among 107,899 early-Rx and 83,292 late-Rx adults, early-Rx had higher crude 5-year MACE incidence (1.94 % vs. 1.14 %, RR 1.70, 95 % CI 1.58–1.84). When stratified by age (< 55 vs. ≥ 55), relative risks were 2.08 and 1.57, respectively.

Introduction

Over 20 % of U.S. adults aged 18–39 meet hypertension criteria under the 2017 ACC/AHA guidelines[1], making early-onset hypertension a public health concern. Lifestyle interventions–such as diet and exercise–often precede pharmacotherapy, but many patients ultimately require medication. Although early-onset HTN conveys established long-term risks (e.g., significantly increased risk of coronary calcification[2]), it remains unclear whether starting antihypertensive medications within one year of diagnosis reduces 5-year rates of myocardial infarction and stroke.

Methods

We conducted a retrospective cohort study using UPMC's i2b2 system to extract data spanning 2005-2025 of adults (≥ 18 years) with the HTN diagnosis defined by ICD-10 I10. Patients were classified as Early-Rx (first antihypertensive prescription ≤ 365 days post-diagnosis) or Late-Rx (> 365 days). The composite outcome of this study included unstable angina (I20.0), acute/subsequent MI (I21–I22), chronic ischemic heart disease (I25), and ischemic stroke (I63) occurring within 0 to 1,825 days of antihypertensive prescription. For statistical analysis we used incidence proportions, risk ratios (Katz 95 % CI), absolute risk differences (Wald 95 % CI), and chi-square tests. Analyses were stratified by age (< 55 vs. ≥ 55).

Results

Table 1. Cohort sizes and 5-year MACE incidence

Cohort	N	Events	Rate (%)	RR (95 % CI)	ARD (pp, 95 % CI)	p-value
Early-Rx	107,899	2,091	1.94	1.70 (1.58–1.84)	0.80 (0.69–0.91)	< 0.0001
Late-Rx	83,292	948	1.14	Reference	Reference	—

Table 2. Age stratified rates (< 55 vs. ≥ 55)

Age Group	N_e	$Rate_e$ (%)	N_L	$Rate_L$ (%)	RR (95 % CI)	ARD (pp, 95 % CI)	p-value
< 55	21,364	0.83	15,585	0.40	2.08 (1.60–2.70)	0.43 (0.33–0.53)	< 0.0001
≥ 55	93,110	2.05	67,707	1.31	1.57 (1.44–1.71)	0.74 (0.66–0.82)	< 0.0001

Discussion

In this cohort, Early-Rx patients showed higher crude 5-year MACE incidence than Late-Rx, with stronger relative differences in younger adults. These results likely reflect confounding by indication and

immortal-time bias rather than a causal effect of early treatment. Limitations of this study include reliance on ICD10 codes, lack of blood pressure data, and other clinical covariates (e.g., comorbidities or medication adherence), and a 5-year follow up that may miss longer-term benefits. Despite these caveats, our study showed i2b2s utility for rapid, large-scale cohort analysis and hypothesis generation around early antihypertensive therapy.

References

1. Rana J, Oldroyd J, Islam MM, Tarazona-Meza CE, Islam RM. Prevalence of hypertension and controlled hypertension among United States adults: Evidence from NHANES 2017-18 survey. Int J Cardiol Hypertens. 2020 Oct 26;7:100061. doi: 10.1016/j.ijchy.2020.100061. PMID: 33447782; PMCID: PMC7803033.
2. Suvila K, McCabe EL, Lehtonen A, et al. Early Onset Hypertension Is Associated With Hypertensive End-Organ Damage Already by MidLife. Hypertension. 2019;74(2):305-312. doi:https://doi.org/10.1161/hypertensionaha.119.13069

Efforts to bridge the gap in cancer recovery: the disparity among rural and urban areas regarding physical activity

Scholar: Siddh Kapil
High School: North Allegheny Senior High School, Wexford, PA
PI of group/lab: Kathryn H Schmitz, PhD, MPH
Mentor(s): Michele Sobolewski
Site: Women's Cancer Research Center

Background: PA Moves is an NCI-funded study to address physical inactivity in rural Pennsylvania–a lead risk factor for cancer. Physical activity lowers the risk by 10-20% for many common cancers. Yet, many Americans remain insufficiently active. PA Moves examines how rurality and the built environment affect physical activity. Rural residents tend to have worse health behaviors than those living in urban areas which may be reflected in their 8% higher cancer mortality rate. This study seeks to examine differences in the built environment across three areas that differ in rurality. We believe that the most urban areas will have better physical activity resources available than the most rural setting.

Methods: We used the Rural Area Living Assessment (RALA) to assess the built environment. The RALA was designed to assess active living attributes of rural environments. The Town-wide assessment, a component of RALA, measures the town's physical activity resources including terrain, infrastructure, and nature. We compared three areas that differ in rurality, Wexford (most urban), Indiana, and Titusville (most rural). Comprehensive audits of each area were compared based on the number, type, and quality of resources available.

Results: Compared to Titusville and Indiana, Wexford had better physical activity opportunities.Though Titusville and Indiana had higher percentages of physical activity resources within the segments examined, Wexford had better infrastructure, with 100% of its segments with good/excellent roads (compared to 71% and 78% for Indiana and Titusville, respectively).

Conclusion: This study supports the hypothesis that urban areas have better physical activity resources than rural areas.

Future Implications: PA Moves hopes that if rural communities are provided with access to resources, their physical activity levels will improve. That may lead to decreased risk of cancer.

Title: Analysis of Hi-C Using Mathematical Modeling Reveals Larger Genomes Have Lower Cohesin Detachment Rates

Scholar: Rachel Kim
High School: Fox Chapel Area High School
Lab: Maria Chikina, PhD
Mentor: Tina Subic, PhD, Maria Chikina, PhD
Site: Computational Biology

Introduction: The way the genome is folded is important for regulating gene expression. Loop extrusion is a process that organizes the 3d genome structure in which cohesin forms "loops" by moving along the chromatin to bring far apart elements together. The distance cohesin travels is regulated by CTCF boundaries and WAPL sites which remove cohesin off the chromatin. Genome size varies between species, however, the number of genes is approximately the same. Therefore genes and their regulatory elements in larger genomes are further apart. This also means that in larger genomes, more further-apart distances have to come in physical contact. Which brings us to the question of how the dynamics of the loop extrusion vary with the genome size so that cohesin can cover longer distances in larger genomes and vice versa. And since regulatory elements in general are further apart, it is reasonable to assume that elements that regulate loop extrusion, such as WAPL sites, are also more spread out. We hypothesize that in species with larger genome sizes, cohesin will take longer to reach a WAPL site and will remain on the chromatin longer. To test this hypothesis, we fit a minimalistic mathematical model of loop extrusion to data from vertebrate species with varying genome sizes to determine how model parameters scale with genome size, with particular focus on the cohesin detachment rate from chromatin.

Method: We obtained publicly available Hi-C contact map data in .hic or .mcool formats from multiple vertebrate species. For each dataset, we computed the average contact probability between pairs of loci as a function of increasing genomic distance. We then fitted these contact probability curves to our mathematical model, which describes chromatin organization through both diffusion and cohesin-mediated loop extrusion. To ensure data quality, we applied a loss threshold of 0.01 and only included fits with errors below this value. The model generates four parameters that characterize chromatin diffusion and cohesin dynamics, including a parameter representing the cohesin detachment rate. We analyzed scaling relationships by plotting the cohesin detachment rate as a function of both total genome size and individual chromosome size across species.

Results: We analyzed Hi-C data from five vertebrate species: zebrafish, chicken, mouse, human, and xenopus. Our results indicate that cohesin detachment rate negatively correlates with both chromosome size and total genome size, suggesting that cohesin tends to remain on chromatin longer in species with larger genomes. This finding supports our hypothesis that smaller

genomes should have higher detachment rates because cohesin travels shorter distances before detaching. Specifically, chicken and zebrafish, which have smaller genomes of approximately 1 Gb, showed higher detachment rates compared to human, mouse, and xenopus, whose genomes are around 3 Gb. However, we also observed some interesting exceptions: xenopus has an unusually high detachment rate for its genome size, and chicken expresses a very strong scaling relationship between detachment rate and chromosome size. These findings suggest there may be additional species-specific factors influencing cohesin dynamics beyond overall genome size.

Conclusion: Our results support our hypothesis that cohesin detachment rate decreases with genome size, allowing cohesin to remain on chromatin longer in larger genomes. The exceptions we observed may reflect unique genomic features: xenopus underwent whole-genome duplication, while chicken has micro-chromosomes with unusually high gene density. Future studies should examine more extreme genome sizes, including very large genomes like lungfish and axolotl, and smaller compact genomes like pufferfish and medaka, to better understand how genome organization and loop extrusion mechanisms work together.

Comparative Genomics of the H. Pylori Bacteria

Kylie M. King[1], Shu-Ting Cho, MS[2]

[1]Moon Area High School, Coraopolis, PA; [2]Department of Computational and Systems Biology, School of Medicine, University of Pittsburgh, Pittsburgh, PA

Abstract

Due to *Helicobacter pylori*'s virulence factors varying in presence and sequence across strains, it is difficult to determine which aspects should be prioritized in treatment. Comparative genomics enables researchers to assess differences in gene content among strains. Using this method, the frequency of key virulence factors such as VacA, CagA, and BabA was recorded, along with how often they co-occurred within the same strain.

Introduction

Helicobacter pylori is a genetically diverse bacterium linked to various gastrointestinal diseases, including ulcers and gastric cancer. Its virulence depends on genes that vary in presence and sequence across strains. This genetic variability complicates treatment decisions, but comparative genomics— the study of similarities and differences in genome sequences—can help eliminate this uncertainty.

Methods

A total of 369 *H. pylori* genomes were obtained from the public NCBI database. Gene content analysis was performed using the DECIPHER package in the R programming language to identify the presence of virulence genes SabA, VacA, CagA, BabA, and OipA. The frequency of each factor, as well as their co-occurrence within the same strains, was recorded and analyzed in a heatmap.

Results

The heatmap revealed notable variation in the presence of virulence genes across the analyzed genomes. SabA, VacA, and OipA showed the highest levels of co-occurrence, frequently appearing together in multiple strains. In contrast, VacA and BabA were detected less consistently in the strains.

Discussion

The findings highlight genetic diversity in *H. pylori* virulence profiles, emphasizing the value of comparative genomics in understanding strain-specific variation. Application would be simple as all resources used were freely available on the internet and only require coding knowledge and a computer to work.

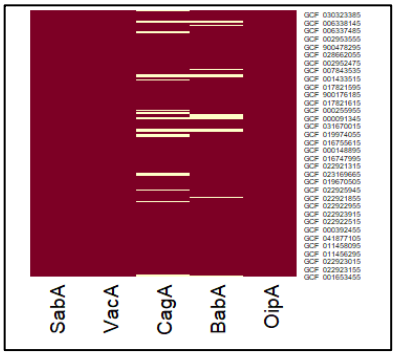

Figure 1. Virulence factor gene presence

Title: The role of APOC3 in Plasma Triglyceride Regulation
Scholar: Christie Ivory Koyo
High School: Perry Traditional Academy. Pittsburgh PA
PI of group/lab: Ali Kohan
Mentor: Rachel Christine Wills
Site: ICI

Background: Triglycerides are fats found in the blood and are important markers of metabolic and cardiovascular health. High triglyceride levels are associated with an increased risk of heart disease. The APOC3 gene plays a key role in lipid metabolism by regulating how triglycerides are broken down. This summer, we investigated how different levels of the APOC3 gene may affect blood triglyceride levels.

METHODS: To conduct this study, we used the following techniques:

- Genotyping, to determine whether each mouse was wild type, Heterozygous, or homozygous mutant for the APOC3 gene.
- qPCR, to analyze gene expression levels.
- Triglyceride Assay (TAG assay), to measure the triglyceride levels in the blood. We visualize two analysis methods: using absorbance values and using calculated concentrations in mg/dL.

RESULT: My genotyping results showed a probable mutant mouse, meaning both copies of the gene were mutated.

Our study demonstrates that elevated APOC3 expression leads to higher triglyceride levels, while reduced APOC3 is correlated with lower triglycerides.

CONCLUSION: These findings suggest that the APOC3 gene may influence blood triglyceride levels and play a significant role in lipid metabolism. This project helped us apply molecular biology techniques and better understand how genetic variations can impact metabolic health.

Designing an *in vitro* Assay to Investigate March5's Role in Membrane Protein Quality Control

Scholar: Einstein "Kevin" Lee

High School: The Kiski School, Saltsburg Pennsylvania

Lab: Matthew Wohlever, PhD

Mentor: Brian Acquaviva

Site: CoSBBI (Computer Science, Biology, Biomedical Informatics)

Introduction: The Wohlever lab studies membrane protein quality control using biochemistry. Protein quality control describes how the cell maintains a proper balance of proteins. If this balance fails, diseases such as cancer, cardiovascular, and neurodegenerative disorders can emerge. The E3 ligase March5 plays a key role in mitochondrial protein degradation and quality control. Inhibition of this protein is a promising avenue for prostate cancer chemotherapy. To identify March5 inhibitors, our lab has developed an *in vitro* assay using purified proteins. While powerful, this assay is time-consuming. One way to improve its speed and sensitivity is to fluorescently label the proteins. My summer research project focuses on using the enzyme sortase to fluorescently label proteins in the March5 assay, thereby improving the workflow for studying March5.

Methods: For thiol coupling, a maleimide dye (AlexaFluor 647) was mixed with a GGGC peptide at a 2:1 molar ratio and incubated overnight at 4°C. The following day, the peptide was mixed with the target protein and sortase at a 100:10:1 molar ratio. After 24 hours of incubation at 4°C, the reaction was analyzed on SDS-PAGE gels. Additionally, March5 was cloned into *E. coli* Golden Gate vectors, then expressed and purified using Ni-NTA affinity chromatography.

Results: Initial March5 purification yielded low expression and insoluble protein. We were able to purify SGTA needed for liposome assays. For sortase labeling, it appears that the substrate is being labeled, but there is an undetermined issue with the fluorophore causing low signal.

Conclusion: We have begun optimizing expression and purification protocols to improve the yield of March5. Once successful, sortase labeling will allow rapid detection of membrane proteins. This method is a high-efficiency alternative to Western blotting. The assay under development may accelerate the discovery of therapeutic inhibitors targeting March5 in cancer and neurodegenerative diseases.

Title: Investigating Stromal Mitochondrial Changes in High-Grade Serous Ovarian Carcinoma

Scholar: Angelina Li

High School/College/City/State: North Allegheny Senior High School, Pittsburgh, PA

PI of group/lab: Dr. Lan G. Coffman, MD, PhD

Mentor(s): Huda I Atiya, PhD

Site: Women's Cancer Research Center (WCRC)

Background: Ovarian cancer (OC) is recognized as the deadliest gynecologic cancer due to late diagnosis and early metastasis. High-grade serous ovarian carcinoma (HGSOC) is the most common OC subtype, with over 70% of patients presenting with metastatic disease at diagnosis. The stromal tumor microenvironment (TME) plays a vital role in OC progression. Our lab focuses on a specific stromal cell population within the TME: mesenchymal stem cells (MSCs). We have shown that cancer-associated MSCs (CA-MSCs) promote OC growth, metastasis, and resistance to therapy. Our lab also showed that CA-MSCs have more total mitochondria compared to nMSCs, and they are functionally different. This study explores the metabolic changes in CA-MSCs that lead to increased mitochondrial mass and enhanced oxidative phosphorylation (OXPHOS), enabling the cells to generate more ATP, which, in turn, promotes OC progression.

Method: (1) RNA-seq gene count data from 31 samples (14 nMSCs and 17 CAMSCs) was used to perform differential expression analysis (DE) and pathway gene set enrichment analysis (GSEA) using R-Studio's DESeq2 and clusterProfiler packages, as well as the Broad Institute's GSEA software, to identify significant genes involved in metabolic function.
(2) To validate the RNA-Seq data, reverse transcription quantitative PCR (RT-qPCR) and western blotting were used.

Results: RNA seq analysis identified 9 genes of interest: CYP24A1, PDK4, TSPO, MTFR2, DNA2, CRLS1, SQOR, SUGCT, and CD36. Multiple rounds of RT-qPCR on different cell lines verified the upregulation of PDK4, CYP24A1, and TSPO and downregulation of MTFR2 and DNA2 in CA-MSCs versus nMSCs. Interestingly, the validated CA-MSCs upregulated genes are associated with increased cellular energy production through metabolic shift from glucose utilization towards fatty acid oxidation. Further, Western blot validation showed that ATP5a (a subunit of the ATP synthase complex) is upregulated in CA-MSC vs nMSCs.

Conclusion: CA-MSCs use different energy production pathways to support OC progression.

Establishing an in vivo imaging system to monitor leukemia development and investigate the role Leukemia-associated macrophage (LAM) in leukemogenesis

Scholar: Joanna Li

High School/College/City/State: Fox Chapel Area High School, Pittsburgh, PA

PI of group/lab: Dr. Wei Du, MD, PhD

Mentor(s): Jiayang Bao PhD; Logan Sund, B.S

Site: Cancer Biology

The tumor microenvironment, particularly macrophages, heavily impacts cancer progression. In leukemia, the bone marrow microenvironment and leukemia-associated macrophages (LAMs) significantly impact leukemia development and progression. While a connection exists between macrophages and leukemia through M1 macrophages, which act as tumor suppressors, and M2 macrophages, which act as tumor promoters, there is still a lack of understanding about how these macrophages contribute to leukemia growth. Immune receptor TREM-1 has been shown to play a role in macrophage polarization, resulting in the production of M1 or M2 macrophages. This study utilized an existing MLL-AF9 (MA9) leukemia model in combination with lentivirus expressing firefly luciferase, as a tool to track leukemia cells in both in vitro/in vivo. We have successfully produced and validated firefly luciferase virus in both adherent 293T, and suspension THP-1 human cell lines through luminescence testing with the luciferin chemical reaction. Additionally, we were able to optimize virus validation procedures in primary mouse bone marrow cells and transduce MA9 leukemia cells. While the preparatory steps—virus production, validation, and in vitro and in vivo transduction—were completed, the final steps, including the bone marrow transplant, TREM-1 deletion in Trem1f/fCsf1RCre mice using tamoxifen, and in vivo time tracking of leukemia development through IVIS imaging in mice and later flow cytometry, remain in progress. Completion of these steps demonstrate that this lentiviral luciferase-based tracking system could serve as a powerful in vivo approach for studying the role of bone marrow-residing LAMs, mechanisms of immunotherapy resistance and for testing novel therapeutic targets for leukemia therapy.

Instrumental Variable Analysis of Environmental and Social Determinants of Poor Mental Health Using County-Level Data

Hannah Luo[1,2], Dr. Eric V. Strobl, MD PhD[3]
[1]South Fayette High School, McDonald, PA; [2]University of Pittsburgh Hillman Cancer Center Academy, Pittsburgh, PA; [3]Department of Biomedical Informatics, University of Pittsburgh, Pittsburgh, PA

Abstract
In this study, instrumental variable analysis was applied to analyze the causal impact of air pollution, social associations, and physical inactivity on poor mental health outcomes across U.S. counties. Traffic volume, broadband access, and access to exercise opportunities were used as instruments to identify significant effects of these exposures on mental health.

Introduction
Mental health is influenced by various environmental and social factors[2]. Traditional studies are often limited by confounding variables, which can bias estimates of the causal effect of an exposure on an outcome. Instrumental variable (IV) analysis offers a way to overcome these challenges by using instruments that influence the exposures but are not directly related to the outcome[1]. This study aims to identify causal effects of particulate air pollution, social interactions, and physical inactivity on poor mental health, applying instrumental variable methods to United States county-level data to mitigate confounding bias.

Methods
County-level data from the County Health Rankings database[3] were used, which included measures of air pollution, social associations, and physical inactivity. Poor mental health days were used as the outcome variable. The dataset included 3,104 U.S. counties with values for the exposures, instruments, and outcomes. Traffic volume, broadband access, and access to exercise opportunities were used as the instrumental variables for air pollution, social associations, and physical inactivity, respectively (Figure 1). First-stage linear regressions were used to test instrument strength using their F-statistics. Two-stage least squares (2SLS) were implemented using the ivreg() function in R. OLS results were also computed for comparison. Model significance and coefficient direction were used to assess plausibility.

Results
Triple 1 (Traffic Volume and Air Pollution) showed strong F-statistics ($F = 54$) but resulted in an implausible negative effect of air pollution on poor mental health days ($\beta = -0.44$, $p < 0.01$), suggesting the presence of other variables influencing the relationship. In Triple 2 (Broadband Access and Social Associations), the instrument was weak ($F = 5$) and the direction of the 2SLS ($\beta = 1.03$, $p < 0.05$) estimate was inconsistent with OLS between social associations and poor mental health days, suggesting that broadband access may not be a valid instrument. Triple 3 (Access to Exercise Opportunities and Physical Inactivity) showed a strong instrument ($F = 686$) and a large, statistically significant IV effect ($\beta = 7.18$, $p < 0.01$), consistent with OLS direction.

Discussion
Of the three instrument-exposure-outcome triples analyzed, only triple 3 (Access to Exercise Opportunities and Physical Inactivity) met all necessary conditions for valid instrumental variable analysis. Specifically, the 2SLS estimate was statistically significant and directionally consistent with both the OLS estimate and prior causal expectations. In contrast, traffic volume and broadband access are likely confounded by factors such as urbanization and access to resources, which can influence mental health through multiple pathways and thus their effects on the outcome cannot be assumed to operate solely through the exposure. As a result, our findings only strengthen the evidence for promoting physical activity as a viable strategy to improve mental health.

Figure 1: Hypothesized relationships among variables in IV analysis. (a) Traffic volume (instrument) increases air pollution (exposure), which is hypothesized to result in more poor mental health days (outcome). (b) Broadband access (instrument) is expected to promote social associations (exposure), which may help protect against poor mental health days (outcome). (c) Access to exercise opportunities (instrument) is posited to increase physical activity (exposure), thereby reducing poor mental health days (outcome).

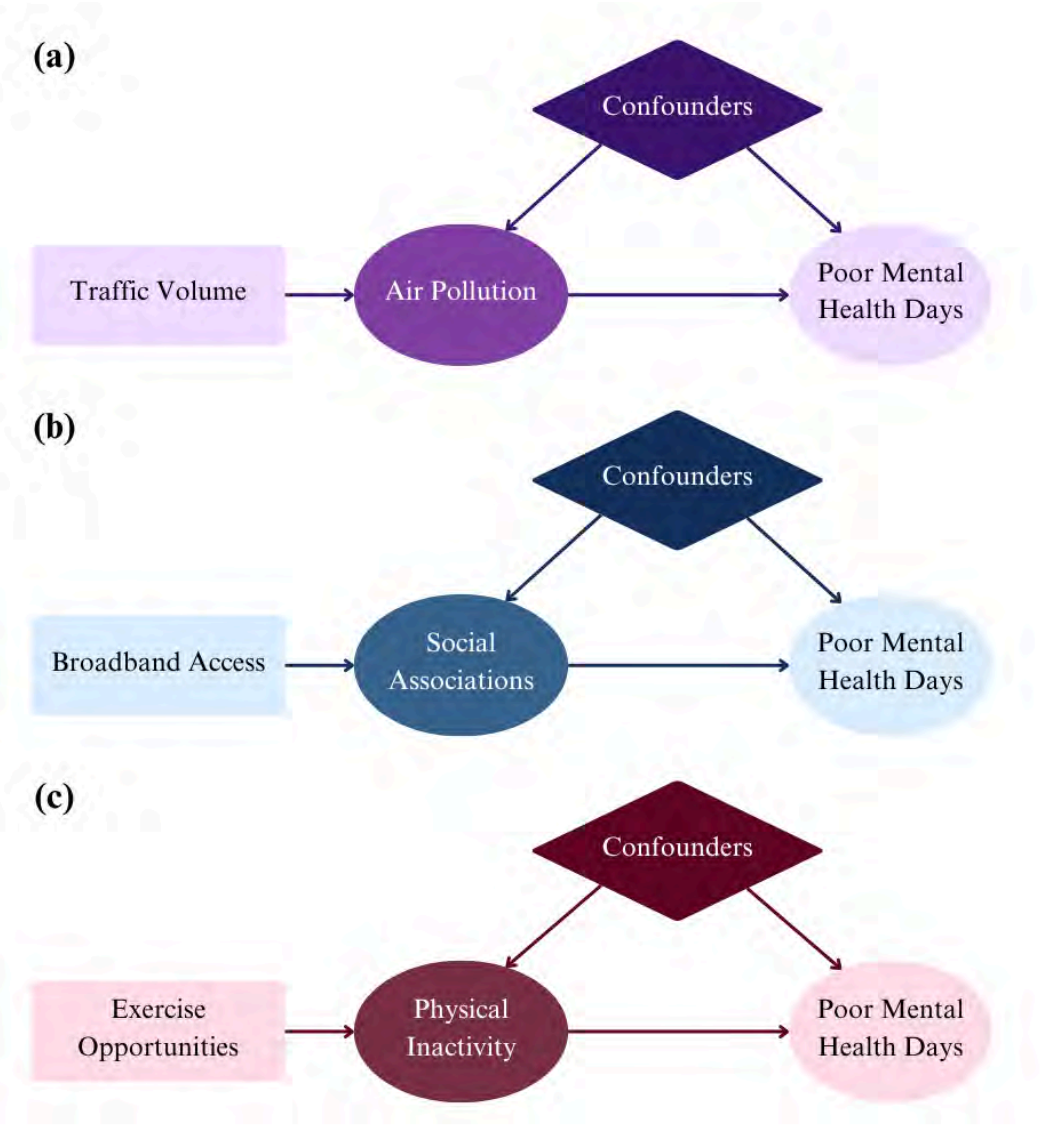

References

1. Baiocchi, Michael, Jing Cheng, and Dylan S. Small. "Instrumental variable methods for causal inference." *Statistics in medicine* 33.13 (2014): 2297-2340.
2. Goetz, Stephan J., Meri Davlasheridze, and Yicheol Han. "County-level determinants of mental health, 2002–2008." *Social Indicators Research* 124.2 (2015): 657-670.
3. University of Wisconsin Population Health Institute. County Health Rankings & Roadmaps: Methodology and sources—data documentation. 2025. Accessed July 23, 2025. https://www.countyhealthrankings.org/health-data/methodology-and-sources/data-documentation

HPV Driven Head and Neck Cancer is Characterized by Tertiary Lymphoid Structures With Enhanced Immune Activity

Rayan Majumdar, La Salle College, Wyndmoor, PA, USA
Mentor: Medard Kazia, PhD, Tullia Bruno, PhD

PI: Tullia Bruno, Ph.D. UPMC Hillman Cancer Center, Pittsburgh, PA, USA

Abstract

In this project, multispectral imaging was used to quantify Tertiary Lymphoid Structure (TLS) and their composition in both HPV driven head and neck squamous cell carcinoma (HNSCC), HPV-positive and HPV-negative disease. The data show that HPV-positive tumors have high density of TLS, and they are composed of high numbers of B cells and T cells. Taken together, the project highlights the importance of TLS in HNSCC.

Introduction

Head and neck squamous cell carcinoma (HNSCC) can be categorized into HPV-positive and HPV-negative subtypes with distinct etiologies and treatment responses. HPV-positive tumors, typically seen in younger individuals, show better prognosis and higher TLS density than HPV-negative ones. TLSs, which resemble lymph nodes, facilitate local immune responses in tumors and are considered promising biomarkers for prognosis. Accurate quantification of TLS in histopathological images is essential for better understanding the immune landscape across cancer subtypes. (MacFawn et al., 2024; Ruffin et al., n.d.)

Methods

A cohort of patients, HPV-positive and HPV-negative were analyzed with a multiplex immunofluorescence panel. QuPath software was used to analyze scanned histological slides. Three automated cell detection techniques—Watershed, StarDist, and Instanseg—were tested on tissue samples from HNSCC patients. Performance was evaluated based on segmentation accuracy, ability to handle overlapping cells, and robustness to staining variation. A TLS pixel classifier was then applied to identify regions of TLS and cells within these TLS were segmented and phenotyped.

Results

TLSs were more frequent and mature in HPV-positive tumors, often exhibiting germinal centers. Instanseg outperformed Watershed and StarDist in detecting cell boundaries, offering cleaner results and higher consistency. HPV-positive images showed denser immune clustering, consistent with previous findings.

Discussion This study validates Instanseg as the optimal QuPath tool for accurate and scalable immune cell detection in TLS analysis. Combining computational pathology tools with immunological insights enables more precise characterization of tumor microenvironments. Further work will include classifying immune cell types and correlating TLS metrics with patient outcomes.

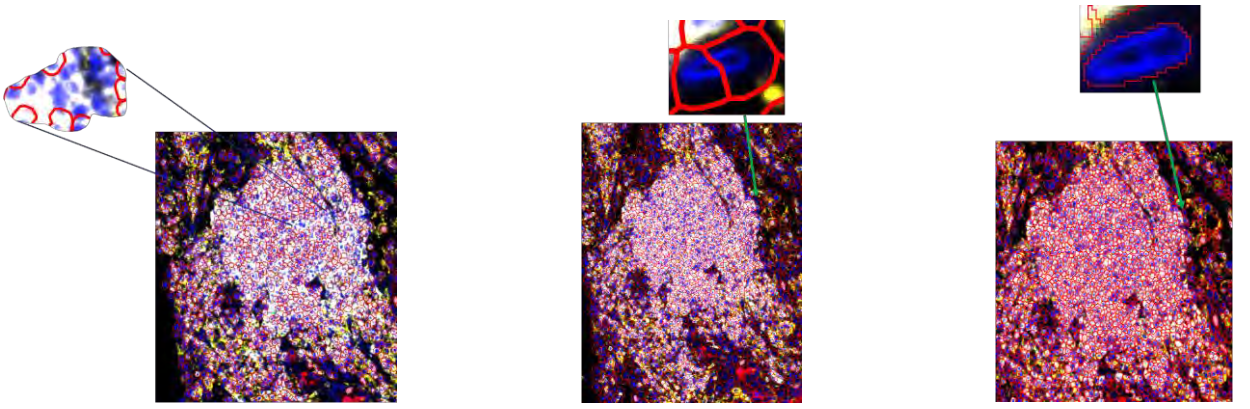

Watershed Cell Detection **Stardist Cell Detection.** **Instanseg Cell Detection**

Figure 1: Methodologies for various cell detection. Instanseg has the best segmentation across variations in staining techniques and works across all image type with the greatest efficiency.

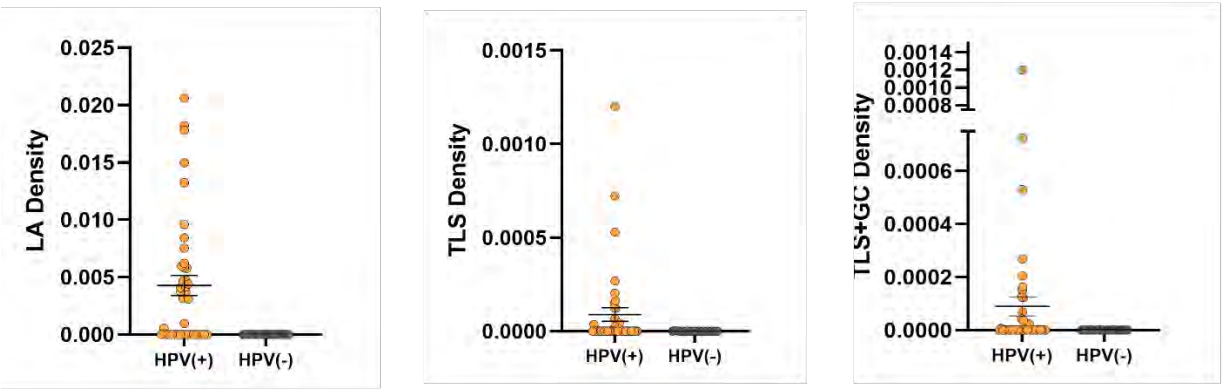

Figure 2: HPV(+) Tumors have higher Lymphoid Aggregate (LA) and Tertiary Lymphoid Structure (TLS) density than HPV(-) tumors

References:

1. MacFawn, I. P., Magnon, G., Gorecki, G., Kunning, S., Rashid, R., Kaiza, M. E., Atiya, H., Ruffin, A. T., Taylor, S., & Soong, T. R. (2024). The activity of tertiary lymphoid structures in high grade serous ovarian cancer is governed by site, stroma, and cellular interactions. *Cancer Cell*, *42*(11), 1864–1881.
2. Ruffin, A. T., Cillo, A. R., Tabib, T., Liu, A., Onkar, S., Kunning, S. R., Lampenfeld, C., Atiya, H. I., Abecassis, I., L Kürten, C. H., Qi, Z., Soose, R., Duvvuri, U., Kim, S., Oesterrich, S., Lafyatis, R., Coffman, L. G., Ferris, R. L., A Vignali, D. A., & Bruno, T. C. (n.d.). *B cell signatures and tertiary lymphoid structures contribute to outcome in head and neck squamous cell carcinoma*. https://doi.org/10.1038/s41467-021-23355-x

Transcriptomic Differences Between Myocardial Infarction and Control Samples

Reina Majumdar, Lansdale Catholic High School, Landsdale, PA

PI of group/lab: Jishnu Das, Ph.D.

Mentor: Mary Cundiff, M.S., Ph.D.

Abstract

This study analyzes transcriptomic data to investigate gene expression differences between myocardial infarction (MI) and healthy heart tissue. Using single-cell RNA sequencing and Seurat in R, we examined fibroblasts from ischemic and fibrotic heart zones. We identified differentially expressed genes (DEGs) linked to tissue repair, fibrosis, and immune response. Our findings help clarify how fibroblasts contribute to cardiac repair and could inform future treatment strategies.

Introduction

Myocardial infarction (MI), commonly known as a heart attack, is a leading cause of death globally. Better understanding of the cellular and molecular changes in heart tissue following MI is critical for improving treatment outcomes. This project investigates the expression of genes involved in tissue repair pathways in MI-affected regions compared to healthy cardiac tissue, focusing specifically on fibroblasts known to be active in fibrosis and wound healing.

Methods

We used a publicly available spatial transcriptomic study (Kuppe et al., 2022, Nature) that developed the public dataset of 23 patients and their genes within their heart tissue before/after a heart attack. Tissue samples were included from the ischemic (IZ), fibrotic (FZ), and control zones of the heart. The study provided a timeline of when the genes were collected and the methods used to collect them (RNA seq).

Results

Comparisons between CTRL vs. IZ, CTRL vs. FZ, and IZ vs. FZ fibroblasts revealed key DEGs. Genes such as CHI3L1, ZBTB20-AS2, and EGOT showed increased expression in MI zones, suggesting a role in extracellular matrix remodeling, fibrosis, and immune response. The fibrotic zone displayed more expression of genes associated with chronic tissue repair, while the ischemic zone showed acute response signatures.

Discussion

This analysis reveals gene expression changes in fibroblasts following myocardial infarction (heart attack). The findings highlight specific targets involved in tissue repair and fibrosis, which can guide therapeutic strategies to help with recovery and future treatments. Work in the future could extend this analysis to other cell types or timepoints.

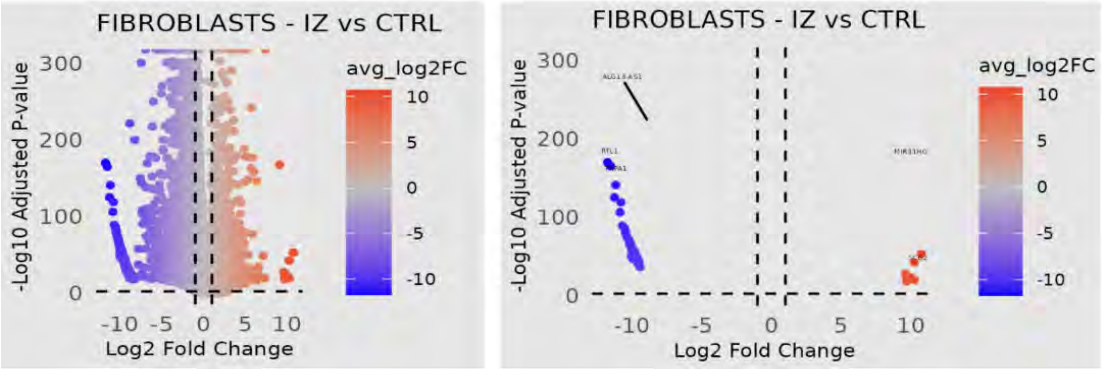

Figure 1: Fibroblast Gene Expression Changes in Ischemic vs. Healthy Heart Tissue

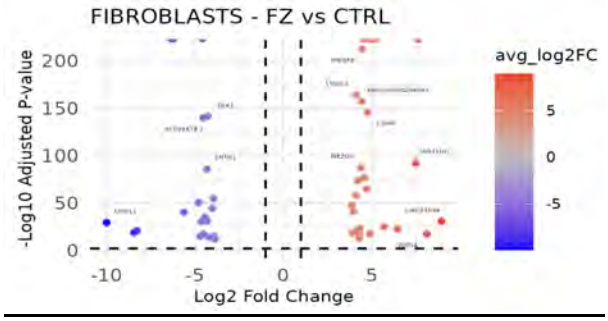

Figure 2: Differential Gene Expression in Fibroblasts: Fibrotic Zone (FZ) vs. Control

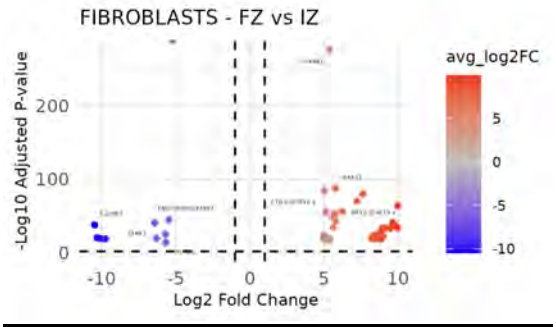

Figure 3: Fibroblast Gene Expression Differences: Fibrotic Zone vs. Ischemic Zone

References:

Rahimikollu J, Xiao H, Rosengart AE, Rosen ABI, Tabib T, Zdinak PM, He K, Bing X, Bunea F, Wegkamp M, Poholek AC, Joglekar AV, Lafyatis RA, Das J.
SLIDE: Significant latent factor interaction discovery and exploration across biological domains. *Nat Methods.* 2024;21(8):835–845. doi:10.1038/s41592-024-02114-3.

Simulating Therapist-Client Dialogues with AI

Oscar Martinez
Claremont High School
Ontario, California, United States

Mentor:
Siyuan Dai, PhD Candidate (Master)
Department of Electrical and Computer Engineering, Swanson School of Engineering
University of Pittsburgh

Abstract
This project explores the use of large language models(LLMs) in simulating therapist-client conversations. In fine-tuning LLaMA over real clinical dialogue data, it seeks to generate emotionally supported and reflective AI output that could assist individuals who are psychologically disturbed when therapy is not readily accessible.

Introduction
Mental illnesses such as depression and anxiety are prevalent and rising world concerns. Professional counseling is still not easily accessible to many, though. AI solutions that can empathically and suitably reply can potentially fill the gap. This study attempts to replicate the dialogue between therapists and clients using large language models (LLMs) with the goal of creating AI-generated dialogue that mirrors therapeutic assistance and imitates real-world clinical communication patterns.

Methods
The material used was 30 anonymized transcripts of real mental health therapy sessions. The dialogue consisted of alternate turns between therapists and clients, emotional well-being, coping, and reflective questioning. Raw transcripts were preprocessed to instruction–input–output form appropriate for LLaMA Factory. Techniques utilized were basic Python scripting, text formatting, and prompt structuring. Preprocessed data were used to fine-tune a LLaMA-3 model on Google Colab. A case study was also developed to assess the empathic response of the model in an actual scenario.

Results
The fine-tuned model generated responses that aligned with therapist-like behavior. Outputs included reflective questions, affirmations, and emotional support statements. Qualitative analysis revealed the AI could have natural, safe, and empathetic dialogue. Initial testing revealed improved alignment with therapeutic tone and goals compared to non-fine-tuned models.

Discussion
This paper shows that fine-tuned LLMs, when trained on real therapy conversation, are capable of producing empathetic and meaningful mental health output. The results show potential for AI augmentation of mental health care delivery, especially in resource-constrained settings. Safety, bias, and clinical effectiveness in extension use need to be the areas of follow-up.

Phenotypically characterizing *wspA* and evolved *wspA* mutants in *Pseudomonas fluorescens*

Scholar: Sophia Mazer

High School: Shaler Area High School, Pittsburgh, PA

PI: Dr. Vaughn Cooper

Mentors: Dr. Abigail Matela, Dr. Erin Nawrocki, Colton Siatkowski

Site: TDX

Biofilms, composed of bacteria and their self-produced matrix, are essential to microbial life. *Pseudomonas fluorescens* SBW25 is often used to study biofilms due to its well-characterized genome and biofilm-related pathways. This study focused on two pathways of *P. fluorescens*: Wsp and Wss. The Wsp operon, a chemosensory-like pathway composed of seven genes, produces cyclic diguanylate monophosphate (c-di-GMP; a secondary messenger) when activated. C-di-GMP turns on many other biofilm-related pathways, including Wss, which is responsible for cellulose synthesis. However, mutations in the Wsp pathway can lead to the constant activation of the operon, thereby resulting in elevated levels of c-di-GMP, ultimately producing colonies with a wrinkled morphology. On agar plates containing Congo red (a dye), these colonies appear bright red due to the dye's ability to bind to sugars such as cellulose. However, after evolving a particular *wspA* mutant, we found colonies that maintained this wrinkled morphology but lost this bright red color, appearing pink instead. This pink color was attributed to the production of another biofilm polysaccharide called poly-β-(1,6)-N-acetylglucosamine (PGA). In this study, our goal was to phenotypically characterize both *wspA* mutants and their evolved mutants by examining potential links between *wspA* mutations and secondary mutations in Wss and by measuring our mutants' rates of growth and c-di-GMP production.

We performed a planktonic selection assay to determine if there was a link between *wspA* mutants and secondary Wss mutations. We used three *wspA* mutants, each having unique mutations that affected c-di-GMP levels differently, and we selected for secondary Wss mutations. In the evolved *wspA* mutants, we selected for suppressors of the wrinkly phenotype. After three transfers over the course of five days, cultures were diluted and plated on Congo red agar to determine their morphology. Each *wspA* mutant produced at least one pink colony and one smooth colony, which were then isolated and sequenced. None of the evolved mutants, however, produced colonies with different morphologies. To further assess growth behavior in our mutants, we performed a growth curve analysis, comparing one *wspA* mutant and two evolved ones to two ancestors, a high-biofilm-producing *wspF* mutant, and engineered Wss and Pga knockouts. The *wspA* mutant showed reduced growth in reference to its ancestor, consistent with the idea that more energy is being used for c-di-GMP production. In a follow-up assay, a GFP-based reporter confirmed these differences in both growth and c-di-GMP production.

These results suggest that certain *wspA* mutations lead to high c-di-GMP levels that may activate secondary biofilm-related pathways, such as Pga, potentially revealing a larger function of the Wsp pathway and the *wspA* gene itself.

Inhibition of Autophagy Effects on Cellular Iron Levels in CCNE1 HGSOC Cells

Scholar: Ava Miller

High School: Plum Senior High School, Plum, PA

Lab: Katherine M. Aird, PhD

Mentor: Naveen Kumar Tangudu, PhD

Site: Women's Cancer Research Center

Background: High-grade serous ovarian carcinoma (HGSOC) is a subtype of epithelial ovarian cancer (OC) that is the most aggressive and common, representing approximately 70% of all cases. Approximately 20% of HGSOCs have cyclin E1 (CCNE1) amplification which corresponds to poor patient outcomes. This correlation is due, in part, to the fact that CCNE1-high HGSOCs have *de novo* resistance to standard-of-care therapy. Dr. Tangudu is exploring alternative therapies for treating CCNE1-high HGSOCs. Interestingly, iron metabolism is elevated in ovarian cancer, and tumor-initiating cells within HGSOCs exhibit higher levels of cellular iron. However, it remains to be investigated whether this increase is due to iron storage proteins or the labile iron pool. In this project I specifically looked at the cellular process, ferritinophagy, to explore if the inhibition of this autophagy would decrease the iron levels in CCNE1-high ovarian cancer cells. All in relation to the idea that iron is important in cell proliferation and tumor progression, making it a promising target to treat cancer.

Methods: Western blot experiments were performed on three types of samples: HGSOC samples, CCNE1-high HGSOC samples, and CCNE1-high HGSOC samples treated with bafilomycinA1 (bafA1), which is an inhibitor of the ferritinophagy process or iron chelator (deferoxamine, DFO). Western blots are a technique for protein analysis. The proteins were denatured and negatively charged. The proteins were then loaded into a well atop an acrylamide gel. An electrical current was passed through the gel, causing the proteins to migrate to the bottom of the wells. In addition to the proteins, a ‘ladder’ was also run. A ‘ladder’ is designed to estimate protein molecular weight. The results from the gels were transferred to a membrane that allowed them to be analyzed in comparison with the ladder. The analyte signal for ferritin (the blood protein that contains iron) was recorded. The analysis was conducted in this way to measure a decrease in iron levels resulting from an increase in ferritin level in CCNE1-high samples.

Results: The results of the western blots were observed through chemiluminescence detection. The bands for ferritin are compared in the HGSOC samples, CCNE1-high HGSOC samples, and CCNE1-high HGSOC samples treated with bafA1 or DFO. There was an increase in ferritin level in CCNE1-high HGSOC samples treated with bafA1 compared to the other samples.

Conclusion: When comparing the results, significant ferritin increases could be seen within the bafA1 treated cells. This shows that labile iron levels in the cell can be decreased by inhibiting the autophagy process ferritinophagy. CCNE1-high HGSOC cells accumulate labile iron pools via degradation of ferritin.

Towards a Comprehensive Variant Effect Map for Polycystin-2 Using the LABEL-seq Platform

Scholar: Avery Mills

High School: The Ellis School, Pittsburgh, PA

Lab: Frederick (Fritz) P. Roth, PhD

Mentor: Warren van Loggerenberg, PhD

Site: Computational Biology

Abstract: Polycystin-2 (PC2), encoded by the gene *PKD2*, regulates cell growth and apoptosis. Genetic variations of PC2 are known to cause Autosomal Dominant Polycystic Kidney Disease (ADPKD), the most common inherited kidney disease, in 15% of patients. However, many disease-associated PC2 variants remain unclassified or unidentified, contributing to the ongoing "variant of uncertain significance" crisis. Multiplexed assays of variant effects (MAVEs) have historically been employed to address this challenge by testing the functional impact of nearly all possible amino acid substitutions. Despite their effectiveness, MAVEs are often limited to single-function assays and require protein-specific optimization. Here, we propose implementing LABEL-seq, a platform for multiplexed protein profiling—including abundance, activity, and intracellular interactions—to evaluate the function of all possible missense variants in PC2. Towards this, we have adapted the LABEL-seq platform to be Gateway-compatible, enabling cDNA libraries to be transferred to the expression vector via *en masse* Gateway LR reactions. A 'truth set' of six pathogenic variants a single benign variant has been generated using site-directed mutagenesis, setting the stage for validating the LABEL-seq abundance assay in human cell lines. When scaled to all possible amino acid substitutions in PC2, this approach will yield a comprehensive 'variant effect map' to enable more rapid and accurate diagnosis of ADPKD.

Title: The removal or overexpression of APOC3's affect on cardiovascular health
Scholar: Luke Morcos
High school/College/City/State: Franklin Regional High School, Pittsburgh, PA
PI of group/lab: Dr. Ali Kohan
Mentor(s): Rachel Wills
Site: ICI

Intro: APOC3 is a protein that regulates triglyceride levels in the blood. Too much of this gene in the body has been shown to increase triglyceride levels. This led to the question: how does the removal or overexpression of APOC3 affect cardiovascular health? By removing or overexpressing the APOC3 gene in mice, we can see the effect on cardiovascular health. In order to do this, we needed to obtain an APOC3 KO mouse (which was determined by genotyping) and view the triglyceride levels in their blood In comparison to the WT and TG APOC3 mice.

Methods: To obtain the mice with the human APOC3 gene, we had to breed the mice. Then we determined who had it by genotyping. We then ran a PCR to amplify the DNA and see which mice were the TG mice (Mice with human APOC3 gene added) we are looking for. We then run a Qpcr to determine the difference in expression between the genes that affect cardiovascular health in the samples with and without the APOC3 gene. Finally, we run a triglyceride assay to quantify the amount of triglyceride in each of the blood samples, telling us the effect of removing or overexpressing the APOC3 gene.

Results: Our triglyceride assay results showed that overexpressing the APOC3 gene led to higher levels of triglyceride in the blood, while the removal of the APOC3 gene led to less triglyceride in the blood.
Conclusion: In conclusion, more APOC3 in one's body causes more triglyceride in the blood. This results in worsened cardiovascular health. Decreasing the prevalence of this gene would cause better cardiovascular health and could help patients who have heart disease or other diseases caused by high triglyceride levels.

Hierarchical Address Event Routing for Large-Scale Communication and Increased Flexibility in Spiking Neural Networks

Lucia Nanda[1] and Inhee Lee[2], PhD.
[1]Billerica Memorial High School, Billerica MA; [2]University of Pittsburgh, Pittsburgh PA

Abstract *Achieving scalable communication and synaptic flexibility in large-scale spiking neural networks (SNNs) remains a major challenge. This project investigates Hierarchical Address Event Routing (HiAER), an architecture that combines Address-Event Representation (AER), multiple routing nodes, and a hierarchically partitioned network. HiAER is assessed for its ability to scale communication across thousands of neurons, support dynamic reconfiguration, and improve SNN performance. We implemented and compared two SNN models to evaluate the architecture's effectiveness.*

Introduction Spiking neural networks (SNNs), computing systems composed of biologically inspired neurons that emit discrete action potentials ("spikes"), have a wide range of applications in neuromorphic computing, robotics, event-based vision, and low-power artificial intelligence [1]. Traditional SNN configurations often implement direct point-to-point (P2P) connectivity between neurons, forming flat or spatially organized layers. However, this setup frequently encounters bandwidth limitations, making it inefficient for large-scale implementations. HiAER introduces a tree-like hierarchical configuration designed to address these communication bottlenecks. It uses Address-Event Representation (AER), a protocol in which each spike is encoded as a packet containing the neuron's unique address and the time of emission. HiAER organizes neurons into independent groups called cores, adds hierarchical layers of routing nodes, and introduces relay neurons that forward spikes between these layers. Each router accesses a Synaptic Routing Table (SRT), a programmable file encoding synaptic connectivity through quadruplets of the form (A_{pre}, A_{post}, w, d), representing pre- and post-synaptic IDs, synaptic weight, and axonal delay [2]. This study explores HiAER's impact on scalability, latency, and flexibility in SNN communication.

Methods Two spiking neural network (SNN) models were developed in Python: a flat model implementing direct P2P connectivity, and one based on the HiAER framework. The flat model was chosen as a baseline not for its scalability but because it represents a conventional, straightforward architecture often used in simpler or non-optimized SNNs. This contrast helps isolate the impact of hierarchical routing on communication efficiency and latency as network size increases. Both models represented neurons, spikes, and routing logic using Python objects and employed time-stepped simulations with identical input parameters to ensure fair comparison. Simulation parameters included total runtime, number of neurons, firing rates, and synaptic connectivity. Parameters were derived from user input as well as SRT files. During execution, real-time spike event timings and latencies were recorded for post-simulation analysis.

Results When simulated with small networks (fewer than 500 neurons) and limited connectivity, both the flat P2P and HiAER models yielded similar results, with the flat model showing slightly better latency due to its simplicity (Figure 1). However, as network size and synaptic density increased, the flat model's performance deteriorated significantly. For instance, in a network of 10000 neurons with 500 synaptic connections per neuron, the flat model exhibited spike latencies up to 500 microseconds (μs), while HiAER maintained latencies in the 1-200 μs range (Figure 2). These differences are attributed to routing congestion and lookup overhead in the flat model, whereas HiAER's hierarchical relay-based structure helped distribute routing workload and reduce bottlenecks.

Discussion The results demonstrate that HiAER provides tangible performance benefits in large-scale SNNs by reducing communication latency and improving scalability. Although the hierarchical routing introduces minor overhead in small networks, the architecture significantly outperforms flat connectivity in systems with high neuron and synapse counts. The flexibility of the SRT files also enables smooth network reconfiguration and modular expansion, which is crucial for experimental and application-specific SNNs. Future work may focus on refining HiAER's routing algorithms through deeper hierarchical layering and optimized partitioning, as well as on hardware-level integration with event-driven sensors and adaptive online learning systems.

a) b)

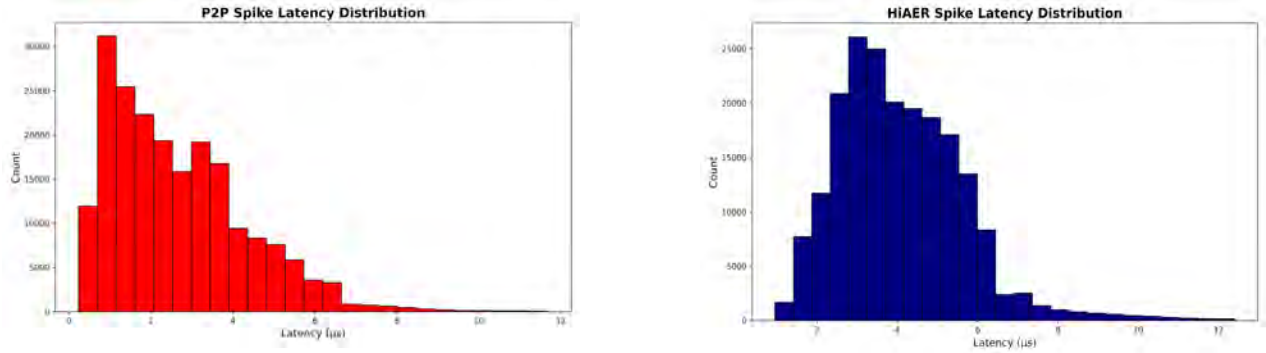

Figure 1. Distributed spike latency in a 128-neuron network with a uniform fan-out of 8 post-synaptic connections per neuron (connections/neuron), sustaining 2.048×10^5 synaptic events per simulated second (synaptic events/s): (a) flat model, (b) HiAER model (2-level hierarchy, *fan-out = 4, d = 0*). Data was collected over 1 simulated second.

a) b)

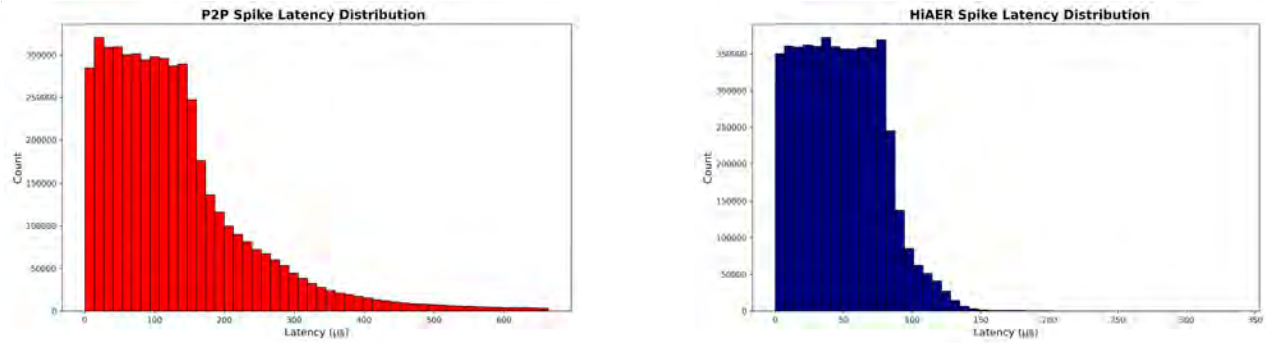

Figure 2. Distributed spike latency in a 10000-neuron network with a uniform fan-out of 500 connections/neuron, sustaining 5×10^6 synaptic events/s: (a) flat model, (b) HiAER model (2-level hierarchy, *fan-out = 4*, *d = 0*). Data was collected over 1 simulated second.

References

1. Yamazaki K, Vo-Ho VK, Bulsara D, Le N. *Spiking Neural Networks and Their Applications: A Review*. Basel, Switzerland: MDPI; 2022.
2. Park J, Yu T, Joshi S, Maier C, *Cauwenberghs G. Hierarchical Address Event Routing for Reconfigurable Large-Scale Neuromorphic Systems*. IEEE Trans Neural Netw Learn Syst. 2017;28(10):2392-2405. doi:10.1109/TNNLS.2016.2572164.

Allostasis and Cancer Outcomes (ALLEGIANT)

Husniya Nurmuhammad, Margaret Rosenzweig, PhD, FNP-BC, Ruth A. Modzelewski, PhD
City Charter High School, Pittsburgh, PA; University of Pittsburgh Hillman Cancer Center Academy, Pittsburgh, PA

Abstract. This study evaluates the associations between lifetime stress and perceived discrimination and the ability to receive the full dose of the first treatment for patients with breast, colorectal, and lung cancers. Longitudinal data collection assessed stress levels, perceived discrimination, resilience, allostatic load (AL), telomere length (TL), and symptom distress at baseline, with the primary outcome of treatment tolerance (treatment prescribed/treatment received) at 6 months. We hypothesize that higher stress and allostatic load (AL) at baseline correlates to poor treatment tolerance and subsequent dose modifications.

Introduction Black and more highly deprived patients with cancer in Western Pennsylvania experience poor outcomes in cancer treatment, including higher symptom distress and dose modifications. The mechanism may be that biological weathering from chronic stress (measured through allostatic load) may directly compromise treatment tolerance. The ALLEGIANT Allostasis, Cellular Aging, and Cancer study addresses this gap by examining how social determinants, stress, financial toxicity, poor quality of life, and perceived discrimination become biologically embedded, compromising the patients' ability to complete prescribed cancer therapies.

Methods: This is an interim analysis of an ongoing study. Biological measures included AL scores (composite of blood pressure ≥130/85 mmHg, BMI ≥30 kg/m², HbA1c ≥6.5%, HDL <50 mg/dL, and C-reactive protein >10 mg/L) and telomere length analysis via Southern blot. Behavioral instruments with established reliability (Perceived Stress Scale α=0.85, Everyday Discrimination Scale α=0.88) captured stress experiences. The Resilience Scale measures the ability to withstand stress. Financial toxicity measures financial concerns during cancer treatment. The Functional Assessment of Cancer Therapy measured quality of life and symptoms. Neighborhood deprivation was quantified and dichotomized using ADI. The chart review measured the percentage of first therapy received. Statistical analysis employed t-tests with $p<0.05$ significance thresholds, Fisher's exact tests for categorical outcomes, and Pearson correlation analysis.

Results: We enrolled 67 patients (21.9% Black/African American, 78.1% White) from UPMC Hillman Cancer Center clinics. Black patients (92%) resided in high-ADI neighborhoods compared to 38% of White. At baseline, Black participants reported significantly higher lifetime/daily discrimination and financial toxicity scores. High vs. low deprived patients report worse quality of life. AL and C-Reactive protein scores showed no racial differences, but patients from more highly deprived areas had higher allostatic load than those from less deprived areas. Resilience scores were higher for Black vs.White patients. For treatment tolerance, (n=48), n=16 (33%) had dose modifications, with no racial or ADI differences. There was a significant correlation between perceptions of lifetime discrimination and dose modifications.

Discussion Our findings demonstrate that racial and economic differences exist at baseline for cancer treatment for perceived stress, discrimination, quality of life, and allostatic load. Resilience is higher at baseline for Black vs. White patients. These baseline differences impacted treatment intensity for perceived discrimination. Among Black patients, resilience may be a learned coping behavior that buffers the effects of such lifetime experiences. We will share these findings with a community forum. We aim to identify modifiable factors to improve outcomes.

Mesenchymal Stem Cell-Derived Extracellular Vesicle and Shear Stress Effect on Endothelial Colony-Forming Cells

Scholar: Angie Odeniyi
High School/City/State: Roy C. Ketcham Senior High School, Wappingers Falls NY
PI of group/lab: Justin Weinbaum, PhD
Mentor(s): Amanda Pellegrino, RN, Kiran Mcloughlin, PhD
Site: Technology Drive X

Background: Endothelialization is the formation of the endothelial cell (EC) monolayer on blood contacting surfaces. Circulating endothelial colony forming cells (ECFCs) contribute to this by attaching and differentiating into ECs. ECFCs differentiate into ECs under conditions of shear stress or in the presence of proteins like vascular endothelial growth factor (VEGF). Mesenchymal stem cell-derived extracellular vesicles (EVs) are nanoparticles secreted from parent cells that contain proteins and RNA, including VEGF. Shear stress is the frictional force that acts on the endothelium via blood flow. We hypothesize that EVs and shear stress, alone or in combination, will increase ECFC differentiation and proliferation.

Methods: For all experiments, ECFCs and ECs (as a control) were treated with Dulbecco's Phosphate Buffered Saline (DPBS), 1e9 and 3e9 particles (P)/mL EVs, and full supplemented media (full supp) under static and dynamic conditions using an orbital shaker for 48hrs, unless stated otherwise. AlamarBlue proliferation assay was run to determine cell growth rate in response to treatments. The dynamic plate was then fluorescently stained after 96hrs to visualize von Willebrand factor (vWf) and VE-Cadherin. 3D fibrin gel tube formation assays were run to observe vasculogenesis after treatment. Fluorescent imaging of phalloidin was then used to quantify vascular area using Fiji. Preliminary flow cytometry was run to determine the percentage of cells expressing CD31, CD34, and VEGF receptor 2 (VEGFR2) after 48hrs of DPBS or full supp under static conditions. Statistics were determined by Graphpad Prism v10.5.

Results: In static conditions at 48h, ECFCs exhibited a significant increase in proliferation when treated with 1e9 P/mL ($P=0.0205$) and 3e9 P/mL ($P=0.0115$) EVs compared to DPBS control. ECs exhibited a significant increase in proliferation under static conditions when treated with 3e9 P/mL ($P=0.0030$) EVs compared to DPBS controls. In dynamic conditions, ECFCs exhibited a significant increase in proliferation at 48h when treated with 3e9 P/mL ($P=0.0411$) EVs. ECs did not significantly respond to EVs in dynamic conditions. Immunofluorescent staining of the cells showed the presence of vWf within cells and VE-Cadherin junctions. For tube formation, there was no significant difference between groups. Preliminary flow cytometry demonstrated altered endothelial cell profiles between ECFCs and ECs based on CD31 and CD34 expression.

Conclusion: The study indicates that EV treatment and shear stress affected ECFCs proliferation but not tube formation. ECFC proliferation showed an overall increase under dynamic + EV conditions. Tube formation results had high variability within groups, possibly due to the analysis process. Flow cytometry demonstrated expected baseline differentiation markers needed before testing if EVs affect ECFC differentiation. Future directions will work to optimize 3D tube formation assays and EV treatment time, and investigate ECFC maturation mechanisms using flow cytometry and qPCR.

Figures:

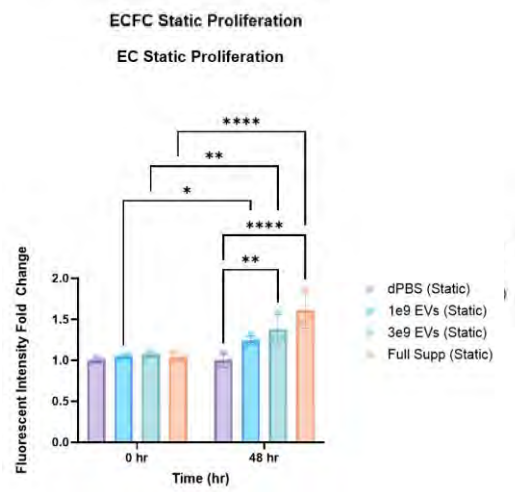
ECFC Static Proliferation
EC Static Proliferation
Fluorescent Intensity Fold Change
2.0
1.5
1.0
0.5
0.0
0 hr
48 hr
Time (hr)
****
**
*
****
**
dPBS (Static)
1e9 EVs (Static)
3e9 EVs (Static)
Full Supp (Static)

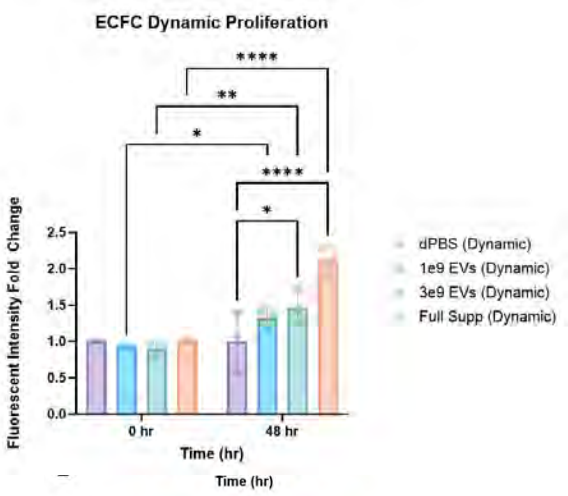
ECFC Dynamic Proliferation
Fluorescent Intensity Fold Change
2.5
2.0
1.5
1.0
0.5
0.0
0 hr
48 hr
Time (hr)
Time (hr)
****
**
*
****
*
dPBS (Dynamic)
1e9 EVs (Dynamic)
3e9 EVs (Dynamic)
Full Supp (Dynamic)

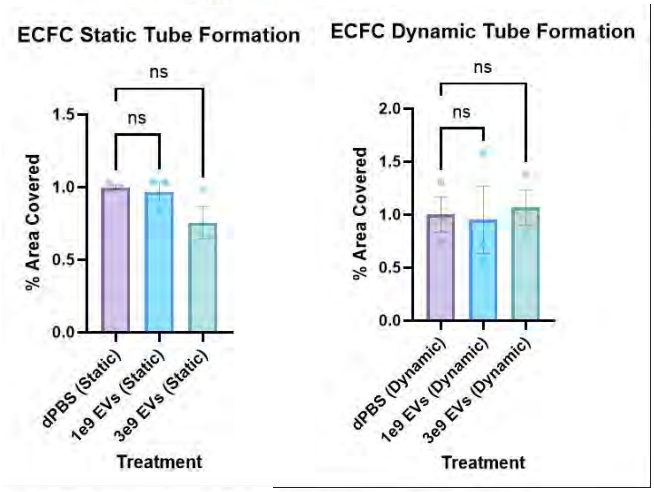
ECFC Static Tube Formation
ECFC Dynamic Tube Formation
% Area Covered
1.5
1.0
0.5
0.0
ns
ns
dPBS (Static)
1e9 EVs (Static)
3e9 EVs (Static)
Treatment
% Area Covered
2.0
1.5
1.0
0.5
0.0
ns
ns
dPBS (Dynamic)
1e9 EVs (Dynamic)
3e9 EVs (Dynamic)
Treatment

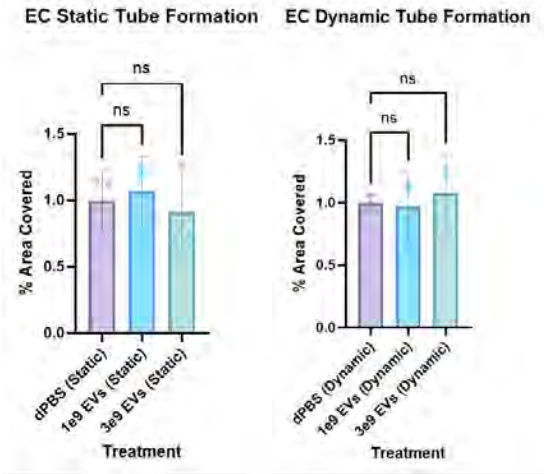
EC Static Tube Formation
EC Dynamic Tube Formation
% Area Covered
1.5
1.0
0.5
0.0
ns
ns
dPBS (Static)
1e9 EVs (Static)
3e9 EVs (Static)
Treatment
% Area Covered
1.5
1.0
0.5
0.0
ns
ns
dPBS (Dynamic)
1e9 EVs (Dynamic)
3e9 EVs (Dynamic)
Treatment

Identifying protein relations between Autism and other Disorders

Asher Peng, M. Ganapathiraju

Background

Autism Spectrum Disorder (ASD) is not just an isolated condition—it often co-occurs with other neurodevelopmental and psychiatric disorders. These include ADHD, cerebral palsy, intellectual disability, epilepsy, anxiety, and eating disorders. While each disorder may appear distinct, recent research suggests they may share similar biological roots, including overlapping genes and protein networks active in brain areas like the hypothalamus, cerebellum, and amygdala. Understanding these overlaps may help explain why these disorders frequently occur together and guide better diagnostic and treatment approaches.

Methods

We used public gene databases and the database generated by Dr. Ganapathiraju to explore these connections. Using Python, we created protein interaction networks (interactomes) for ASD and related conditions. Data sources included SFARI Gene, BioGRID, and Dr. Ganapathiraju's curated dataset. We analyzed co-occurrence data from published studies, focusing on common gene traits and the number of interacting proteins across conditions.

Results

Protein interaction mapping revealed that ASD shares hundreds of protein interactors with conditions like eating disorders and anxiety. For example, ASD and anxiety shared 56 genes and 675 protein interactors, while ASD and eating disorders shared 49 genes and 580 interactors. These overlaps suggest that the same molecular pathways may contribute to different symptoms in each disorder. Genes such as NECAB2, PKM2, and FLNA—found in autism-specific network studies—are part of these shared pathways.

Conclusion

Our findings support the idea that ASD is biologically connected to other developmental and mental health disorders through shared genes and protein networks. Instead of being viewed independently, autism may be better understood as part of a larger system of interconnected conditions. This understanding could lead to earlier diagnosis and more targeted, whole-person care strategies.

Title: Development of a Robust Breast Cancer Liver Metastasis Mouse Model

Scholar Name: Sunny Pham

High School: The Ellis School, Pittsburgh, PA

PI: Dr. Michelle Williams

Mentor(s): Angelica Phan

Site: Women's Cancer Research Center

Background: Breast cancer (BC) is one of the most common malignant cancers in women. BC can travel or metastasize throughout the body and commonly spreads to the liver. However, breast cancer liver metastasis (BCLM) remains understudied. The Williams lab has identified heme oxygenase-1 (HO-1) as a possible driver of BCLM. We are developing a reliable mouse model of BCLM to test the effects of targeting HO-1 on liver metastasis. We injected parental mouse mammary carcinoma cells (66Cl-4-luc-ZSgreen) into the portal vein and spleen of mice. The resulting liver metastases were developed into cell lines (MW01 and MW03, respectively). I am evaluating the applicability of the 66Cl-4-luc-ZSgreen, MW01, and MW03 cell lines as possible BCLM models. I hypothesized that these cell lines will exhibit similar growth rates, colony-forming abilities, and HO-1 expression.

Methods: Cell viability and colony growth were assessed with a 2D and 3D growth assay. HO-1 expression was determined with a Western Blot. The 2D colony assay was repeated with Tin Mesoporphyrin (SnMP) and Cobalt Protoporphyrin (CoPP), a HO-1 inhibitor and activator respectively.

Results: The 2D growth assay revealed that MW03 cells were ~50% less viable than 66Cl-4-luc-ZSgreen and MW01 cells. MW03 cells grown in 3D formed the fewest number of colonies, but their colonies size was the largest. The Western Blot showed that MW03 cells had twice as much HO-1 than the parentals. Conversely, the MW01 cells had about half of the parental's HO-1 expression. Lastly, the drug treatment assay revealed that MW01 cells were the most sensitive to SnMP.

Conclusion: The 66Cl-4 and MW01 cell lines exhibited faster growth rates and stronger colony-forming abilities than the MW03 cell line. These results suggest that the MW01 line would be a better candidate for further BCLM model development, and to test if SnMP inhibits liver metastasis formation.

Investigating the effectiveness of Vaccinia Virus on the formation of tertiary lymphoid structure in tumor mouse models

Anabella Phelps, Caroline Sweeney, Hye Mi Kim, Tullia C. Bruno
Mt. Lebanon High School, PA; University of Pittsburgh Hillman Cancer Center Academy, Pittsburgh, PA

Spatial analysis of subcutaneous and orthotopic murine model tissue samples explores whether treatment with oncolytic virus (OV) with transgenes of interest enhances the formation and organization of tertiary lymphoid structures within tumors, leading to new potential immunotherapies for the treatment of NSCLC.

Lung Adenocarcinoma (LUAD) is the most common type of non-small cell lung cancer, having a 5-year survival rate between 15-20%. Within this cancer, a promising target for therapy lies in tertiary lymphoid structures (TLS), ectopic immune structures that arise in sites of chronic inflammation. Acting as a hub for B cell and T cell activation and proliferation, the presence of TLS with germinal centers (GC) has shown prognostic benefit, including in LUAD patients. In order to induce the infiltration of these immune structures within tumors, it is important to understand what factors drive TLS formation and maturity. To understand the factors driving TLS formation, our lab evaluated TLS complexity in human LUAD using multispectral imaging and spatial transcriptomics. Due to the heterogenous nature of TLS, we have found that in LUAD patients TLS show incomplete expression of factors like LIGHT/LTβ, CXCL13, CD40 ligand (CD40L), and IL-21. In order to induce TLS formation and maturity, an oncolytic virus was engineered to deliver these factors while generating immunogenic antigens and releasing inflammatory cytokines to support TLS formation within tumors. ELISA analysis initially verified that OV can express key factors in LLC and FVBW-17 cell lines. The assay showed an increase of key factors like LIGHT/LTβ, CXCL13, CD40 ligand (CD40L), and IL-21 with the addition of oncolytic virus with transgenes. To further evaluate TLS formation and tumor reduction, we employed a subcutaneous syngeneic tumor murine model. LLC and FVBW-17 cell lines were implanted in mice and subsequently received vaccinia virus treatment; tumor collection occurred on day 11. Analysis of LLC mice exhibited a significant decrease in growth rate and volume of tumors. While FVBW-17 did not show significant response to treatment; further analysis of IHC images revealed infiltration of CD-19 positive B cells within the tumor. To transition to an orthotopic model, a new syngeneic lung cancer model is vital to further evaluate OV-mediated TLS modulation: KPAR, developed through CRISPR/Cas9-targeted gene deletion. Initial IHC results of orthotopic models without OV treatment confirmed the expression of CD-19 positive B cell aggregates within KPAR mouse model, making KPAR a more viable option than FVBW-17 due to its resistance to treatment in subcutaneous models. To further validate and explore the interaction between OV and TLS formation, we must transition to orthotopic models with OV treatment delivery via tail vein and analyze with multispectral staining and flow cytometry. These studies aim to provide deeper insights into TLS biology and support the development of novel immunotherapeutic strategies for NSCLC, potentially offering improved treatment options for patients.

References

1. Boumelha, Jesse et al. “An Immunogenic Model of KRAS-Mutant Lung Cancer Enables Evaluation of Targeted Therapy and Immunotherapy Combinations.” *Cancer research* vol. 82,19 (2022): 3435-3448. doi:10.1158/0008-5472.CAN-22-0325
2. Ng, Kevin W et al. “Antibodies against endogenous retroviruses promote lung cancer immunotherapy.” *Nature* vol. 616,7957 (2023): 563-573. doi:10.1038/s41586-023-05771-9
3. Schumacher TN, Thommen DS. Tertiary lymphoid structures in cancer. Science. 2022;375:eabf9419. doi: 10.1126/science.abf9419.

Title: Exogenous RFP as a tool to study cellular origins of MBV cargo

Scholar: Rose-Carlie Pierre

High School/College/City/State: Pittsburgh Obama Academy, Pittsburgh, PA

PI of group/lab: Dr. Melanie Scott, MD, PhD

Mentor(s): Dr.Yekaterina Krutsenko, PhD

Site: Surgery

Introduction: Matrix-bound nanovesicles (MBVs) are nanosized (~50–300 nm), membrane-bound vesicles tightly embedded within the extracellular matrix (ECM). MBVs are distinct from other extracellular vesicles due to their location and unique cargo. MBVs play important roles in tissue remodeling, immune regulation, and maintaining tissue homeostasis. MBVs can be found in various tissues, including the liver, and are believed to act as a reservoir for bioactive signaling molecules, such as proteins, lipids, and RNA. However, the primary cellular origin of MBVs remains largely unknown. To explore whether MBV cargo reflects the identity of the originating cell, we investigated whether exogenously expressed fluorescent proteins, such as red fluorescent protein (RFP), can be incorporated into MBVs. In future studies, this approach could help trace the cellular source of MBV content, using cell-specific expression of RFP.

Methods: MBVs were isolated from the livers of CMV-Cre, RFP-floxed mice using collagenase digestion, followed by an established centrifugation protocol. The yield and purity of the isolated MBVs were assessed using nanoparticle tracking analysis (NTA). Cultured RAW 264.7 macrophages were treated with MBVs derived from the RFP-positive livers at a concentration of 1×10^7 particles/mL and incubated for 2 hours. After incubation, cells were fixed with 2% paraformaldehyde and stained with anti-RFP antibody. Nuclei were counterstained with DAPI, and cytoskeleton with phalloidin. Confocal imaging was used to assess the presence of MBVs within macrophages.

Results: Confocal imaging showed detectable RFP signal within RAW macrophages exposed to MBVs from RFP-positive livers, while no signal was observed in macrophages treated with control media.

Conclusion. These findings suggest that exogenously expressed fluorescent proteins can be incorporated into MBV cargo and detected after uptake by recipient cells. This supports the use of cell-specific RFP expression in future studies aimed at uncovering the cellular origins and functional properties of MBVs in the liver and other organs.

Understanding the Role of AP-2β in Mammary Epithelium and Applying it to Invasive Lobular Carcinoma

Scholar: Shamael Rahamani
High School/College/City/State: The Ellis School, Pittsburgh, PA
PI of group/lab: Adrian Lee, Steffi Oesterreich
Mentor: Christopher Merkel
Site: Women's Cancer Research Center

Introduction

Invasive Lobular Carcinoma (ILC) is characterized by discohesive morphology of single file strand shaped tumors. This is due to the loss of the protein E-Cadherin which plays a pivotal role in cell-adhesion. Patients with ILC do not have targeted therapies for this disease and tend to have worse long term outcomes. In ILC, the overexpression of AP-2β, which is a known transcription factor that helps with early development in embryogenesis, can possibly combat the loss of E-cadherin. This alludes that AP-2β has an understudied involvement in ILC.

Hypothesis

We are studying the expression of AP-2β and other proteins expressed in the ducts of mammary fat pads of healthy mice to create a baseline to compare cells that are capable of tumorigenesis.

Research Methods

We used indirect immunofluorescence to visualize cells that have an expression of AP-2β in the brain, lung, kidney, liver, to confirm that the staining of AP-2β was specific as well as the targeted mammary fat pad. We also did PCR and genotyping to expand the mouse model that will have a conditional overexpression of AP-2β that will be used in further experimentation.

Results

When imaging AP-2β, the staining was specific and was expressed within the luminal epithelial tissue surrounding the mammary ducts as expected. The antibodies for CK8/18 and HER2 did not directly target these proteins and will need further experimentation. E-Cadherin, CK14, and GATA3 were expressed with specific staining. E-Cadherin was expressed in all cells within the mammary ducts and GATA3 was only expressed within the luminal epithelium tissue and overlapped with the AP-2β staining. CK14 however, was only expressed in the myoepithelium cells.

Conclusion

These results show the expression of AP-2β and GATA3 are commonly co-expressed in ductal luminal epithelium; however, CK14 was expressed in myoepithelium. This will allow for further experimentation about the importance of the involvement of other luminal proteins such as GATA3 and the loss of E-Cadherin and how these interact with AP-2β in ILC formation.

Trem1-Deficient Macrophages Impair HSC Homeostasis via Eotaxin-2 Mediated Disruption of the Bone Marrow Niche

Scholar: Hussain Raza

High School: Gateway High School, Monroeville, Pennsylvania

PI: Wei Du, MD, PhD

Mentors: Jian Xu, PhD; Logan Sund B.S.

Site: Cancer Biology

Macrophages are specialized immune cells that play a central role in host defense and inflammation. It is also known that BM microphages support HSC retention, survival, and quiescence through direct cell-cell interactions and the secretion of signaling molecules, therefore maintain hematopoietic stem cell (HSC) homeostasis within the bone marrow (BM). Recent studies show that macrophage-specific deletion of Trem1, an immune receptor known to regulate macrophage polarization, leads to HSC dysfunction using a novel *Trem1f/f;Csf1Rcre* mouse model. This is characterized by increased apoptosis and aberrant HSC quiescence. Cytokine profiling revealed a significant reduction in Eotaxin-2 (CCL24) in *Trem1*-deficient bone marrow, which may be a key factor linking the HSC defects observed in *Trem1f/f;Csf1Rcrde* mice. These findings were validated using another macrophage specifically Trem-1 knockout mouse model (*Trem1f/f;LysM-Cre*). To explore how Eotaxin-2 influences hematopoiesis in BM, we investigated changes in niche components using immunostaining for endothelial cells (MECA 32), mesenchymal stromal cells (Leptin Receptor), and Osteolineage cells (Collagen I). Our data suggested that Trem1-deficient macrophages disrupt the structural and functional integrity of the HSC niche, particularly through altered interactions between HSC and niche stromal elements. Furthermore, analysis shows that the deletion of Trem1 in macrophages alters HSC-niche interaction in the bone marrow microenvironment. In summary, our study identifies a novel macrophage Eotaxin-2 niche axis critical for HSC maintenance and highlights a potential therapeutic target for preserving hematopoietic function under inflammatory or pathological conditions.

Classification of the S-phase cells using a convolutional neural network

Allison Shi[1, 3], Gaohan Yu[2], Lu Yong[3], Zheng Zhiqian[3], Jianhua Xing[2, 3]
1. Shady Side Academy, Pittsburgh, PA; 2. Department of Physics and Astronomy, University of Pittsburgh, Pittsburgh, PA; 3. Department of Computational and System Biology, University of Pittsburgh, Pittsburgh, PA

Abstract

The development of live-cell imaging techniques allows researchers to access real-time protein dynamics. However, tracking cell-cycle progression remains a challenge; PCNA protein is a robust marker for distinguishing cell cycle phases. This study creates two convolutional neural networks (CNN) with different model architectures to predict if a PCNA cell image is in the S-phase of the cell cycle. Overall, the CNN with three convolutional layers had better performance compared to the two layered network.

Introduction

A convolutional neural network (CNN) is a popular deep learning method commonly used in computer vision fields[1,2]. These networks contain convolutional layers that apply a number of learnable filters to the input data. The CNN can overall detect shapes, textures, edges, and patterns within an image. The purpose of this study was to train a CNN that can accurately predict whether a proliferating cell nuclear antigen (PCNA) cell nucleus image is in the S-phase or not. PCNA is a protein crucial to DNA replication and repair in cells[3]. It helps DNA polymerases move along the DNA strand, coordinates various DNA repair processes, and is involved in cell cycle control and chromatin assembly.

Methods

This study uses the python programming language. The code was run with T4 GPU on google colab. We used Cellpose-SAM[4] to segment PCNA cells images from MCF10A cells. To generate a ground-truth data set, we manually grouped images into two classes: S-phase, and non-S-phase. We then cropped each cell using their cell nucleus masks and separated them into a file for the CNN to use. The raw image groups of non-S-phase to S-phase cells had a ratio of 253:144. We applied data augmentation to randomly blur, rotate, and flip these cell images. Each cell image had a total of 16 variants. The final ratio of non-S-phase to S-phase cells was 4,048:2,304 images. These images were separated into a training and validation dataset. In the training set, the ratio was 3,238:1,843; in the validation set, the ratio was 810:461. We created two CNNs: one with 3 convolutional layers, the other with 2. Both used the same training and validation sets. Each training set had 100 epochs. Finally, we reported the validation losses, accuracy, precision, recall, true negative rate, false positive rate, false negative rate, and F1 score of each CNN model.

Results

The 3-layer CNN outperformed the 2-layer CNN. Its validation metrics had better scores (Table 1). It had a better performance for accuracy, precision, recall, true negative rate, false positive rate, false negative rate, and F1 score.

Discussion

This study shows the capability of analyzing biomedical images using deep learning methods. With only a small set of labeled images and a very light CNN model, we could achieve a decent performance for S-phase classification. The S-phase is especially crucial to research development, as this is when DNA is replicated and genetic information is split evenly. This model can enhance the understanding of DNA synthesis, which can be researched further to prevent DNA mutations like cancer and other genetic abnormalities. Machine and deep learning can analyze large amounts of data from living cells. Live-cell analysis enables researchers to observe more accurate cell functions. Live-cell analysis allows researchers to study the impact of diseases on cells, leading to medicinal discoveries and new preventative methods. There are a few reasons why the 3-layer CNN performed better. Firstly, each layer in a CNN increases the number of parameters during training and minimizes errors. Secondly, adding more layers reduces the risk of underfitting. The 3-layer CNN has better learning capacity and can process complex images with data augmentation which prevents underfitting. Lastly, CNNs recognize patterns in a hierarchical sequence. Earlier layers process simple features while later layers combine what they learned into intricate shapes and object parts, leading to more accurate predictions.

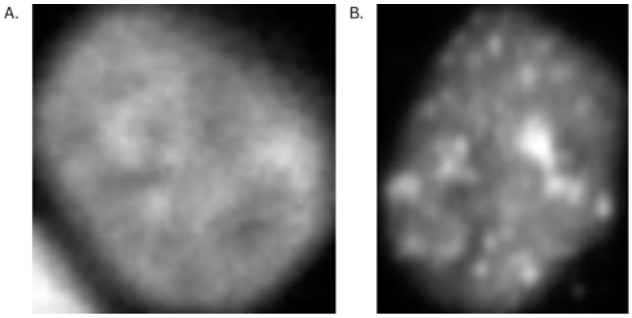

Figure 1: MCF10A PCNA Cell Nucleus (A): Non-S-phase; (B): S-phase

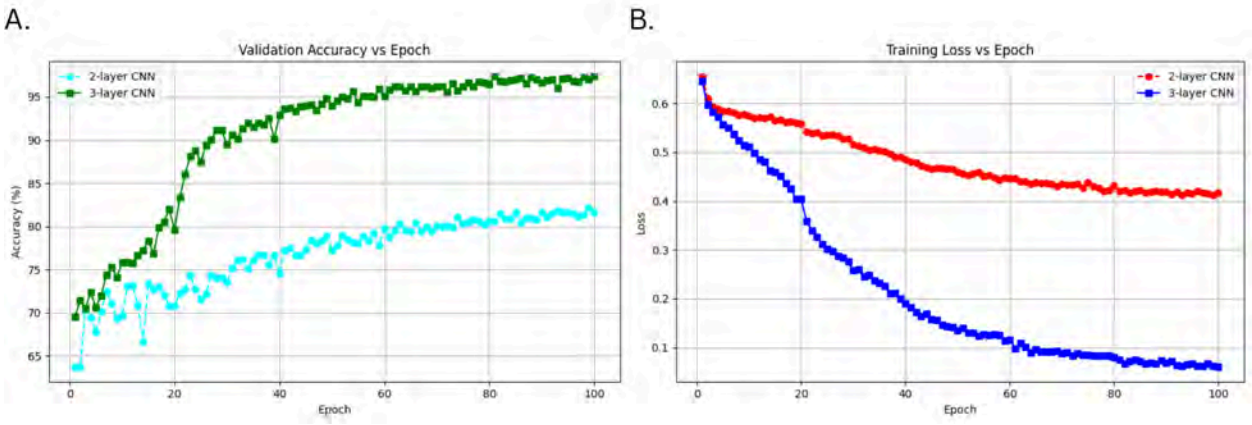

Figure 2. Validation Metric and Training Loss Comparison with each CNN Model (A): Validation Accuracy VS Number of Epochs of both 2 and 3-layer CNNs; (B): Training Loss VS Number of Epochs of both 2 and 3-layer CNNs

Table 1. Validation Metrics for each CNN Model Type

Model Type	Accuracy (%)	Precision (PPV) (%)	Recall/True Positive Rate (%)	True Negative Rate (%)	False Positive Rate (%)	False Negative Rate (%)	F1 Score (%)
3-Layer CNN	97.80	95.58	98.48	97.41	2.59	1.52	97.01
2-Layer CNN	81.75	74.95	74.62	85.80	14.20	25.38	74.78

References

1. Ronneberger, Olaf & Fischer, Philipp & Brox, Thomas. (2015). U-Net: Convolutional Networks for Biomedical Image Segmentation. 10.48550/arXiv.1505.04597.
2. K. He, X. Zhang, S. Ren and J. Sun, "Deep Residual Learning for Image Recognition," *2016 IEEE Conference on Computer Vision and Pattern Recognition (CVPR)*, Las Vegas, NV, USA, 2016, pp. 770-778, doi: 10.1109/CVPR.2016.90.
3. Zerjatke, T., Gak, I. A., Kirova, D., ..., Muller, D., Glauche, I., & Mansfeld, J. (2017). Quantitative Cell Cycle Analysis Based on an Endogenous All-in-One Reporter for Cell Tracking and Classification. Cell Reports, 19(9), 1953-1966..
4. Pachitariu, M., Rariden, M., & Stringer, C. (2025). Cellpose-SAM: superhuman generalization for cellular segmentation. bioRxiv.

Acknowledgements

I would like to sincerely thank and express my gratitude to Prof. Jianhua Xing, Dr. Yong Lu, Gaohan Yu and Zhiqian Zheng who have helped me complete this project by answering my questions and explaining complex topics to me.

Imaging Immune Cells in the Living Eye of Patients with Age-Related Macular Degeneration

Scholar: Alexander B. Small
High School: Hillel Academy of Pittsburgh, Pittsburgh, PA
PI of group/lab: Ethan A. Rossi, PhD
Mentors: Ethan A. Rossi, PhD; Robert L. Draham, PhD
Site: VISION

Background: Age-Related Macular Degeneration (AMD) is the leading cause of irreversible blindness in older adults. Early and intermediate AMD are characterized by drusen, extracellular deposits below the Retinal Pigmented Epithelium (RPE). While drusen can remain stable, their enlargement and collapse often precedes geographic atrophy in late AMD, causing vision loss. Understanding AMD progression is crucial for developing treatments to halt progression as early as possible. Histological studies have shown that immune cells accumulate around large drusen. Here we hypothesized that immune cells may also be active around smaller deposits.
Methods: Our study imaged 13 patients with early and intermediate AMD using multi-modal Adaptive Optics Scanning Light Ophthalmoscopy (AOSLO) with confocal, autofluorescence and non-confocal phase contrast modalities. We observed putative immune cells in 7 of these patients. Cells and drusen were manually measured. Through a systematic approach of analyzing histological reports, clinical studies, and trials, we evaluated various hypotheses for the identity of these objects.
Results: Drusen diameter ranged from 57.4-355.3 μm. Around these drusen, we identified numerous circular (range: 3.8-38.1 μm; mean=11.6 SD=(7.8)), elliptical (major axes: 5.7-87.1 μm; 23.4 (19.7) and minor axes 3.5-34.4 μm; 12.3 (8.2)), and irregularly-shaped phase objects. The size of these structures and their morphologies were consistent with microglial cells.
Conclusion: The high-contrast phase objects around drusen likely represent activated microglial cells, especially the large objects. This suggests that immune responses in AMD may start earlier than expected, with microglial activation around small drusen. Better understanding and monitoring of the inflammatory response to drusen in earlier stages of AMD may offer potential early biomarkers and targets for therapies to slow down or halt AMD in its earliest stages before irreversible vision loss occurs.

Auditory Attention Detection using Common Spatial Patterns Algorithm and Convolutional Neural Networks

Ethan L. Small, Dr. Murat Akcakaya, Yifan Zuo, Richard T. Gall,
Pennsylvania State College

Abstract: This project investigates applying Electroencephalography (EEG) signals for auditory attention detection (AAD) to classify attended speakers in multi-speaker environments. The methodology combines Common Spatial Patterns (CSP) and Convolutional Neural Networks (CNNs), leveraging EEG's temporal and spatial characteristics to improve speaker classification accuracy in complex auditory scenes.

Introduction: Attending to a single speaker in noisy environments is challenging, especially for those with hearing impairments. AAD using EEG offers a promising solution for next-generation hearing aids. This project addresses limitations of traditional AAD methods by combining CSP and CNNs to enhance speaker classification accuracy, aiming to significantly contribute to advanced brain-computer interfaces and dynamically adaptive hearing aids.

Methods: EEG data were acquired from 18 subjects, sampled at 512 Hz, with 60 trials per session. Each trial involved 50 seconds of audio with two distinct speakers (male/female) and varied reverberation levels. Raw EEG underwent preprocessing: 50 Hz notch filter, re-referencing to mastoid channels, 3-32 Hz band-pass filter, and downsampling to 70 Hz. Concurrently, audio speech envelopes were extracted using a gammatone filterbank (150-4000 Hz, 150 Hz increments), followed by Hilbert transform for absolute speech envelopes, a 32 Hz low-pass filter, and downsampling to 70 Hz to match EEG. Both processed speech envelopes and EEG data were normalized.

Results: Classification model performance varied with window lengths (Figure 2). CNN accuracy was 66.7% (1-second window), 69.3% (2-second), and 70.8% (5-second). The combined CNN + CSP model showed an average 8-9% accuracy improvement, yielding 75.3%, 78.1%, and 80.2% for 1, 2, and 5 seconds, respectively. These results indicate CSP significantly enhances speaker classification, with longer window lengths correlating with higher accuracy for both configurations.

Discussion: This project demonstrates the significant potential of machine learning, specifically the combined application of CSP and CNNs, in enhancing AAD using EEG signals. The observed improvements in classification accuracy, particularly with CSP integration, highlight the methodology's effectiveness. These findings have profound implications for developing advanced assistive technologies like next-generation hearing aids that can dynamically adapt to and isolate attended speech in complex, noisy environments, improving communication and quality of life for individuals with hearing impairments.

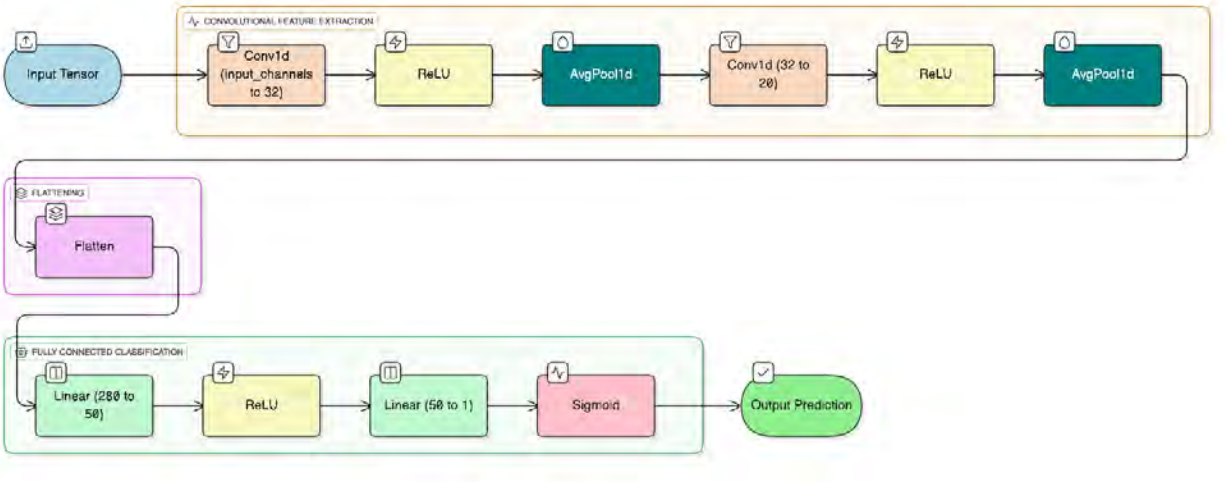

Figure 1. Model Architecture

Window Length	Accuracy (CNN)	Accuracy (CNN + CSP)
1 seconds	66.7%	75.3%
2 seconds	69.3%	78.1%
5 seconds	70.8%	80.2%

Figure 2. Model Results

References

Fuglsang, S. A., et al. EEG and Audio Dataset for Auditory Attention Decoding. 1, Zenodo, 15 Mar. 2018, doi:10.5281/zenodo.1199011.

Understanding Real-World Eye Movements

Scholar: Aubrey Sudor

High School: Bishop Canevin, Pittsburgh, PA

Lab: Dr. Patrick Mayo

Mentors: Dr. Patrick Mayo

Site: Vision

Studying eye movements helps us understand how the brain processes visual information in real-world settings. The jerky, jumping movement “saccades” and continuous tracking movement “smooth pursuit” are two key types of eye movements we make thousands of times per day. For example, saccades occur when you are reading, smooth pursuits occur when watching a fly moving through the air. While these types of eye movements have been studied extensively in laboratory settings, less is known about how often we make these eye movements in everyday life. Also, it is unclear how our eye behavior changes based on the surrounding environment or task at hand. In this project, we collected over forty hours of eye tracking data from a subject performing a variety of everyday activities, such as walking outdoors, reading, writing, using a computer, scrolling on phone, and more—all while recording natural, unconstrained viewing. The eye tracking data were collected using Tobii Pro Glasses 3, which recorded the focus of gaze and pupil size. We compared various eye movement metrics (e.g., number of saccades, pupil diameter) across four different types of activities. The mobile glasses give us the ability to measure the saccades and smooth pursuits that occur naturally, and identify the real-world stimuli that evoke the visual activities. In the future, this improved understanding of eye behavior in naturalistic settings could help inform the design of more functional and realistic accessibility technologies.

Macrophage and Chronic Inflammation Contribution to Osteosarcoma Prognosis and Survival

Scholar: Christian Tabler

High School/College/City/State: Bethel Park High School, Pittsburgh, PA

PI of group/lab: Dr. Ines Lohse, PhD, Dr. Kurt Weiss, MD

Mentor(s): Dr. Karen Schoedel, MD

Site: Cancer Biology

Abstract

Osteosarcoma is the most common primary malignant bone tumor in children and adolescents, yet outcomes are poor for patients with metastasis.[1] The tumor immune microenvironment (TIME) plays a critical role in cancer progression, but its composition in osteosarcoma, particularly the balance of immune cell subsets, has not been substantially explored.[2] Macrophages are a point of interest in the TIME, as higher M2, or tumor promoting, macrophages are linked to worse prognosis in patients.[3] In the present study, we analyzed a tissue microarrays derived from OS patient cores using Vectra staining, a method for the analysis of multiple biomarkers in tissue sections, including macrophages. We analyzed macrophage subsets (M1/ M2) in the context of patient demographics and treatment history. We observed marked differences in M2/M1 ratios between individual patients as well as between samples derived from primary tumors and metastasis. Indeed, samples in both groups separated into three distinct subgroups with low, medium, and high M2/M1 ratios. Additionally, our results revealed a relationship between low M2/M1 ratios, chronic inflammation, and patient survival. 5 patients survived in the 13-patient group observed. 4 of those 5 patients presented with chronic inflammation comorbidities and low M2/M1 ratios. Patients without chronic inflammation showed lower survival probabilities and higher chances of complications. The significant differences in ratios may be caused by monocyte differentiation in response to comorbidities and mass immune responses related to inflammation. However, the limitations of our dataset size prevented us from drawing definitive conclusions. Nevertheless, our data suggests that future research is needed to better characterize the TIME of Osteosarcoma to better predict and understand the direction of the Osteosarcoma diagnosis.

Citations:

1. Misaghi A, et al. SICOT-J. 4:12. doi:10.1051/sicotj/2017028
2. Tian H, et al. Bone Res. 2023;11(1):11. doi:10.1038/s41413-023-00246-z
3. Cersosimo F, et al. Int J Mol Sci. 2020;21(15):5207. doi:10.3390/ijms21155207

The Role of IGF-1 in Retinal Ganglion Cell Axon Outgrowth in a Human Stem Cell-Derived Organoid Model

Scholar: Jacquelyn Tang

High School/College/City/State: Mt. Lebanon High School, Pittsburgh, PA

PI of group/lab: Kun-Che Chang, PhD

Mentor(s): Kun-Che Chang, Ya-Ling Lin

Site: VISION

Retinal ganglion cells (RGC) are specialized neurons which play an imperative role in the eye, transmitting visual information from the eye to the brain. When RGCs are damaged in humans, such as from glaucoma and other optic diseases, they have an extremely detrimental effect on the subject's vision and lead to permanent blindness. As of now, there are no treatments for such visual impairment. Accordingly, there is an unmet need for further studies into RGC-replacement therapies using human-derived cells. Insulin-like growth factor 1 (IGF-1) has been shown to promote RGC differentiation and neural axonal growth, suggesting it may also be effective in promoting RGC axon growth in a human stem cell-derived model. Human stem cell-derived retinal organoids were first cultured and then transferred to grow in RC2 media containing IGF-1 along with in PBS acting as a control for a total of 5 days. We expected to observe RGC axon growth in an *ex vivo* model. Screening scope fluorescence imaging was then done to observe the length of RGC axon growth from the retinal organoids every day until day 5. Our data showed that IGF-1 does promote RGC axon growth in the retinal organoids. These results demonstrate that IGF-1 is a potential treatment for vision impairment in cases of RGC damage. Further studies should be done to reinforce this result with comparison to other growth factors before applying to *in vivo* experiments as well as studies to further explore the mechanism by which IGF-1 promotes RGC axon growth.

Comparative Analysis of RNA-Seq Tools Across Multiple Stages of Analysis

Scholar: Roshini Umesh

High School/College/City/State: Seneca Valley, Cranberry Township, PA

PI of Group/Lab: Adrian Lee, PhD & Steffi Oesterreich, PhD

Mentor: Rahul Kumar, PhD

Site: Women's Cancer Research Center (WCRC)

Background: RNA Sequencing (RNA-Seq) is widely used in cancer research for gene expression analysis. However, the analysis pipeline involves multiple steps such as quality control, read alignment, quantification, and differential expressions. While utilizing breast cancer as a biological context, this project performs a comparative analysis of tools in Bulk RNA-Seq data processing to evaluate their data quality, efficiency, and reproducibility.

Methods: Multiple RNA-Seq pipelines were tested for this project. For quality control, FastQC and Fastp were utilized: both tools provide a visual graph to output the base quality scores, GC content, adapter content, and other quality control measures. For trimming low-quality reads and adapter sequences, Trimmomatic and Trim Galore were utilized with their own customization options. For alignment tools, STAR and HISAT 2 were employed. HTSeq and Salmone were used for quantification purposes. Finally, DESeq2 and Limma were used for Differential Expression Analysis (DEA).

Results: The results focused on evaluating each tool's output across different parameters such as run time, mapping efficiency, user friendliness, and quality improvement of the data. Fastp was preferred for quality control because it generates QC reports and trims low-quality data in a single step. For trimming, Trimmomatic outperformed Trim Galore through greater customization of options and faster runtimes. Comparing alignment tools, STAR resulted in an overall more efficient process than HISAT2. For quantification, Salmon was faster and provided transcript-level resolution, whereas HTSeq was simpler but slower to process. For DEA, DESeq2 and Limma both produced similar and consistent results, but Limma is preferred because of its greater flexibility for complex experimental designs.

Conclusion: This comparative analysis demonstrates that tool selection can significantly influence RNA-Seq data quality and efficiency. A pipeline should be tailored to the dataset, intended purpose of the project, and resource availability for efficient and reproducible performance.

Exogenous estrogen and progesterone regulate skeletal muscle architecture in a dose-dependent manner in female mice

Scholar: Nithila Vijayan

High School: South Fayette High School, McDonald, Pennsylvania

Lab: Amrita Sahu, PhD

Mentor: Jagruti Kosaraju, MS; Abraham Brown

Site: Technology Drive X

Background: Women are disproportionately affected by musculoskeletal injuries, however, female-specific musculoskeletal research remains limited. Hormonal contraceptives (HCs), widely used clinically, contain exogenous estrogen and/or progesterone that influence skeletal muscle health. Emerging evidence suggests HCs may enhance muscle strength, with some studies indicating that hormone fluctuations across the menstrual cycle may alter susceptibility to muscle injury, raising the question of whether cycle regulation via HCs could support muscle resilience and recovery. The goal of this study is to investigate the effect of exogenous sex hormones on skeletal muscle health.

Methods: Twelve-week-old female C57BL/6J mice were divided into three groups and orally administered exogenous sex hormones (Group 1: Control, Group 2: 2 mg/kg ethinyl estradiol and 200 mg/kg progesterone [L-EE/PG], Group 3: 5 mg/kg ethinyl estradiol and 200 mg/kg progesterone [H-EE/PG]) for six weeks. Estrus cycling was confirmed with daily vaginal cytology. Tibialis anterior (TA) muscles were collected and frozen for histological analysis of myofiber size, collagen-2, lipid, and mitochondrial health (SDHA).

Results: We found a significantly higher percentage of large muscle fibers ($>2{,}500\mu m^2$) in the H-EE/PG group compared to both the control and L-EE/PG groups ($p < 0.05$), suggesting hormone dosage impacts fiber size distribution. Although there was a trend in increased expression of collagen II, lipid, and SDHA with the high dose group, the results were not significantly different across groups.

Conclusion: These findings demonstrated that high-dose HCs increased myofiber size. However, only modest increases in collagen, mitochondrial content, and lipid levels were observed, indicating that our study was not powered enough to see significant muscle effects in response to the hormones. Further research will be conducted to assess how these changes impact muscle strength and endurance, with the ultimate goal of filling a critical knowledge gap for novel rehabilitation strategies for women.

Exploring the conservation of protogene trafficking mechanisms in zebrafish

Matayo V. Wankiiri-Hale; Alison Guyer; Nathan D. Lord, Ph.D
Eden Christian Academy, Pittsburgh, PA; Hillman Academy, Pittsburgh, PA

Genomic regions deemed as coding regions is the current definition of a gene. However, previous work has recognized the birth of *de novo* genes called protogenes derived from non-coding “junk” DNA. How these protogenes adapt to the existing cellular environment and what fitness advantages they provide is an area of active research. Recent work in yeast suggests that protogenes harness the endoplasmic reticulum (ER) insertional pathways to traffic throughout the cell. Genomic studies suggest that protogenes may be conserved across multiple species. To further test protogene conservation and trafficking dynamics, I injected the yeast protogene YBR-196C-A in early-stage zebrafish (*Danio rerio*) embryos and tracked protogene localization using an ER marker. I observed that the protogene was localized to the ER. This suggests that the protogene is indeed being trafficked in the ER the same way that it was in yeast. These preliminary data support the hypothesis that protogenes utilize similar trafficking mechanisms across species.

References:

1. Levy, A. (2019, October 16). *How evolution builds genes from scratch*. Nature News. https://www.nature.com/articles/d41586-019-03061-x
2. **Houghton CJH, Castilho Coelho N, Chiang A, Hedayati S, Parikh SB, Ozbaki-Yagan N, et al.** De novo proteins integrate cellular systems using ancient protein targeting and degradation pathways. *bioRxiv*. 2025. doi:10.1101/2024.08.28.610198v3
3. **Carvunis Lab, University of Pittsburgh.** Research. [Internet]. Available from: https://carvunislab.csb.pitt.edu/research/ [Accessed 2025 Jul 25]

Thymidine Rescue of ATRi-Induced DNA Damage at Telomeres

Scholar: Alastair Watt

College: University of Pittsburgh, Pittsburgh, PA

PI of lab: Dr. Patricia Opresko

Mentor(s): Dr. Samantha Sanford

Site: Cancer biology

Background Telomere maintenance at chromosome ends is essential for cancer cell growth. Telomerase, which is active in 90% of cancers, extends telomeres using nucleotides, which can make it sensitive to nucleotide pool imbalances. These highly mutagenic nucleotide imbalances can be caused by cancers or induced by chemotherapeutics. While inhibitors of the critical DNA damage response (DDR) kinase ATR are in clinical trials to sensitize tumors to genotoxic therapies, the ATRi, Ceralasertib (AZD6738), alters nucleotide metabolism and increases deoxyuridine (dU) in the genome which can lead to DNA replication errors. Supplementing with thymidine (dT), but not other deoxyribonucleosides, can rescue ATRi-induced dU contamination and cancer cell death.

Methods: To determine whether ATR inhibition disrupts telomere length homeostasis, HeLa LT cells were treated chronically for 7 days with low doses (0.2, 0.4 and 0.8 μM) of AZD6738 with and without thymidine. Metaphase chromosome spreads were conducted to determine if the treatment caused telomere aberrations and decreased telomere length. Cells were arrested in metaphase with colcemid, swollen in hypotonic KCl, and fixed. The cell suspension was then dropped onto slides to disperse chromosomes for analysis. Slides were hybridized with telomere specific fluorescent probes, allowing telomeric defects to be visualized by fluorescence microscopy.

Results: Quantitative TeloFISH on metaphase chromosomes revealed a dramatic reduction in telomere signal intensity. After one week, HeLa LT exhibited increased telomere fragility with ATRi, but thymidine partially rescued this fragility. Signal-free chromosome ends increased in HeLa LT cells at the higher 0.8 μM dose.

Conclusions: This data suggests that ATRi impairs telomere maintenance by inducing dU incorporation at telomeres, leading to telomere shortening and increased telomere defects in telomerase-positive cancer cells, and that thymidine can partially rescue these effects.

Title: Establishment of a Stable Non-Cancerous Cell Line Expressing CHD7:BEND2 in an In-Vitro System

Scholar: Andy Weng

High School: Seneca Valley Senior High School, Harmony PA

PI: Dennis Hsu, MD

Mentor(s): David Man, Ph.D.

Site: Cancer Biology

Background: Fusion proteins form when two separate genes are joined, often due to the result of chromosomal rearrangements. These fusions can have abnormal or enhanced functions, contributing to the progression or development of diseases like cancer. One fusion protein, CHD7:BEND2, involves CHD7 and BEND2, the latter of which is thought to be involved with transcription regulation and chromatin structuring. This fusion has recently been found to be aberrantly expressed in a subset of aggressive pancreatic neuroendocrine tumors. Although the role of CHD7:BEND2 is unclear, its presence suggests that it may act as an oncogenic driver by disrupting normal chromatin structure and gene regulation. To investigate the CHD7:BEND2 fusion, we establish it in a non-cancerous cell line to assess the effects in an untransformed cellular context.

Methods: pcDNA3.1+ encoding the *CHD7:BEND2* fusion gene were constructed via standard molecular cloning techniques (polymerase chain reaction, restriction digestion, agarose gel purification). DNA was ligated and transformed into E. coli DH5alpha for amplification, followed by mini prep to retrieve the DNA. HEK293 cells were transfected with purified pcDNA3.1+ *CHD7: BEND2*, BCA assay, SDS-PAGE, RT-PCR, and Western Blotting are used to verify protein expression.

Results: The pcDNA3.1+ *CHD7: BEND2* fusion construct was successfully created, amplified in E. coli DH5alpha, and purified for downstream applications. The plasmid was transfected into HEK293 cells. RT-PCR demonstrates the fusion construct recombinantly incorporated into the genome from the cell pool.

Conclusion: A stable cell line expressing CHD7:BEND2 is nearing completion. RT-PCR has confirmed the fusion protein expressed at the mRNA level. Once a single clone is isolated, western blot will verify protein expression. Future work may entail using chromatin immunoprecipitation sequencing (ChIP-seq) to identify DNA-protein interactions or conducting ATAC-seq to assess genome-wide chromatin accessibility. These approaches can reveal how CHD7:BEND2 alters chromatin structure and identify gene targets in oncogenic reprogramming.

Title: AMT effectiveness on TBIs

Scholar: Blake Whiteman

High School/College/City/State: Shaler Area High School, Pittsburgh, PA

PI of group/lab: Justin Wideman

Mentor(s): Dr. Brown and Dr. Leeper

Site: Surgery

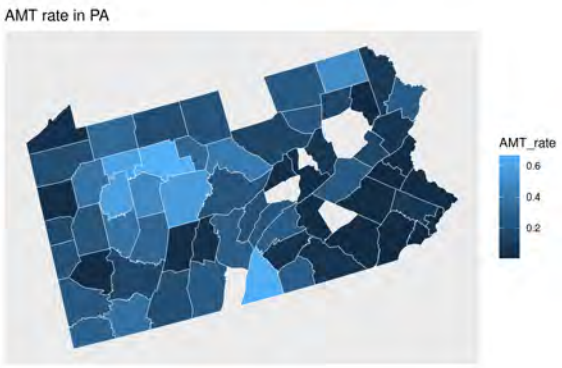

Background

Traumatic brain injury (TBI) is a leading cause of death after injury. Increased time to treatment results in higher mortality rates, signifying fast transport to trauma centers is ideal. Air medical transport (AMT) with helicopters is faster than ambulances, and prior research shows AMT for TBI increases survival. It is unclear how much AMT is used for TBI. Our objective was to evaluate the use of AMT for TBI patients in Pennsylvania and differences across urban and rural counties.

Methods

County-level age-adjusted TBI fatality rates in Pennsylvania from 2018-2020 were obtained from the CDC. The Pennsylvania Trauma Outcomes Study (PTOS) was utilized to calculate county-level AMT rates. Choropleth maps were created to visualize relationships between AMT rates and TBI fatality rates across counties. AMT, fatality, and Years of Productive Life Lost (YPLL) rates were compared between rural and urban counties using t-tests.

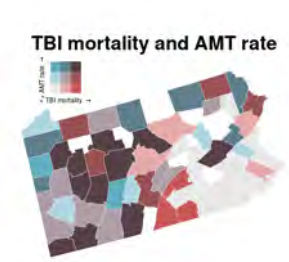

Results

The AMT rate varies across Pennsylvania (Figure 1). Geographic analysis of AMT and fatality rates shows outlier counties where there are high TBI fatality rates but low AMT utilization (red counties, Figure 2). When comparing urban to rural counties, the AMT rate is higher in rural areas (27.3% vs 4.4%, $p<0.01$). The TBI fatality rate was also higher in rural counties (23.3±5.9 vs 15.7±3.4 per 100,000 people, $p<0.01$), but the YPLL was higher in urban counties (3902.6±4157.4 vs 840.0±545.6 years, $p<0.01$).

Conclusion

We identified counties that have high TBI fatality rates but low AMT use. This allows us to target these areas to educate first responders about the benefits of AMT, so they could improve utilization and ultimately help to save lives. Rural and urban counties differ with higher fatality rates in rural areas from TBI, but younger patients dying from TBI in urban areas leading to more YPLL. This can inform prevention strategies in rural versus urban areas.

Title: The Characterization of iPSCs

Scholar: Brandon Williams

High School: Winchester Thurston Upper School, Pittsburgh, Pennsylvania

Lab PI: Rodrigo Florentino, PhD

Mentor: Rodrigo Florentino, PhD

Site: Pathobiology

iPSCs, or induced pluripotent stem cells, are a type of stem cell that are able to differentiate into any cell type in the body. These cells are useful for researching diseases due to their ability to model other cell types. However, due to the inefficiency of the reprogramming process, some iPSCs may not be consistent compared to normal iPSCs. Therefore, the goal of this study is to characterize iPS 167 WT and iPS 167 gene edited cells to make sure they can be used for lab research. Well plates that contained iPS 167 WT cells and iPS 167 gene edited cells were blocked and stained with the primary antibodies Nanog, TRA-1-60, or SSEA4. Each well plate also was stained with DAPI and a secondary antibody specific for Nanog and TRA-1-60. Pictures of the well plates were taken using EVOS M500. iPS 167 WT and iPS 167 gene edited cells were collected and their RNA was extracted. The extracted RNA was used to make cDNA using a Thermal Cycler. The analysis of the cDNA was done using a qPCR machine with control iPSC being the reference sample and Lin 28, OCT ¾, MYC, Nanog, and Sox 2 being the targets with ACTB being the internal control. Immunofluorescent staining showed the presence of Nanog, TRA-1-60, and SSEA4 in iPS 167 WT and iPS 167 gene edited cells. Control iPS cells showed a consistent fold change under each target. iPS 167 WT cells and iPS 167 edited cells showed a somewhat consistent fold change under each target. This study confirmed that iPS 167 cells had most of the characterization necessary in order to be used in lab research. In the future, collected iPS 167 WT and iPS 167 gene edited cells will have their DNA sequenced using genotyping to fully characterize the cells.

LIF Gene Therapy Potential for Retinal Degeneration

Scholar: Sarah Beth Winikoff
High School: CAPA 6-12, Pittsburgh, Pennsylvania
Lab: John Ash, PhD
Mentors: Constanza Potilinski, John Ash
Site: VISION

Background: The leading causes of blindness are degenerative retinal diseases including glaucoma, age-related macular degeneration, and retinitis pigmentosa. Early treatment is crucial, however, patients who notice vision impairment may have irreversible and debilitating disease progression. Understanding the protective mechanisms that help retinal cells adapt and survive during disease is key to unlocking new treatments. Currently, gene therapies are being invented to activate stress response pathways to protect photoreceptors and help cells stay alive and functional for longer. Therefore, understanding the molecular mechanisms behind stress response pathways is crucial.

Leukemia Inhibitory factor is a cytokine produced by the immune system that is neuroprotective of the retina. It is activated by the STAT-3 transcription pathway and leads to the production and activity of immunoproteasomes, which degrades and processes protein peptides and prepares them for antigen presentation in immune cells. Our study analyzes the specific antibody production and upregulation of IRF transcription factors in relationship to this effect.

Hormesis, an adaptive response to repair mechanisms of the cell, occurs when LIF stimulates inflammation. Thus, this hypothesis-driven study investigates the regulation and activity of the immunoproteasome in response to LIF as a potential new treatment strategy for patients with neurodegenerative retinal disorders.

Methods: Mouse retinas were obtained from enucleated eyes from intravitreally injected albino mouse eyes with PBS 1 ul or LIF 1 ul with a concentration of 2 ug/ul. The retinas were sonicated for 10 seconds at 10 kHz and then the samples were centrifuged at 4 degrees for 20 minutes at 17000 g. Supernatants were quantified by BCA to address protein concentration. Samples were stored at -80 degrees upon use. Immunoblotting techniques and chemiluminescence-based assays were used to obtain protein expression levels.

Results: After LIF exposure, transcription factors IRF-1 and IRF-9 increase in relation to post-transcriptional binding. The 20S-core proteasome subunit and the immunoproteasome subunits PSMB-5 and PSMB-8 are activated in both male and female samples. Differences in expression level were located between female and male quantifications, possibly due to differences between female genetic composition or sex-related traits. Validations for other antibodies including 11s, PSMB-9, PSMB-11, and PSME-2 did not show significant results compared to the PBS control samples.

Conclusion: Our study shows that specific transcription factors and immunoproteasome activity increase upon LIF treatment in mouse retinal models. Therefore, the mechanism behind the stress-induced resistance and resilience to degeneration may be explained by the immune functions of the 20s core, PSMB-5 and PSMB-8 subunits, and IRFs. We will continue to investigate the mechanisms of immune protection to develop therapies for neurodegeneration to prevent vision loss.

Developing an Antiviral for Influenza A by Targeting the Polymerase Acidic Protein

Scholar: Casey Yang

High School: North Allegheny Senior High School, Pittsburgh, Pennsylvania

PI: Yuan Liu

Mentors: Bill Chen, Yanwen Chen

Site: Tech Drive X

Background: Influenza A causes severe respiratory illness and has caused many pandemics globally. Due to the rapid evolution of Influenza A, current vaccines and antivirals vary in efficacy. Therefore, developing new antivirals for Influenza A is imperative. The Polymerase Acidic (PA) protein, a subunit of the heterotrimeric RNA-dependent RNA Polymerase of Influenza A, is a vital protein that plays a key role in cap snatching, a process that Influenza A undergoes to replicate its RNA. Furthermore, due to PA's significance, it is highly conserved in different variants of Influenza A, making it an optimal target for potential antivirals. Thus, this study investigates potential compounds to induce the degradation of PA and the effects these compounds have on Influenza A.

Methods: High-throughput screening of ChemDiv Diversity Library and a qPCR were performed to choose hit compounds. Beas-2B cells and Madin-Darby Canine Kidney (MDCK) cells were treated with Influenza A (H1N1-PR8) and Compound 500. Immunoblotting was used to study PA and nucleoprotein levels. By comparing co-treatment with proteasome, lysosome, or E1 inhibitors, the mechanism of degradation of Compound 500 was deduced. A Hemagglutination Assay was performed with turkey red blood cells to detect virus titer. Immunoprecipitation was executed to evaluate the levels of PA ubiquitination.

Results: Through initial testing, it was concluded that Compound 500 is the hit compound. Further testing of Compound 500 revealed that PA is degraded through the ubiquitin proteasome pathway. Cells treated with Compound 500 and Influenza A were shown to have decreased levels of viral protein and less virus in comparison to a control.

Conclusion: Compound 500 has proven to be a promising degrader of PA and a potential antiviral for Influenza A. Further studies will be done to identify superior derivatives of Compound 500 and to investigate the E3 ligase responsible for the degradation of PA.

Title: Functional Validation of RAX Enhancers in the Developing Retina

Scholar: William Zhang
High School: Hampton High School/ Pittsburgh, PA
Affiliations: Al Diri Lab, UPMC Vision Institute, University of Pittsburgh, Department of Ophthalmology
Mentors: Issam Al Diri, Ph.D., Kamakshi Mehta, Ph.D.

Background: Retinal neurogenesis is a precisely regulated process in which retinal progenitor cells (RPCs) exit cell cycle and differentiate into neurons or glial cells. This highly conserved process is governed by a complex gene regulatory network consisting of transcription factors expressed in multipotent RPCs. One such transcription factor is the Retina and Anterior Neural Fold Homeobox (RAX) gene, which is essential for retinogenesis. Disrupting RAX function can have serious consequences on eye development in humans. Previous epigenomic studies mapping the cis-regulatory landscape of retinal cells in mice and humans have identified potential non-coding enhancer elements associated with the RAX gene. However, whether these elements act as bona fide enhancers to regulate RAX expression in the developing retina is not known.

Methods: I first cloned one putative RAX enhancer (EN3) into a STAGIA3 vector (a plasmid containing two reporter genes with minimal promoter), and confirmed the cloning was successful using sequencing methods. Next, to functionally validate whether the enhancer is active in the developing mouse retina, I performed ex vivo electroporation of STAGIA3 plasmid with the RAX putative enhancer element in retinae dissected at embryonic stage 14.5 (E14.5). I also electroporated SATAGIA3 empty vector (no enhancer) as a negative control. Successfully electroporated retinae were cultured ex vivo for two days and followed by an Alkaline Phosphatase (AP) staining to visualize the spatial pattern of the enhancer activities.

Results: Cloning of the candidate RAX enhancer region into the STAGIA3 reporter vector was confirmed by Plasmidsauras sequencing, with the enhancer sequence fully aligned to the reference sequence, thus verifying successful insertion and correct orientation. Following ex vivo electroporation into E14.5 mouse retinal tissue, the STAGIA3 enhancer-reporter construct showed robust and localized reporter activity. AP staining revealed distinct expression patterns in the central region of the retina, consistent with zones of active retinal progenitor cells (RPCs). Notably, reporter expression was absent in control tissues electroporated with empty vector, confirming enhancer-specific activity.

Conclusions: My study indicates that the candidate RAX enhancer is active in embryonic developing retina at E14.5, suggesting that it may act as an enhancer regulating RAX expression during retinal development.

Large-language models for extraction of methodological details from infectious disease modeling papers

Matei Zivanov[1], Eddie Perez[2], Harry Hochheiser[2]
[1]Allderdice High School, Pittsburgh, PA
[2]Department of Biomedical Informatics, University of Pittsburgh, Pittsburgh, PA

Abstract

This project investigates the use and benefit of large language models (LLMs) in combination with few shot example prompting and RAG to extract key relationships and entities from a dataset of scientific literature regarding infectious diseases. This approach demonstrates the potential of these pipelines to quickly and efficiently provide insights on disease information, but the content extracted remains insufficient.

Introduction

As infectious diseases remain a global health concern, utilizing scientific literature to study these diseases likewise remains crucial for controlling spread, developing treatments, and protecting vulnerable populations. However, manual extraction of information from this literature to create an illustrative gold standard of knowledge poses challenges: the growing volume of publications renders manual extraction tedious. Thus, using LLMs[3], in combination with RAG and Few shot architectures, to automate information processing can enhance extraction of key relationships from scientific papers on infectious diseases.[1,2]

Methods

Two corpora of infectious disease-related abstracts were selected: one set of 47 training documents, and one pool of 5736 modeling documents for extraction, both in JSON format. The first 200 modeling documents were used to create a vector store of embeddings for retrieval. Two RAG, Retrieval Augmented Generation, retrievals were designed, graph and generic RAG, that were then implemented into the LLM QA pipeline. The graph RAG infused pipeline took significantly longer to build; around 200 minutes, compared to the 4 second generic RAG. Once built, the LLM - in this case Llama 3.2 - was prompted to develop a summary of one of the 5736 modeling documents. The extracted summary was then run through a transformer routine for graph extraction, printing a graph of key relationships. The few shot pipeline employed a set of 11 ideal example relationships as context for the LLM A similar graph transformer extracted crucial relationships from a selected modeling document. After, analyzing those results, the few-shot approach was then extended by implementing 15 additional ideal example relationships. The number of distinct nodes and relationships for each method for a randomly selected set of 10 documents were counted and concatenated into a data frame and plotted as a distribution in a violin plot. All coding was done through Python.

Results

The few shot pipelines, specifically the FS method, typically extracted more key relationships and distinct nodes compared to the RAG approaches for the 10-document set. This can be observed in the increase in width as the count increases in both plots for the FS approach. Document ID 3820 is identified as an outlier for the FSImproved method, with a count of 31 distinct nodes and 20 relationships, compared to the median 4.5 nodes and 4.5 relationships. This suggests that the FS methods are more effective in extracting key relationships, namely extracting a larger count of relationships. Furthermore, extending the few shot approach by incorporating more example relationships has the potential to extract a significantly larger amount of information, however this may be on a document-by-document basis, and requires more testing.

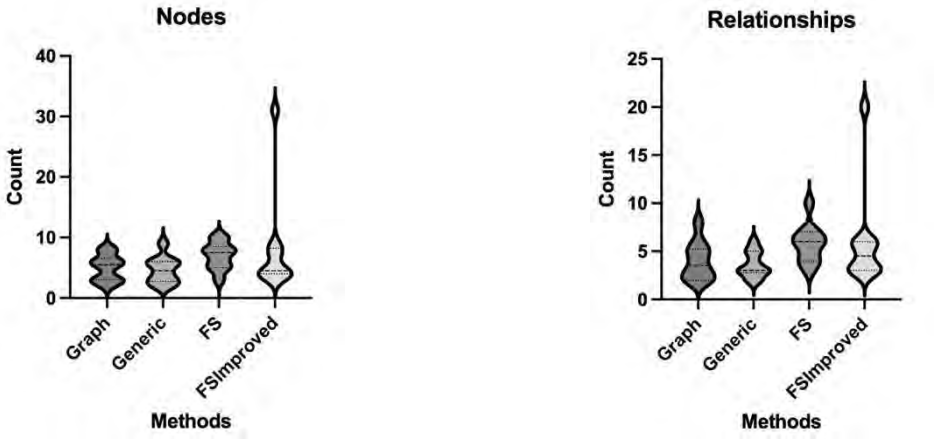

(a) **(b)**

Figure 1. Violin Plots of (a) node counts and (b) relationship counts extracted from 10 documents, using four different approaches: Graph RAG, Generic RAG, Few Shot Prompting, Few Shot Prompting Improved

Discussion

The results indicate that augmented LLM pipelines show promising potential to extract key relationships from scientific literature on infectious diseases. The graph and generic RAG integrated pipelines performed similarly, and the few shot prompted pipelines displayed the most abundant outputs. While the speed of completion poses a clear advantage, the overall benefit of LLM assistance to extract information from papers remains limited, lagging behind manual human extraction.

References

1. Sujau, M., Wada, M., Vallée, E., Hillis, N., & Sušnjak, T. (2025). Accelerating Disease Model Parameter Extraction: An LLM-Based Ranking Approach to Select Initial Studies for Literature Review Automation. Machine Learning and Knowledge Extraction, 7(2), 28. https://doi.org/10.3390/make7020028
2. Hang, T., Liu, S., Feng, J., Djigal, H., & Huang, J. (2024). Few-shot relation extraction based on prompt learning: A taxonomy, survey, challenges and future directions. ACM Computing Surveys. https://doi.org/10.1145/3746281
3. Dagdelen, J., Dunn, A., Lee, S. et al. Structured information extraction from scientific text with large language models. Nat Commun 15, 1418 (2024). https://doi.org/10.1038/s41467-024-45563-x